A MODELING AND MEASUREMENT STUDY OF ACOUSTIC HORNS

by

John T. Post
and
Elmer L. Hixson

May 1994

Electroacoustics Research Laboratory
Department of Electrical and Computer Engineering
The University of Texas at Austin

Acknowledgements

I would like to express my most sincere gratitude to the many people who contributed to my completion of this dissertation. First I must thank my advisor, Professor E. L. Hixson, for his prodigious patience, support, and counselling throughout the duration of the project. Hopefully I have inherited some of his experimental prowess. I greatly appreciate the efforts expended by the committee in overseeing my work, especially Professor F. X. Bostick, who was always there to help me overcome mathematical obstacles in the theory of wave propagation. Thanks to Dr. Jim McLean for proof-reading the text and verifying much of the mathematical content. I also appreciate the many hours of interesting and insightful discussions concerning horns and countless other topics. Thanks also go to Mr. Tom Kite, for taking most of the photographs of the experimental apparatus (a couple were taken by Dr. Hixson), and for proof-reading the text.

Thanks to Mr. Marty Ringuette of the Electrical Engineering Department staff, for supporting the experimental work and constructing several of the more intricate pieces of the experimental apparatus. I owe several favors to Mr. Hank Franklin of the Mechanical Engineering Department staff, who was responsible for the expert machining needed in the construction of much of the experimental apparatus.

I would like to recognize Klipsch Professional for fabricating (by hand) the exponential and tractrix horns used in the experiments. I would also like to acknowledge the support from Electro-Voice in supplying compression horn drivers for use in the experiments. Thanks to Ms. Karen Hunt of Boner and

Associates for her assistance in obtaining support from Klipsch and Electro-Voice. Many thanks to Mr. Mark Botner and Convex Computer Corporation for the final runs of the boundary element code.

I am also very thankful for the support of my friends (those not yet mentioned), classmates, and family during my graduate education. Thanks to Mr. Paul Colestock for his continuous moral support, technical advice, and great bike rides. Special thanks to my parents for having faith in me throughout the many years of my college education, and for always being there when I needed them.

A MODELING AND MEASUREMENT STUDY OF ACOUSTIC HORNS

Although acoustic horns have been in use for thousands of years, formal horn design only began approximately 80 years ago with the pioneering effort of A. G. Webster. In this dissertation, the improvements to Webster's original horn model are reviewed and the lack of analytical progress since Webster is noted.

In an attempt to augment the traditional methods of analysis, a semi-analytical technique presented by Rayleigh is extended. Although Rayleigh's method is not based on one-dimensional wave propagation, it is found not to offer significant improvement over Webster's model.

In order to be free of the limitations associated with analytical techniques, a numerical method based on boundary elements has been developed. It is suitable for solving radiation problems that can be modeled as a source in an infinite baffle. The exterior boundary element formulation is exchanged for an interior formulation by placing a hemisphere over the baffled source and using an analytical expansion of the field in the exterior half space. The boundary element method is demonstrated by solving the baffled piston problem, and is then used to obtain the acoustic throat impedance and far-field directivity of axisymmetric horns having exponential and tractrix contours.

Experiments are performed to measure the throat impedance and the far-field directivity of two axisymmetric horns mounted in a rigid baffle. An exponential horn and a tractrix horn with equal throat radius (2.54 cm), length

(55.9 cm), and mouth radius (27.1 cm) are critically examined. A modern implementation of the "reaction on the source" method is compared with a new implementation of the two-microphone method for measuring acoustic impedance. The modified two-microphone method is found to be extremely simple and accurate, but the "reaction on the source" method has the advantage of *in situ* measurements. The far-field directivity is measured by a new technique that allows the far-field pressure to be calculated from the measured near-field pressure. Experimental results compare very well with the numerical predictions obtained by the boundary element method.

The annotated bibliography is 34 pages in length and features approximately 200 references that are useful in the general study of acoustic horns.

Table of Contents

List of Figures

Chapter 1

Introduction

At the turn of this century, the invention of audio recording gave the millennia-old acoustic horn new purpose. The traditional uses of the acoustic horn included music, summoning, and listening. In these roles, the resonances in the horn were exploited for sound production or increased hearing sensitivity. With the invention of audio recording, the acoustic horn assumed a role as a device for impedance matching and directivity control in the field of sound reproduction, where the resonances existing in previous horns are not desirable.

The first section of this chapter summarizes the analytical progress in the study of horns over the past eighty years. The advent of the digital computer made possible the application of numerical techniques to the analyses of acoustic horns. Previous numerical modeling efforts are reported, and weak points needing further development are identified. At the end of the chapter, the work contained herein is discussed and the organization of the dissertation is presented.

1.1 Analytical Developments in the Theory of Horns

Although acoustic horns have been in use for thousands of years, formal horn design began relatively recently with A. G. Webster's landmark paper, "Acous-

tical Impedance, and the Theory of Horns and of the Phonograph" [11],* published in 1919. The primary contribution of Webster's paper was the introduction of the concept of acoustic impedance, but it also introduced techniques for the analysis of horns that have remained virtually unchanged during the past 80 years. Webster derived an equation modeling one-dimensional plane-wave propagation in horns, which is known as Webster's horn equation. He also mentioned that complicated horn geometries can be handled by dividing them into sections, and presented a general technique for finding the two-port parameters of each section. These sections can then be cascaded to form a transmission-line model of the horn. The number of subsequent publications dealing with one-dimensional horn theory is staggering, and no attempt will be made to discuss them individually. Most of these either present solution techniques for, or properties of certain solutions to Webster's horn equation. The interested reader is referred to the annotated bibliography of the present work, and in particular to the papers by Salmon [66], Mawardi [70], Eisner [106], and Campos [151].

One practical aspect of horns which was not discussed in detail by Webster is that of the proper size for the horn mouth. In the experimental verification of his theory [12], Webster terminated the horns by using an end correction length of 0.6 times the radius at the mouth. Long, narrow horns were tested at relatively low frequencies, the highest being $ka = 0.79$ (k is the wave number, a is the mouth radius). The proper size for the horn mouth is discussed at length by Hanna and Slepian [16], who introduce the concept of one-dimensional wave propagation that is not necessarily planar. Their paper contains drawings of spherically expanding wavefronts, and the concept that the horn mouth need be at least one wavelength in circumference at the lowest frequency of operation. The end correction used by Webster is replaced with the impedance "seen" by

*All references are found in the bibliography, which is ordered chronologically.

a hemispherical source with a radius equal to that of the horn mouth.

Although Hanna and Slepian's work depicted spherical wavefronts inside the horn, the cross-sectional area $S(x)$ of the horn in Webster's one-dimensional theory is usually chosen to be a plane for lack of a method to obtain a more accurate estimate of the rate of area expansion. An attempt to improve on the plane-wave assumption has been made by Weibel, who has shown [91] that the stream functions for constant flow in a horn lead to an equation identical to Webster's, but the coefficients are more complicated and, in general, would require solution by a sophisticated numerical method such as the finite element technique. Such a technique would be difficult to justify for obtaining an approximation. Perhaps the most important contribution of Weibel's work is the verification of the applicability of Webster's horn equation at low frequencies, where its correctness had been questioned [16, 24, 73].

During their tests of the resonances in musical instrument horns, Benade and Jansson [122, 123] found that plane-wave assumptions and spherical wave assumptions lead to predicted resonances which tend to bound the measured resonance frequency. This idea has recently been extended by Holland, Fahy, and Morfey [185], who assumed the rate of area expansion to be the arithmetic mean of the planar cross-section and a spherical area that contacted the wall normally, which lead to good agreement between the predicted and measured values of throat impedance.

Many researchers have investigated the assumptions involved in Webster's theory. Attempting to explain the complex directivity patterns measured by Stewart, Hoersch suspected and showed [18] that non-planar vibrations can exist inside a conical horn. Hall [40] measured the acoustic pressure inside an exponential and conical horn and showed that the wavefronts curve in a spherical manner at low frequencies but become complicated at higher frequencies. Hall's paper is a major contribution to experimental data for horns, and he

felt that it would lead to improved horn design methods when he stated, "The impossibility of verifying more exact theories experimentally has heretofore justified the use of the present horn theory. However, this restriction is rapidly being removed, and it is to be expected that refinements in the theory will be made to keep pace with the experimental technique." The theory has actually not kept pace with the experimental progress as Hall predicted, because the problem of wave propagation within a general waveguide cannot easily be solved.

The analytical history of horns discussed in this section reveals that only minor improvements to Webster's horn model have been made in the past 80 years. A more sophisticated mathematical model has not been practicable because of the corresponding increase in difficulty of solution. The useful contributions that various researchers have made to Webster's original model equation are *i*) choosing the appropriate size of the mouth of the horn, and *ii*) choosing the rate of area expansion with more accuracy than that afforded by assuming plane waves.

1.2 Application of Numerical Methods to Horn Modeling

Because of the falling cost and increasing speed of digital computers, the numerical solution of horn models containing fewer simplifying assumptions than Webster's model has become possible, but very little work has yet been done in this area.

Kyouno et al. [150] have modeled a complete horn loudspeaker by using circuit models for the horn driver and a finite element model for the horn. The measured electrical impedance and far-field response show reasonable agreement with numerical predictions. Shindo, Yoshioka, and Fukuyama [179] have used sections of multi-moded rectangular waveguide (first presented by Steven-

son [79]) combined with the boundary element method to model radiation from a horn into free space. The acoustic field in the mouth of the horn is found under the assumption that the horn is mounted in a rigid, infinite baffle. The resulting acoustic field in the mouth is then used as the source in an exterior boundary element formulation to find the far-field directivity. The measured and far-field directivity are plotted at two frequencies and agree well.

1.3 Need for Further Study

Webster's equation is a practical tool for the study of the throat impedance of horns, but no criteria exist to determine the frequency range of applicability for Webster's equation. Several estimates have been given for the accuracy of plane-wave approximations [172, 176], but the wave propagation can be nearly one-dimensional without the requirement of being plane, and there have not been any estimates for the range of validity of one-dimensional propagation in general. Webster's model is probably quite good for horns that taper slowly and/or have relatively small mouths with respect to the propagated wavelengths, but the practitioner must exercise some caution before interpreting the results based on Webster's model for horns that flare quickly or have relatively large mouths. Therefore one area of focus is to investigate the range of applicability of Webster's equation. In researcher's efforts to extend the range of applicability of the horn equation, the greatest gain has resulted from making an improved approximation for the rate of area expansion. This correction is currently limited to averaging the areas of cross-sectional plane and spherical surfaces. The utility of Webster's equation could be extended if an efficient technique is found for computing the proper rate of area expansion, which would then be substituted into Webster's equation.

The wave equation can be solved with the aid of a digital computer without the assumptions inherent in Webster's model, but the number of completed

numerical solutions is still too sparse at this time for general conclusions. It is important that the efficiency, accuracy, and flexibility of particular numerical methods be made clear, so that the reader can ascertain the usefulness of the method for his application. Progress in this area has been hampered by the lack of rigorous, explicit development of the methods. More numerical work needs to be done that is capable of simultaneously predicting the throat impedance and directivity (although directivity is currently more important than throat impedance). In many of the current generation of acoustic horns, directivity control is optimized at the expense of throat impedance [136]. This trade-off is necessary to reduce the complexity (and associated cost) involved in empirical design. A major drawback of the current design method is that it results in a non-optimal loading of the compression horn driver. If significant deviations in the frequency response of the horn result from this procedure, electronic compensation can be employed, but no amount of electronic equalization can make up for an impedance mismatch when it comes to distortion and power handling specifications. The diaphragm displacement becomes excessive for a poor impedance match. Excessive diaphragm displacement results in increased distortion and reduced power handling for the horn loudspeaker. The impedance mismatch in high-quality, constant-directivity horns has been shown to be as large as 10:1 [191].

Although the quantity of literature concerning horns is quite large, there are very few publications which confirm analytical or numerical solutions by laboratory measurement. This is largely due to the difficulty in measuring the acoustic impedance of horns. It would be of considerable benefit to develop a simple and robust measurement method for measuring the throat impedance with both a high degree of accuracy and precision.

1.4 Organization of Dissertation

This dissertation is organized into three primary chapters. The need to define a range of validity and an accurate rate of area expansion for Webster's horn equation inspired the work contained in Chapter 2, which is based on a technique first presented by Rayleigh. This technique may offer the possibility of providing error bounds for Webster's horn equation, and defining the correct rate of area expansion, which is likely to be frequency dependent. The technique presents some interesting results, but analytical difficulties have prevented the achieving of the desired goals. Nevertheless, the chapter is presented here because of the possibilities the method offers.

Chapter 3 introduces the boundary element method, and presents the difficulties inherent in this approach. The boundary integral equation is derived, and a particular implementation of the numerical method is chosen that circumvents the difficulties typically associated with the boundary element method. The dimension of the boundary integral equation is reduced by taking advantage of the axisymmetric horn geometry, and then a numerical implementation is described which uses isoparametric quadratic elements. The chapter finishes by implementing the technique and testing it by solving the problem of a rigid piston in an infinite baffle and comparing the computed solution with the analytical one.

In Chapter 4, two techniques for measuring acoustic impedance are developed and compared. The more robust of these is then used to measure the throat impedance of axisymmetric exponential, and tractrix horns. The measured impedances are compared to those computed by the boundary element program developed in Chapter 3. A measurement technique for predicting the far-field directivity by measuring the pressure in the near field is then described and implemented. In the final section of the chapter, the measured results are compared to computed predictions.

In the course of investigating various techniques that might be useful for acoustic horns, some thought was put toward using the tremendous volume of work in the electromagnetics area by way of analogy. No particular results from this are used in the text, but the investigation itself may be useful to others, and is therefore included in the appendix.

Also a word is in order concerning the bibliography. It contains more references than are actually cited in the text, and many of these are annotated. The annotations were originally intended only to jog the author's memory, but have been included here along with all of the references in the hope that they will be useful for those who may be interested in pursuing portions of this work further. The references are ordered chronologically.

Chapter 2

An Approximate Analytical Method

To find a general solution of the wave equation in the interior of an acoustic horn is an ambitious, if not impossible, task. If an exact solution to the wave equation cannot be obtained analytically, alternative possibilities exist.

Simplifying approximations may be made that result in a modeling differential equation that can be solved analytically without losing all of the relevant physical information. Webster [11] chose this approach by assuming one-dimensional, plane-wave propagation within a horn, yielding "Webster's horn equation,"

$$\phi'' + \frac{S'}{S}\phi' + k^2\phi = 0 \tag{2.1}$$

where ϕ represents the velocity potential, $S(x)$ the cross-sectional area of the horn, and k the wave number. This equation is very useful for predicting the throat impedance of acoustic horns. A limitation of Webster's horn equation is the lack of information concerning the acoustic wave field interior to the horn.

If an approximate model loses the ability to predict the desired physical results, it is still sometimes possible to find an approximate analytical (or semi-analytical) solution to the more exact model for some restricted regions or parameter conditions. This is the approach so aptly demonstrated by Rayleigh [10].* Webster first presented his technique at a meeting of the American Physical Society at Philadelphia in December of 1914. In all likelihood, Rayleigh

*John William Strutt, Baron Rayleigh III (1842–1919).

did not know of Webster's presentation before he developed "Webster's horn equation" as a zeroth-order approximation to the wave equation within a tapered waveguide. Rayleigh published this work in 1916, but had presented the method of solution for an electrostatics problem 40 years earlier [1] to the Mathematical Society of London.

If a simplified model or a semi-analytical solution is not possible, a numerical solution can be employed. This will be developed in Chapter 3.

In the following sections Rayleigh's work has been the underlying basis, but the fundamentals of his work are expanded to clarify the method, and the results are extended to include, among other details, the off-axis acoustic field.

2.1 Rayleigh's Iterative Method

For the case of time-harmonic[†] acoustic vibrations, the differential equation of the physical model is the Helmholtz equation. In a lossless, source-free, axisymmetric region, the appropriate form is

$$\frac{\partial^2\phi}{\partial r^2} + \frac{1}{r}\frac{\partial\phi}{\partial r} + \frac{\partial^2\phi}{\partial x^2} + k^2\phi = 0 \tag{2.2}$$

where ϕ represents the complex velocity potential, k the wave number, and x and r the longitudinal and radial coordinates respectively as seen in figure 2.1. The volume of the horn is generated by rotating the contour $y(x)$ about the x axis. Equation (2.2) may be rewritten as

$$\frac{\partial^2\phi}{\partial r^2} + \frac{1}{r}\frac{\partial\phi}{\partial r} + \left(\frac{\partial^2}{\partial x^2} + k^2\right)\phi = 0 \tag{2.3}$$

which would be Bessel's differential equation if the quantity in parentheses were constant. This suggests a solution of the form

$$\phi = J_0\left(r\sqrt{d^2/dx^2 + k^2}\right)F(x) \tag{2.4}$$

[†]The time dependence is taken to be $e^{j\omega t}$.

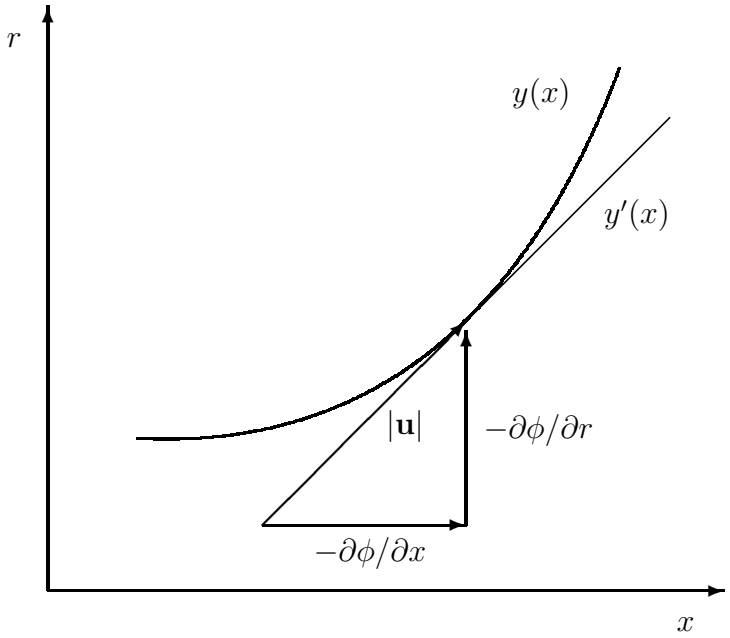

Figure 2.1: Rigid wall boundary conditions illustrating tangential velocity.

where J_0 represents the Bessel series of order zero. The differential argument in the Bessel series is understood to operate on the function $F(x)$. The function $F(x)$ is the on-axis value of $\phi(x, r)$, which can be written

$$F(x) = \phi(x, r)|_{r=0} \,. \tag{2.5}$$

Equation (2.4) is in fact an *exact* solution, as can be verified by substitution into equation (2.2).

The rigid wall of the horn requires the normal component of the velocity to vanish on the boundaries,

$$\left.\frac{\partial \phi}{\partial n}\right|_{r=y(x)} = 0 \tag{2.6}$$

where n represents the coordinate axis normal to the boundary. This requirement is equivalent to stating that the velocity vector at the boundary must be tangent to the boundary. The ratio of the r and x components of the velocity ($\mathbf{u} = -\nabla\phi$) must be equal to the slope of the boundary contour. This is

illustrated in figure 2.1. Mathematically,

$$\left[-\frac{\partial\phi}{\partial x}\frac{dy}{dx}+\frac{\partial\phi}{\partial r}=0\right]_{r=y(x)} \tag{2.7}$$

where it is understood that the expression must be evaluated on the boundary.

To enforce the rigid boundary condition, first expand equation (2.4) to get[‡]

$$\phi(x,r)=F(x)-\frac{r^2}{4}\mathcal{D}F(x)+\frac{r^4}{64}\mathcal{D}^2F(x)-\frac{r^6}{2304}\mathcal{D}^3F(x)+\frac{r^8}{147456}\mathcal{D}^4F(x)-\cdots \tag{2.8}$$

where the linear operator $\mathcal{D}$ has been defined as

$$\mathcal{D}\equiv\frac{d^2}{dx^2}+k^2 \tag{2.9}$$

and substituted for brevity. Higher powers of the differential operator $\mathcal{D}$ are defined by $\mathcal{D}^{n+1}\equiv\mathcal{D}\mathcal{D}^n$ and represent repeated applications of the operator. Differentiating the velocity potential with respect to longitudinal and radial coordinates gives

$$\frac{\partial\phi}{\partial x}=F'(x)-\frac{r^2}{4}\mathcal{D}F'(x)+\frac{r^4}{64}\mathcal{D}^2F'(x)-\frac{r^6}{2304}\mathcal{D}^3F'(x)+\cdots \tag{2.10}$$

$$\frac{\partial\phi}{\partial r}=-\frac{r}{2}\mathcal{D}F(x)+\frac{r^3}{16}\mathcal{D}^2F(x)-\frac{r^5}{384}\mathcal{D}^3F(x)+\frac{r^7}{18432}\mathcal{D}^4F(x)-\cdots \tag{2.11}$$

which can be substituted into the boundary condition, equation (2.7). The boundary condition equation can be rearranged to become

$$\begin{aligned}\mathcal{D}(yF)=y''F+\frac{y^2}{2}y'\mathcal{D}F'-\frac{y^4}{32}y'\mathcal{D}^2F'+\frac{y^6}{1152}y'\mathcal{D}^3F'-\cdots\\ +\frac{y^3}{8}\mathcal{D}^2F-\frac{y^5}{192}\mathcal{D}^3F+\frac{y^7}{9216}\mathcal{D}^4F-\cdots,\end{aligned} \tag{2.12}$$

which is an ordinary differential equation of infinite order to be solved for $F(x)$. This equation is still exact. The original partial differential equation has been

[‡]The series expansion for the Bessel function is $J_0(x)=1+\sum_{n=1}^{\infty}\frac{(-1)^n}{(n!)^2}\left(\frac{x}{2}\right)^{2n}$.

exchanged for an ordinary differential equation of infinite order. The infinite order of this equation would normally be alarming, but the repeated applications of the differential operator $\mathcal{D}$ will be of rapidly diminishing influence if this technique is to be useful.

To find an approximate analytical solution, a modified "method of successive approximations" will be used.[§] The method of successive approximations assumes an approximate solution to an exact differential equation and iterates until the solution is sufficiently accurate, usually gaining one additional correct term in a power series with each integration of every iteration. An example of this method applied to a partial differential equation of the elliptic type can be found in the *Encyclopedic Dictionary of Mathematics* [140], which also includes criteria for convergence.

Rayleigh's modified method of successive approximations assumes an exact solution to an approximate differential equation and iterates until the differential equation is sufficiently accurate. This method is intuitively plausible because each iteration keeps no more terms in the differential equation than are justified by the accuracy of the current approximation to the solution.

Before an initial approximation of the differential equation is made, it may be useful to find a measure by which the problem can be scaled. This would allow the elimination of high-order terms to be justified while quantifying the range of validity for the resulting solution. Since this problem is a geometric one, it suggests that the modeling equations be regrouped in the dimensionless variable γx, where γ is the frequency-dependent wave number. Unfortunately, the solution of the problem precedes the knowledge of γ so another choice must be made. It is convenient to choose kx as the dimensionless parameter. This

[§]Also known as Picard's "iteration method," after E. Picard (1856–1941), who developed a rigorous proof for convergence [4]. See Boyce & DiPrima [134], page 72.

choice is a good one for waveguides that exhibit relatively small amounts of dispersion.¶

The velocity potential in equation (2.8) can now be rearranged as

$$\phi = F - \frac{(kr)^2}{4}DF + \frac{(kr)^4}{64}D^2F - \frac{(kr)^6}{2304}D^3F + \frac{(kr)^8}{147456}D^4F - \cdots, \quad (2.13)$$

where the linear operator D is defined as

$$D \equiv \frac{d^2(\cdot)}{d(kx)^2} + 1. \quad (2.14)$$

Equations (2.10) and (2.11) can be rewritten as

$$\frac{\partial\phi}{\partial(kx)} = F' - \frac{(kr)^2}{4}DF' + \frac{(kr)^4}{64}D^2F' - \frac{(kr)^6}{2304}D^3F' + \cdots \quad (2.15)$$

$$\frac{\partial\phi}{\partial(kr)} = -\frac{kr}{2}DF + \frac{(kr)^3}{16}D^2F - \frac{(kr)^5}{384}D^3F + \frac{(kr)^7}{18432}D^4F - \cdots \quad (2.16)$$

where the primes $(\cdot)'$ now indicate differentiation with respect to kx. The scaled equation for the boundary condition is

$$D(kyF) = (ky)''F + \frac{(ky)^2}{2}(ky)'DF' - \frac{(ky)^4}{32}(ky)'D^2F' + \frac{(ky)^6}{1152}(ky)'D^3F' - \cdots$$
$$+\frac{(ky)^3}{8}D^2F - \frac{(ky)^5}{192}D^3F + \frac{(ky)^7}{9216}D^4F - \cdots. \quad (2.17)$$

Because the derivatives in the previous equations are taken on the order of the changes with respect to kx, it is reasonable to suspect that they will remain of the same order. The convergence of equation (2.13) is very rapid for values of kr much less than unity but the series is still useful for larger values. For example, using the first two terms results in a 2% error when kr is equal to unity. Rescaling these equations does not establish convergence of this method though, because the proper scaling measure is really not known. It only suggests where the equations might be useful. The consistency of this

¶Conical horns are not dispersive in the fundamental mode of propagation but experimental evidence confirms that the exponential horn is strongly dispersive at low frequencies.

method can be checked after the velocity potential has been found by examining the relative significance of neglected terms. Because the advantage of rescaling the equations seems dubious and adds additional mathematical confusion, the original form of the system equations will be used instead.

For the first approximation of the modeling differential equation (which will be referred to as the zeroth-order approximation), all terms on the right side of equation (2.12) are neglected, because they are assumed to be small relative to the term on the left side. The resulting zeroth-order approximation

$$\mathcal{D}(yF_0) = (yF_0)'' + k^2(yF_0) = 0, \tag{2.18}$$

where the subscript identifies the order of the approximation, can be solved to yield the zeroth-order solution

$$F_0 = \frac{Ae^{-jkx} + Be^{jkx}}{y}. \tag{2.19}$$

The zeroth-order solution must now be substituted into the right side of equation (2.12) and expanded to reveal which terms must be kept and discarded for the next iteration. If the terms are not getting smaller in some manner, then the first approximation is not close enough to the truth. After neglecting "high-order" terms, solving the resulting equation will yield the first-order solution. For this purpose, it is sufficient to rewrite equation (2.18) (neglecting y'') as

$$\mathcal{D}F_0 = F_0'' + k^2F_0 = -\frac{2y'}{y}F_0' \tag{2.20}$$

which is Webster's equation, as can be seen by comparing it to equation (2.1) with $S(x) = \pi y^2(x)$. Rayleigh was interested in this equation only to the extent that it is used to expand the differential operators $\mathcal{D}$ on the right side of equation (2.12) for obtaining the first-order approximation. Examining the neglected terms reveals that equation (2.18) is only equivalent to equation (2.20) if $y'' \ll k^2y$. (If the contour were exponential, this implies $f \gg f_c$.) As a first

approximation then, Webster's equation is on the same order as equation (2.18), and can be used to expand the right side of equation (2.12).

Rayleigh might have chosen Webster's equation as a first approximation to equation (2.12), but a closed form solution to Webster's equation is not known for arbitrary contour profiles $y(x)$, which would prevent an iterative procedure in the general case.[‖] The next section covers the case of using Webster's equation as a zeroth-order approximation.

All of the terms previously neglected on the right side of equation (2.12) must be of diminishing significance or the first approximation is not consistent. This can be verified while making the second approximation. Substituting the zeroth-order solution into the right side of equation (2.12) and keeping terms of increased "order" will yield a nonhomogeneous equation that can be solved to give the first-order solution. The tediousness of this work can be lessened by noticing that the linearly independent solutions to equation (2.18) are complex conjugates. Rewrite equation (2.19) as

$$F_0 = A\frac{e^{-jkx}}{y} + B\frac{e^{jkx}}{y} = A(F_0)_+ + B(F_0)_-. \tag{2.21}$$

The linear operator $\mathcal{D}$ is commutative with complex conjugation, so only one of the solutions need be operated on, and this result added to itself after taking the complex conjugate and exchanging the constants A and B. In this manner, the expansions on the right side of equation (2.12) may be handled more efficiently. Following this approach, $\mathcal{D}$ operates on $(F_0)_+$ to give

$$\mathcal{D}(F_0)_+ = \left\{\left(\frac{1}{y}\right)'' - 2jk\left(\frac{1}{y}\right)'\right\} y(F_0)_+ \tag{2.22}$$

and differentiation with respect to x results in

$$\mathcal{D}(F_0')_+ = \left\{-3jk\left(\frac{1}{y}\right)'' - 2k^2\left(\frac{1}{y}\right)'\right\} (yF_0)_+. \tag{2.23}$$

[‖]In principle an iterative technique such as the WKB method could be used for each iteration step at the price of increasing the computations.

Operating with $\mathcal{D}$ once again on equation (2.22) shows

$$\mathcal{D}^2(F_0)_+ = -4k^2 \left(\frac{1}{y}\right)'' y(F_0)_+, \tag{2.24}$$

which results in

$$\mathcal{D}^2(F_0')_+ = 4jk^3 \left(\frac{1}{y}\right)'' y(F_0)_+ \tag{2.25}$$

after differentiation. Applying $\mathcal{D}$ once more to equation (2.24) reveals that

$$\mathcal{D}^3(F_0)_+ = 0 \quad \text{and} \quad \mathcal{D}^3(F_0')_+ = 0 \tag{2.26}$$

to the order of the present approximation. Equations (2.23)–(2.26) have been derived under the assumption that the high-order terms are a result of differentiating $(1/y)$ and that in general

$$\left(\frac{1}{y}\right)^{(n+1)} \ll k \left(\frac{1}{y}\right)^{(n)} \tag{2.27}$$

where the nth derivative is denoted by (n).

Before proceeding, the above results can be utilized to find the velocity potential by substituting them into equation (2.8) and ignoring terms of order $(1/y)''$ (relative to $k(1/y)'$) and higher (since they have already been ignored once in obtaining the first approximation) to get

$$\phi_0 = \left\{1 - j\frac{y'}{2ky}(kr)^2\right\} A(F_0)_+ + \left\{1 + j\frac{y'}{2ky}(kr)^2\right\} B(F_0)_-. \tag{2.28}$$

For plane waves to be a sufficiently accurate approximation of ϕ_0, the variation with respect to r must be small, i.e.

$$\left|j\frac{y'}{2ky}(kr)^2\right| \ll 1, \tag{2.29}$$

and this term is largest on the horn walls where $r = y(x)$ so the expression reduces to

$$\left|\frac{kyy'}{2}\right| \ll 1 \tag{2.30}$$

which is the same criterion as that derived by Pierce [176, page 360] for validity of Webster's horn equation.

After substituting equations (2.22)–(2.26) into equation (2.12), the equation reduces to the first-order approximation,

$$\begin{aligned} D(yF_1) &= y''F_0 - \frac{1}{2}(y)^2 y'' F_0'' \\ &= \left(1 + \frac{1}{2}k^2y^2\right) y''F_0 \end{aligned} \tag{2.31}$$

where F_1 is defined as the first-order solution. This equation is a linear, non-homogeneous, ordinary differential equation whose solution can be found by variation of parameters** to be

$$F_1 = \left\{ \frac{1}{-2jk} \int^x Y(A + Be^{2jkx})dx \right\} (F_0)_+ + \left\{ \frac{1}{2jk} \int^x Y(B + Ae^{-2jkx})dx \right\} (F_0)_- \tag{2.32}$$

where the function Y is defined by

$$Y \equiv \left(1 + \frac{1}{2}k^2y^2\right) \frac{y''}{y}. \tag{2.33}$$

In the throat of the horn the cross section is very small relative to a wavelength, and the slope of the horn wall is very small relative to unity, so F_0 should be a sufficiently accurate solution in this region. This allows the determination of the arbitrary constants in equation (2.32) by requiring the solution to identify with F_0 for $x \leq 0$, which gives

$$\begin{aligned} F_1 =& \left\{ A - \frac{1}{2jk} \int_0^x Y(A + Be^{2jkx})dx \right\} (F_0)_+ \\ &+ \left\{ B + \frac{1}{2jk} \int_0^x Y(B + Ae^{-2jkx})dx \right\} (F_0)_-. \end{aligned} \tag{2.34}$$

To find the velocity potential, the higher order terms in equation (2.8) may be dropped so that

$$\phi_1(x, r) = F_1 - \frac{r^2}{4}\mathcal{D}F_1 + \frac{r^4}{64}\mathcal{D}^2F_1 \tag{2.35}$$

**See Boyce & DiPrima [134], page 123.

which after expanding $\mathcal{D}F_1$ and $\mathcal{D}^2F_1$ may be written

$$\phi_1(x,r) = F_1 - \frac{r^2}{4}\left\{\mathcal{D}F_0 + YF_0\right\} + \frac{r^4}{64}\mathcal{D}^2F_0. \tag{2.36}$$

2.1.1 Conical Horn

Rayleigh's solution given in integral form can be expanded for special cases. If the horn contour is conical, $y(x) = \alpha(x + x_0)$ where α is the slope of the horn and x_0 is the distance from the origin to the vertex of the cone. The zeroth-order approximation can be found as

$$\begin{aligned}\phi_0 =&\left\{1 - \left(\frac{1}{(x+x_0)^2} + \frac{jk}{(x+x_0)}\right)\frac{r^2}{2}\right\}A\frac{e^{-jkx}}{y}\\ &+\left\{1 - \left(\frac{1}{(x+x_0)^2} - \frac{jk}{(x+x_0)}\right)\frac{r^2}{2}\right\}B\frac{e^{jkx}}{y}.\end{aligned} \tag{2.37}$$

and the second approximation is just as easily found since the conical case results in $y'' = 0$, $F_1 = F_0$ so the first-order velocity potential is

$$\begin{aligned}\phi_1 =&\left\{1 - \left(\frac{1}{(x+x_0)^2} + \frac{jk}{(x+x_0)}\right)\frac{r^2}{2} - \frac{k^2r^4}{8(x+x_0)^2}\right\}A\frac{e^{-jkx}}{y}\\ &+\left\{1 - \left(\frac{1}{(x+x_0)^2} - \frac{jk}{(x+x_0)}\right)\frac{r^2}{2} - \frac{k^2r^4}{8(x+x_0)^2}\right\}B\frac{e^{jkx}}{y}.\end{aligned} \tag{2.38}$$

These equations reveal how a plane wave at the throat of a conical horn transforms as it propagates along the horn. For $r = 0$ the solution is the same as that found by assuming plane waves inside the horn, but off-axis the wavefronts curve to maintain the proper boundary condition. Checking the previous assumptions shows that the solution is consistent if

$$k(x + x_0) \gg 1 \tag{2.39}$$

so as the horn opens at smaller angles, the vertex x_0 of the cone is increasingly distant from the origin and $k(x+x_0)$ is much greater than unity for all practical wave numbers even at the mouth of the cone. As the angle of the cone increases,

the solution is only applicable at a certain distance from the mouth of the cone. The region of applicability is also bounded by the convergence of the velocity potential. Examination of equation (2.38) shows that the solution converges if

$$\frac{(kr)^2}{k(x+x_0)} \leq 1. \tag{2.40}$$

This restricts the solution to a limited radial distance. Taken in union, equations (2.39) and (2.40) establish a region of validity of the solution between some a and b such that the solution is useful for $a \leq x \leq b$.

2.1.2 Exponential Horn

If the horn contour is exponential, $y(x) = y_0 e^{\alpha x}$ and

$$\begin{aligned} F_1 =& \left\{1 + \frac{j(\alpha x)}{2(k/\alpha)} + \frac{j(k/\alpha)}{8}\left[(y')^2 - (y_0')^2\right]\right\} A(F_0)_+ \\ &+ \left\{1 + \frac{-j(\alpha x)}{2(k/\alpha)} + \frac{-j(k/\alpha)}{8}\left[(y')^2 - (y_0')^2\right]\right\} B(F_0)_- \\ &+ \left\{\frac{-j\sin(kx)}{2(k/\alpha)^2} + \frac{-j(k/\alpha)}{8(1-j(k/\alpha))}\left[(y')^2 e^{-jkx} - (y_0')^2 e^{jkx}\right]\right\} \frac{A}{y} \\ &+ \left\{\frac{j\sin(kx)}{2(k/\alpha)^2} + \frac{j(k/\alpha)}{8(1+j(k/\alpha))}\left[(y')^2 e^{jkx} - (y_0')^2 e^{-jkx}\right]\right\} \frac{B}{y}. \end{aligned} \tag{2.41}$$

In general, the constants A and B are coupled to both e^{-jkx} and e^{jkx}, which makes it difficult to find one constant in terms of the other. In equation (2.28), each of the constants only couple to one of the two basis solutions. This is a result of the basis solution chosen for the iteration scheme. To study the solution, it will be necessary to add a boundary condition at the mouth of the horn, or to assume that no mode conversion takes place after the waves have traveled a certain distance. The boundary condition at the horn mouth is represented by the Rayleigh integral [176, page 214], but the present problem formulation precludes the effect of mode conversion at the mouth of the horn. The effect of mode conversion at the mouth of the horn is certainly not negli-

gible though, and if ignored will restrict the applicability of the present results to lower frequencies.[††]

2.2 Webster's Equation as Basis

If Rayleigh had chosen Webster's equation as the basis of the method of successive approximation, equation (2.12) would be rearranged as

$$F'' + \frac{2y'}{y}F' + k^2F = \frac{y}{2}y'\mathcal{D}F' - \frac{y^3}{32}y'\mathcal{D}^2F' + \frac{y^5}{1152}y'\mathcal{D}^3F' - \cdots + \frac{y^2}{8}\mathcal{D}^2F - \frac{y^4}{192}\mathcal{D}^3F + \frac{y^6}{9216}\mathcal{D}^4F - \cdots \quad (2.42)$$

For the first approximation of this differential equation, all terms on the right side of equation (2.42) are neglected, yielding Webster's horn equation. This equation can be solved exactly for only a few horn geometries although others may be handled sufficiently well by the WKB method. Consider the conical and exponential contours.

2.2.1 Conical Horn

The cross sectional radius for a conical horn contour is expressed by

$$y(x) = \frac{y_0}{x_0}(x + x_0) \quad (2.43)$$

or $y = \alpha X$ where $\alpha \equiv y_0/x_0$ and $X \equiv (x - x_0)$. This reduces equation (2.42) to

$$\mathcal{D}(XF) = \frac{\alpha^2X^2}{2}\mathcal{D}F' - \frac{\alpha^4X^4}{32}\mathcal{D}^2F' + \frac{\alpha^6X^6}{1152}\mathcal{D}^3F' - \cdots + \frac{\alpha^2X^3}{8}\mathcal{D}^2F - \frac{\alpha^4X^5}{192}\mathcal{D}^3F + \frac{\alpha^6X^7}{9216}\mathcal{D}^4F - \cdots \quad (2.44)$$

[††]To witness the importance of mode conversion at the mouth of a conical horn, see Hall [40].

which may be collected as

$$\mathcal{D}(XF) = \alpha^2 X^2 \left\{ \frac{\mathcal{D}F'}{2} + \frac{X\mathcal{D}^2F}{8} \right\} - \frac{\alpha^4 X^4}{4} \left\{ \frac{\mathcal{D}^2F'}{8} + \frac{X\mathcal{D}^3F}{48} \right\} + \frac{\alpha^6 X^6}{24} \left\{ \frac{\mathcal{D}^3F'}{48} + \frac{X\mathcal{D}^4F}{384} \right\} - \cdots. \tag{2.45}$$

If all terms on the right side are ignored,

$$\mathcal{D}(XF_0) = (XF_0)'' + k^2(XF_0) = 0 \tag{2.46}$$

where the subscript identifies the zeroth-order approximation. This has the solution

$$F_0 = \frac{Ae^{-jk(x-x_0)} + Be^{jk(x-x_0)}}{x - x_0}. \tag{2.47}$$

This solution *exactly* satisfies the infinite order differential equation, as can be seen by expanding and substituting into the right side of equation (2.45). Successive iteration is not necessary. As many terms of the solution can be found as desired by substituting F_0 into equation (2.8) and expanding. Both Rayleigh's method in the last section and the modified Rayleigh method in this section yield the same result for the conical horn and furthermore, this solution is the same on axis as predicted by Webster's equation.

2.2.2 Exponential Horn

An exponential horn radius is given by

$$y(x) = y_0 e^{\alpha x} \tag{2.48}$$

which, when substituted into equation (2.42), results in

$$F'' + 2\alpha F' + k^2 F = \frac{y^2}{2} \left\{ \alpha\mathcal{D}F' + \frac{1}{4}\mathcal{D}^2F \right\} - \frac{y^4}{32} \left\{ \alpha\mathcal{D}^2F' + \frac{1}{6}\mathcal{D}^3F \right\} + \frac{y^6}{1152} \left\{ \alpha\mathcal{D}^3F' + \frac{1}{8}\mathcal{D}^4F \right\} - \cdots. \tag{2.49}$$

For the zeroth-order approximation, all terms on the right side are ignored and the resulting equation can be solved for the zeroth-order solution,

$$F_0(x) = Ae^{-\lambda_1 x} + Be^{-\lambda_2 x}$$

$$= A(F_0)_+ + B(F_0)_- \tag{2.50}$$

where the λ's are given by

$$\begin{aligned} \lambda_1 &= \alpha + \sqrt{\alpha^2 - k^2} \\ \lambda_2 &= \alpha - \sqrt{\alpha^2 - k^2}. \end{aligned} \tag{2.51}$$

This is the solution of the one-dimensional Webster's equation for an exponential cross sectional area and leads to the definition of a critical quantity $k_c \equiv \alpha$, frequently referred to as the "cutoff" wave number. The definition of cutoff frequency and wave number follow in the obvious way. These are the natural definitions since the acoustic waves go from evanescent to propagating at this critical frequency.

Expanding solutions is a simple process for the present approximation. Operation on the zeroth-order solution results in

$$\begin{aligned} \mathcal{D}^n(F_0)_+ &= (2\alpha\lambda_1)^n(F_0)_+ \\ \mathcal{D}^n(F_0')_+ &= -\lambda_1(2\alpha\lambda_1)^n(F_0)_+. \end{aligned} \tag{2.52}$$

Now substituting equation (2.50) into equation (2.4), the zeroth-order approximation to the velocity potential can be expressed as

$$\phi_0 = AJ_0(\alpha r\sqrt{2\lambda_1/\alpha})(F_0)_+ + BJ_0(\alpha r\sqrt{2\lambda_2/\alpha})(F_0)_- \tag{2.53}$$

or, after expanding the Bessel series, as

$$\phi_0 = \left\{1 - \frac{\lambda_1}{2\alpha}(\alpha r)^2\right\} A(F_0)_+ + \left\{1 - \frac{\lambda_2}{2\alpha}(\alpha r)^2\right\} B(F_0)_-. \tag{2.54}$$

The ϕ_0 solution is consistent with the assumptions made in obtaining it if

$$\frac{1}{2}(y')^2 \ll 1. \tag{2.55}$$

For a plane-wave approximation to be sufficiently accurate, the variation over r must be small, i.e.

$$\left|\frac{\lambda_1}{2\alpha}(\alpha r)^2\right| \ll 1 \tag{2.56}$$

and this quantity is largest on the contour where $r = y(x)$ so

$$\left|\frac{\lambda_1 y y'}{2}\right| \ll 1 \tag{2.57}$$

where y' has been substituted for αy. Above cutoff, the magnitude of λ_1 is equal to k and the plane-wave criterion is the same as previously shown in equation (2.30). Below cutoff, the expression is more complicated and it is best to use equation (2.57) directly.

To find the first-order approximations, the methods outlined in section (2.1) can be utilized to minimize the tedious nature of the manipulations. Substituting F_0 into the right side of equation (2.49) gives

$$F_1'' + 2\alpha F_1' + k^2 F_1 = \left\{-\frac{1}{2}\lambda_1^2 (y')^2\right\} A(F_0)_+ + \left\{-\frac{1}{2}\lambda_2^2 (y')^2\right\} B(F_0)_- \tag{2.58}$$

which can be solved by the method of undetermined coefficients yielding

$$F_1 = \underbrace{A_1(F_0)_+ + B_1(F_0)_-}_{\text{homogeneous solution}} - \frac{\lambda_1^2}{8\alpha\lambda_2}(y')^2 A(F_0)_+ - \frac{\lambda_2^2}{8\alpha\lambda_1}(y')^2 B(F_0)_-. \tag{2.59}$$

If this solution is required to identify with F_0 in the throat of the horn, then the constants in the homogeneous portion of the solution can be determined such that the first-order solution is

$$F_1 = \left\{1 - \frac{\lambda_1^2}{8\alpha\lambda_2}\left[(y')^2 - (y_0')^2\right]\right\} A(F_0)_+ + \left\{1 - \frac{\lambda_2^2}{8\alpha\lambda_1}\left[(y')^2 - (y_0')^2\right]\right\} B(F_0)_-. \tag{2.60}$$

This iteration yields an additional term in the solution which qualifies the validity of the zeroth-order solution. The solution F_0 is sufficiently accurate if

$$\left|\frac{\lambda_1^2}{8\alpha\lambda_2}(y')^2\right| \ll 1. \tag{2.61}$$

Above cutoff this reduces to

$$\frac{1}{8} k y y' \ll 1, \tag{2.62}$$

which may be compared to Pierce's estimate. This shows that Webster's solution is applicable over four times the frequency range as predicted by the plane-wave criterion, if the solution is interpreted as in equation (2.54).

To examine the range of validity of the first-order solution, it is necessary to find the second order solution F_2. Substitute F_1 into the right side of equation (2.49) and keep one additional term[‡‡] to get

$$F_2'' + 2\alpha F_2' + k^2 F_2 = \left\{ -\frac{1}{2}\lambda_1^2 (y')^2 - \frac{\lambda_1^2(9\lambda_2 - 4\lambda_1)}{48\alpha}(y')^4 \right\} A(F_0)_+ \tag{2.63}$$

which can be solved to yield

$$(F_2)_+ = \left\{ 1 - \frac{1}{8}\frac{\lambda_1^2}{\alpha\lambda_2}\left[(y')^2 - (y_0')^2\right] - \frac{1}{384}\frac{\lambda_1^2(9\lambda_2 - 4\lambda_1)}{\alpha^2(\alpha + \lambda_2)}\left[(y')^4 - (y_0')^4\right] \right\} (F_0)_+ \tag{2.64}$$

where the constants of integration were determined by requiring the solution to match F_1 at the throat of the horn. The additional term in equation (2.63) must be small relative to the term kept in equation (2.58) if F_1 is to be a consistent solution. This can be restated as

$$\left(\frac{3}{8}\frac{\lambda_2}{\alpha} - \frac{1}{6}\frac{\lambda_1}{\alpha} \right) (y')^2 \ll 1. \tag{2.65}$$

The equation (2.64) above for F_2 contains an additional term which allows us to qualify the accuracy of F_1 as sufficient if

$$\left| \frac{1}{384}\frac{\lambda_1^2(9\lambda_2 - 4\lambda_1)}{\alpha^2(\alpha + \lambda_2)}(y')^4 \right| \ll 1. \tag{2.66}$$

The first approximation to the velocity potential is

$$\begin{aligned} \phi_1 = & \left\{ R_1 - \frac{1}{8}\frac{\lambda_1^2}{\alpha\lambda_2}\left[(y')^2 - (y_0')^2\right] R_2 \right\} A(F_0)_+ \\ & + \left\{ R_2 - \frac{1}{8}\frac{\lambda_2^2}{\alpha\lambda_1}\left[(y')^2 - (y_0')^2\right] R_1 \right\} B(F_0)_- \end{aligned} \tag{2.67}$$

[‡‡]It is only possible to increase the accuracy by one additional term each iteration so there is no need to expend effort by calculating meaningless terms in the series.

where R_1 and R_2 are given by

$$R_1(r) \equiv 1 - \frac{\lambda_1}{2\alpha}(\alpha r)^2 + \frac{\lambda_1^2}{16\alpha^2}(\alpha r)^4 - \cdots$$
$$R_2(r) \equiv 1 - \frac{\lambda_2}{2\alpha}(\alpha r)^2 + \frac{\lambda_2^2}{16\alpha^2}(\alpha r)^4 - \cdots. \tag{2.68}$$

In the throat of the horn where $k_c r \ll 1$, R_1 and R_2 are practically unity as can be seen by rewriting them as

$$R_1 = 1 - \frac{1}{2}\left(1 + \sqrt{1-(k/k_c)^2}\right)(k_c r)^2 + \frac{1}{16}\left(1 + \sqrt{1-(k/k_c)^2}\right)^2 (k_c r)^4$$
$$R_2 = 1 - \frac{1}{2}\left(1 - \sqrt{1-(k/k_c)^2}\right)(k_c r)^2 + \frac{1}{16}\left(1 - \sqrt{1-(k/k_c)^2}\right)^2 (k_c r)^4$$

which allows the specific acoustic impedance at the throat of the horn to be expressed as

$$\frac{z_1}{z_0} = \frac{1}{1 + \frac{1}{4}\frac{\lambda_1}{\lambda_2}(y_0')^2} \tag{2.69}$$

where z_0 is the throat impedance of the exponential horn from plane-wave theory, which is

$$z_0 = j\rho_0 c_0 \frac{k}{\lambda_1} \tag{2.70}$$
$$= j\rho_0 c_0 \left\{ \frac{f_c}{f} + \sqrt{\left(\frac{f_c}{f}\right)^2 - 1} \right\}^{-1}. \tag{2.71}$$

For all practical purposes, the throat impedance is the same at that predicted by Webster's plane-wave theory, since it has been previously assumed that the slope of the horn wall near the throat is very small. Below the cutoff frequency though, the term λ_1/λ_2 in equation (2.69) gets very large and causes an appreciable discrepancy with plane-wave theory.

The results presented in this chapter are both disappointing and interesting. It is disappointing that a more accurate expression for the throat impedance has not been found. At the same time, it is interesting that a more

accurate expression for the throat impedance has not been found. Although the present solution procedure takes into account the effect of mode conversion along the contour of the horn, the mode conversion does not result in a significant change in the impedance. This seems to indicate that Webster's equation, which was derived assuming plane waves, may be a better approximation than one might first believe.

Chapter 3

The Boundary Element Method

In this chapter a formulation of the boundary element method is developed for acoustic radiation problems, and a practical numerical algorithm which is suitable for implementation on a digital computer is described in detail. In the boundary element method, the wave equation is first combined with the boundary conditions to arrive at an integral equation, where the integration is over the surface bounding the domain of interest. Radiation problems have one surface of integration coinciding with the source geometry, and an exterior surface that is allowed to extend to infinity, forcing the contribution from that surface to vanish. Thus, radiation problems are often described as "exterior" problems, because the domain of interest is exterior to the surface of integration.

One difficulty with the boundary element method is that the integral formulation of the radiation problem is not unique. The wave numbers at which the exterior Neumann (Dirichlet) problem is not unique correspond to the wave numbers at which the associated interior Dirichlet (Neumann) problem has resonances. This has long been known and has been discussed by Lamb [38] and more recently by Schenck [107], who also presents a method of making the problem unique, which he refers to as CHIEF (combined Helmholtz integral equation formulation). Practically speaking, if the difficulty were only encountered at the discrete eigenvalues or resonance frequencies of the interior problem, then the discrete wave numbers could be avoided, but unfortunately the system matrix is ill-conditioned in the neighborhood of these wave numbers.

For a source positioned on an infinite baffle, the exterior formulation of the radiation problem can be exchanged for an interior formulation by placing a fictitious hemisphere over the source. In the region exterior to the hemisphere, the problem is posed as a hemispherical source positioned in an infinite baffle. This problem has been solved and is presented in many elementary textbooks. Only the knowledge of the pressure or normal velocity on the hemisphere is required. In the present formulation for acoustic horns, the pressure is chosen as the unknown over the entire surface of integration, which includes the hemisphere at the mouth of the horn, coincides with the walls, and makes a plane in the throat of the horn. The horn walls are assumed to be rigid, forcing the normal velocity to vanish there, while the amplitude of the normal velocity is prescribed as unity in the throat. Assuming a constant velocity over the throat area is valid if the horn is driven by a rigid piston source, or approximately valid if the acoustic wavelengths are much greater than the throat diameter.

The cornerstone of the boundary element method is the Helmholtz integral formula. Because this formula is vital to the understanding and implementation of the boundary element method, it is carefully derived, then customized for boundary element methods. The formulation is then modified to take advantage of the axisymmetric geometry and the boundary conditions.

3.1 Derivation of the Helmholtz Integral Formula

An appropriate beginning point for deriving the Helmholtz integral formula is the divergence* theorem,

$$\int_V \nabla \cdot \mathbf{F} dV = \oint_S \mathbf{F} \cdot \hat{\boldsymbol{\eta}}\, dS \tag{3.1}$$

which is only valid if the vector field $\mathbf{F}$ has C^1 continuity, meaning it is at least once differentiable in V, the domain of interest. The unit vector $\hat{\boldsymbol{\eta}}$ is normal

*Also referred to as Gauss' theorem or Ostrogradsky's theorem.

to the surface S of integration and directed out of the volume V. Now let the vector field $\mathbf{F}$ be replaced by

$$\mathbf{F} = \phi \nabla G \tag{3.2}$$

where ϕ and G are arbitrary scalar fields. Equation (3.1) can be rewritten as

$$\int_V \nabla \cdot (\phi \nabla G) dV = \oint_S (\phi \nabla G) \cdot \hat{\boldsymbol{\eta}} \, dS \tag{3.3}$$

which expands to what is commonly known as Green's first identity

$$\int_V \left[\nabla \phi \cdot \nabla G + \phi \nabla^2 G \right] dV = \oint_S \phi \frac{\partial G}{\partial \eta} dS \tag{3.4}$$

where the relation

$$\frac{\partial G}{\partial \eta} \equiv \nabla G \cdot \hat{\boldsymbol{\eta}} \tag{3.5}$$

has been defined and will be used throughout this work. Because the functions ϕ and G in equation (3.4) are arbitrary, the equation must also hold for ϕ and G interchanged,

$$\int_V \left[\nabla G \cdot \nabla \phi + G \nabla^2 \phi \right] dV = \oint_S G \frac{\partial \phi}{\partial \eta} dS. \tag{3.6}$$

Subtracting equation (3.6) from equation (3.4) results in Green's second identity (also known as Green's theorem or Green's symmetric identity),

$$\int_V \left[\phi \nabla^2 G - G \nabla^2 \phi \right] dV = \oint_S \left[\phi \frac{\partial G}{\partial \eta} - G \frac{\partial \phi}{\partial \eta} \right] dS \tag{3.7}$$

which requires that both ϕ and G be twice differentiable.

If the function ϕ satisfies the time-harmonic wave equation (the Helmholtz equation),

$$\nabla^2 \phi + k^2 \phi = 0, \tag{3.8}$$

then equation (3.7) can be rewritten as

$$\int_V \phi \left[\nabla^2 G + k^2 G \right] dV = \oint_S \left[\phi \frac{\partial G}{\partial \eta} - G \frac{\partial \phi}{\partial \eta} \right] dS. \tag{3.9}$$

If the values of ϕ and $\partial\phi/\partial\eta$ were known on the boundary surface S, and the function G satisfied the Helmholtz equation in the domain V except in a very small neighborhood V_ϵ of a particular point $\mathbf{x}_i$, then an approximate integral equation for the value of ϕ at the point $\mathbf{x}_i$ could be written as

$$\phi(\mathbf{x}_i)\int_{V_\epsilon}\left[\nabla^2 G + k^2 G\right]dV \approx \oint_S \left[\phi\frac{\partial G}{\partial\eta} - G\frac{\partial\phi}{\partial\eta}\right]dS. \tag{3.10}$$

The smaller the neighborhood V_ϵ, the less error there is in assuming that the value of the field ϕ is approximately constant over that neighborhood. A function that would allow sampling the field at a single point would be the Green's function.

Recall that the Green's function is the solution to the nonhomogeneous Helmholtz equation in three-dimensional space,

$$\nabla^2 G(\mathbf{x}|\mathbf{x}_i) + k^2 G(\mathbf{x}|\mathbf{x}_i) = -4\pi\delta(|\mathbf{x}-\mathbf{x}_i|). \tag{3.11}$$

The forcing function on the right side of equation (3.11) incorporates the Dirac delta function $\delta(|\mathbf{x}-\mathbf{x}_i|)$, which represents a volume source of unity magnitude located at the point identified by the vector $\mathbf{x}_i$. The solution of this equation is the Green's function and can be shown to be [144]

$$G(\mathbf{x}|\mathbf{x}_i) = \frac{e^{-jk|\mathbf{x}-\mathbf{x}_i|}}{|\mathbf{x}-\mathbf{x}_i|}, \tag{3.12}$$

which will often be written as

$$G(\mathbf{x}|\mathbf{x}_i) = \frac{e^{-jkR}}{R} \tag{3.13}$$

where R has been defined as

$$R \equiv |\mathbf{x}-\mathbf{x}_i|. \tag{3.14}$$

It is tempting to now assume that the function G in equation (3.9) is the free-space Green's function for the Helmholtz equation. This would allow the

neighborhood to vanish and the approximation to become exact, but the free-space Green's function does not satisfy the continuity requirements of Green's identity when $|\mathbf{x} - \mathbf{x}_i| \to 0$ and the Green's function becomes singular.[†] This

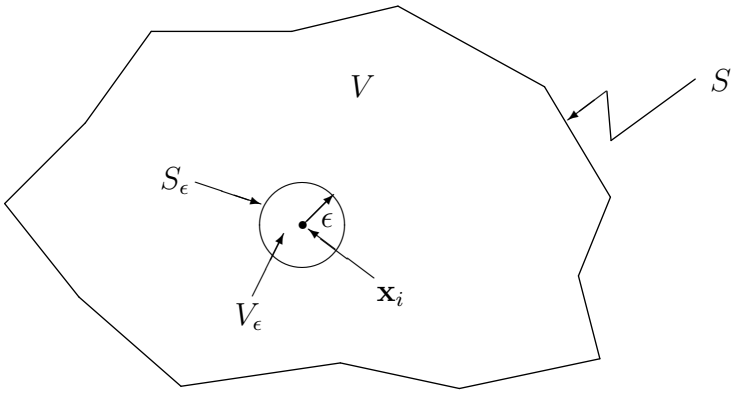

Figure 3.1: Sphere of vanishing radius ϵ used to remove the singularity at $\mathbf{x}_i$ from the domain V of integration.

difficulty can be overcome by removing the singular point from the volume V in Green's second identity. The volume V can be modified to exclude the singular point by placing a sphere of radius ϵ, surface area S_ϵ, and volume V_ϵ, about the singularity $\mathbf{x}_i$ as shown in figure 3.1. Equation (3.9) can now be written as

$$\int_{V-V_\epsilon} \phi \left[\nabla^2 G + k^2 G\right] dV = \oint_{S+S_\epsilon} \left[\phi \frac{\partial G}{\partial \eta} - G \frac{\partial \phi}{\partial \eta}\right] dS. \tag{3.15}$$

Because the Green's function G is of C^2 continuity and satisfies the homogeneous Helmholtz equation in the volume $V - V_\epsilon$, equation (3.15) can be written as

$$0 = \oint_{S+S_\epsilon} \left[\phi \frac{\partial G}{\partial \eta} - G \frac{\partial \phi}{\partial \eta}\right] dS \tag{3.16}$$

which may be further divided into integrations over the external and internal

[†]Recall that Green's identity requires that the field have C^2 continuity throughout the volume V.

surfaces,

$$0 = \oint_S \left[\phi \frac{\partial G}{\partial \eta} - G \frac{\partial \phi}{\partial \eta}\right] dS + \oint_{S_\epsilon} \phi \frac{\partial G}{\partial \eta} dS - \oint_{S_\epsilon} G \frac{\partial \phi}{\partial \eta} dS. \tag{3.17}$$

The integrations over the surface S_ϵ can be done in spherical coordinates centered about the point $\mathbf{x}_i$ such that $|\mathbf{x} - \mathbf{x}_i| = \epsilon$ and the unit normal $\hat{\boldsymbol{\eta}}$ points into the sphere so

$$\frac{\partial G}{\partial \eta} = -\frac{\partial G}{\partial \epsilon}. \tag{3.18}$$

In this spherical coordinate system the Green's function and its normal derivative can be expressed as

$$G(\mathbf{x}|\mathbf{x}_i) = \frac{e^{-jk\epsilon}}{\epsilon} \quad \text{and} \quad \frac{\partial G}{\partial \eta} = [1 + jk\epsilon] \frac{e^{-jk\epsilon}}{\epsilon^2}, \tag{3.19}$$

which are both constant over the surface for a fixed value of ϵ.

Now the magnitude of the integrals over S_ϵ in equation (3.17) can be inspected.[‡] If there is a finite positive constant K such that

$$\left|\frac{\partial \phi}{\partial \eta}\right| \leq K \tag{3.20}$$

over the surface S_ϵ, then

$$\left|\oint_{S_\epsilon} G \frac{\partial \phi}{\partial \eta} dS\right| \leq \left|\frac{e^{-jk\epsilon}}{\epsilon}\right| [K][4\pi\epsilon^2] = 4\pi K\epsilon \tag{3.21}$$

which vanishes as ϵ approaches zero so

$$\lim_{\epsilon \to 0} \oint_{S_\epsilon} G \frac{\partial \phi}{\partial \eta} dS = 0. \tag{3.22}$$

The remaining integral over S_ϵ in equation (3.17) will result in a nonzero contribution. Assume that the velocity potential ϕ is smooth in such a manner that

$$|\phi(\mathbf{x}) - \phi(\mathbf{x}_i)| \leq K\epsilon, \tag{3.23}$$

[‡]See chapter VI (especially pages 160–164) in Kellogg [28] for rigorous proofs of this kind.

and write the remaining integral as

$$\oint_{S_\epsilon} \phi \frac{\partial G}{\partial \eta} dS = \phi(\mathbf{x}_i) \oint_{S_\epsilon} \frac{\partial G}{\partial \eta} dS + \oint_{S_\epsilon} \left[\phi(\mathbf{x}) - \phi(\mathbf{x}_i)\right] \frac{\partial G}{\partial \eta} dS \tag{3.24}$$

in which the value of the velocity potential at the point $\mathbf{x}_i$ has been added and subtracted. With the results from equation (3.19) and (3.23), we obtain

$$\left| \oint_{S_\epsilon} \left[\phi(\mathbf{x}) - \phi(\mathbf{x}_i)\right] \frac{\partial G}{\partial \eta} dS \right| \leq K\epsilon \left[\frac{1 + k^2\epsilon^2}{\epsilon^2}\right] 4\pi\epsilon^2 \tag{3.25}$$

which vanishes as $\epsilon \to 0$, whereas

$$\phi(\mathbf{x}_i) \oint_{S_\epsilon} \frac{\partial G}{\partial \eta} dS = \phi(\mathbf{x}_i) \left[1 + jk\epsilon\right] \frac{e^{-jk\epsilon}}{\epsilon^2} 4\pi\epsilon^2 = 4\pi\phi(\mathbf{x}_i) \left[1 + jk\epsilon\right] e^{-jk\epsilon} \tag{3.26}$$

approaches $4\pi\phi(\mathbf{x}_i)$ as $\epsilon \to 0$ so

$$\lim_{\epsilon \to 0} \oint_{S_\epsilon} \phi(\mathbf{x}) \frac{\partial G(\mathbf{x}|\mathbf{x}_i)}{\partial \eta} dS = 4\pi\phi(\mathbf{x}_i). \tag{3.27}$$

Combining the results of equations (3.27), and (3.22), equation (3.17) can be expressed as

$$4\pi\phi(\mathbf{x}_i) = \oint_S \left[G \frac{\partial \phi}{\partial \eta} - \phi \frac{\partial G}{\partial \eta}\right] dS. \tag{3.28}$$

which is valid for any point $\mathbf{x}_i$ within the volume V. Equation (3.28) is commonly known as the Helmholtz integral theorem and is a special case ([28], page 219) of Green's third identity.

3.2 Development of the Boundary Integral Equation

To establish an equation that is expressed solely in terms of boundary values, referred to as a boundary integral equation, it is necessary to move the interior point $\mathbf{x}_i$ to the boundary surface. Because the Green's function is singular, the point cannot be moved onto the boundary without some care. The singular point can be removed from the domain of interest by defining a small sphere of

radius ϵ centered on a point located on the boundary and taking the surface of integration to be the original surface minus that which is now contained in the sphere, plus the portion of the added sphere that is contained in the domain of interest. This situation is pictured in figure 3.2. Because the point of interest

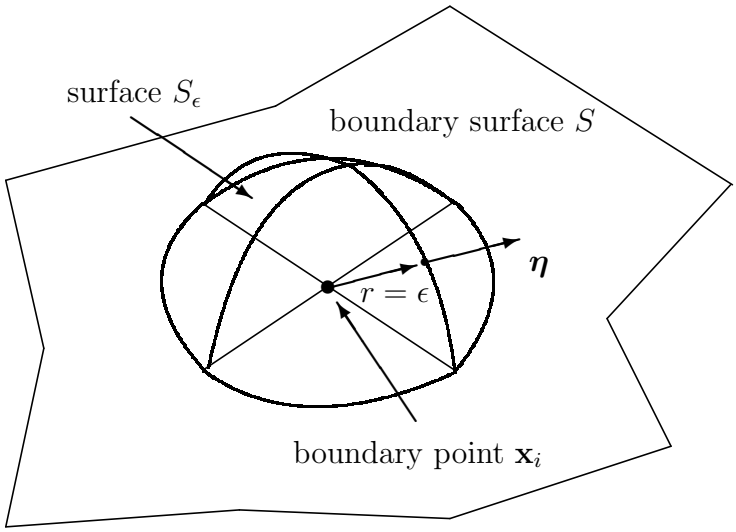

Figure 3.2: Boundary point augmented by a small hemisphere.

$\mathbf{x}_i$ is not in the volume $V - V_\epsilon$, Green's second identity (equation (3.7)) reduces to

$$0 = \oint_{S-S_\epsilon} \left[\phi \frac{\partial G}{\partial \eta} - G \frac{\partial \phi}{\partial \eta}\right] dS + \oint_{S_\epsilon} \phi \frac{\partial G}{\partial \eta} dS - \oint_{S_\epsilon} G \frac{\partial \phi}{\partial \eta} dS, \tag{3.29}$$

just as in equation (3.17), except that the surfaces of integration have been changed. The surface $S - S_\epsilon$ is the surface of the domain minus that part of the surface contained in the exclusion sphere, and the surface S_ϵ is that portion of the exclusion sphere surface contained in the domain of interest before the sphere was added. From this point onward, the analysis is identical to that already presented in the previous section except that the integration surface of the exclusion sphere is no longer $4\pi\epsilon^2$, but equal to $\Omega(\epsilon)\epsilon^2$, where $\Omega(\epsilon)$ is the solid angle contained in the original domain V and depends on the value

of ϵ. The only portion of the analysis in which this is important is the surface integration of equation (3.26), which produced a non-zero contribution. For the present analysis, it can be rewritten as

$$\phi(\mathbf{x}_i) \oint_{S_\epsilon} \frac{\partial G}{\partial \eta} dS = \phi(\mathbf{x}_i) \left[1 + jk\epsilon\right] \frac{e^{-jk\epsilon}}{\epsilon^2} \Omega(\epsilon)\epsilon^2 = \phi(\mathbf{x}_i)\Omega(\epsilon) \left[1 + jk\epsilon\right] e^{-jk\epsilon}. \tag{3.30}$$

In the limit of shrinking sphere radius, this reduces to

$$\lim_{\epsilon \to 0} \left[\phi(\mathbf{x}_i) \oint_{S_\epsilon} \frac{\partial G}{\partial \eta} dS \right] = C(\mathbf{x}_i)\phi(\mathbf{x}_i) \tag{3.31}$$

where $C(\mathbf{x}_i)$ has been defined as

$$C(\mathbf{x}_i) \equiv \lim_{\epsilon \to 0} \oint_{S_\epsilon} \frac{\partial G}{\partial \eta} dS = \lim_{\epsilon \to 0} \Omega(\epsilon) = \Omega_0. \tag{3.32}$$

Combining this result with those obtained in the previous section yields a boundary integral equation that is valid for any location of the evaluation point $\mathbf{x}_i$,

$$C(\mathbf{x}_i)\phi(\mathbf{x}_i) = \text{p.v.} \oint_S \left[G \frac{\partial \phi}{\partial \eta} - \phi \frac{\partial G}{\partial \eta} \right] dS. \tag{3.33}$$

When $\mathbf{x}_i$ is inside the volume V, $C = 4\pi$; when outside the volume V, $C = 0$; and when on the surface S, C is given by equation (3.32). If the surface is smooth, $C = 2\pi$ since the solid angle subtended by a smooth surface or half-space is 2π steradians; if the surface resembles the intersection of a wall with the floor (1/4 space), $C = \pi$, and if the intersection resembles the corner of a rectangular room, $C = \pi/2$. Because the integration over the surface S in equation (3.33) was obtained in the limit as $S_\epsilon \to 0$, it must be understood in the Cauchy principle value sense, which is denoted by 'p.v.' preceding the integral. However, the 'p.v.' notation is usually not expressed explicitly in the current literature and will not be repeatedly shown in this work unless it is felt that confusion would ensue without it.

Equation (3.33) is the most frequently used starting point for developing a numerical procedure for general geometries. This numerical procedure is

typically referred to as the boundary element method. One remaining difficulty is the practical computation of $C(\mathbf{x}_i)$. The definition of $C(\mathbf{x}_i)$ in equation (3.32) shows that the value depends on the geometry alone, but to find an efficient numerical procedure for determining the solid angle subtended by the surface in the general case of a piecewise continuous surface is a difficult geometry problem.

An alternative technique for evaluating $C(\mathbf{x}_i)$ can be found by first realizing that the derivation of the boundary integral in equation (3.33) is equally valid for Laplace's equation,

$$\nabla^2\phi = 0, \tag{3.34}$$

which is approached by the Helmholtz equation as the wave number k vanishes. The vanishing wave number does not alter any of the results previously derived. The only change that need be made is to substitute the free-space Green's function from the nonhomogeneous Laplace's equation (the Poisson equation),

$$\nabla^2 G_0(\mathbf{x}|\mathbf{x}_i) = -4\pi\delta(|\mathbf{x}-\mathbf{x}_i|), \tag{3.35}$$

which can be shown to be

$$G_0(\mathbf{x}|\mathbf{x}_i) = \frac{1}{|\mathbf{x}-\mathbf{x}_i|} = \frac{1}{R}, \tag{3.36}$$

in the place of the Helmholtz free-space Green's function $G(\mathbf{x}|\mathbf{x}_i)$. The zero subscript used above is suggestive of viewing Laplace's equation as a limiting case of the Helmholtz equation when the wave number k approaches zero. Equation (3.33) can now be written as

$$C_0(\mathbf{x}_i)\phi(\mathbf{x}_i) = \text{p.v.} \oint_S \left[G_0 \frac{\partial\phi}{\partial\eta} - \phi \frac{\partial G_0}{\partial\eta} \right] dS. \tag{3.37}$$

The coefficient $C_0(\mathbf{x}_i)$ is defined just as $C(\mathbf{x}_i)$ was in equations (3.30) and (3.32) with $k = 0$,

$$C_0(\mathbf{x}_i) \equiv \lim_{\epsilon\to 0} \oint_{S_\epsilon} \frac{\partial G_0}{\partial\eta} dS = \lim_{\epsilon\to 0} \left[\frac{1}{\epsilon^2}\Omega(\epsilon)\epsilon^2 \right] = \Omega_0. \tag{3.38}$$

It can be seen from this that $C_0(\mathbf{x}_i) = C(\mathbf{x}_i)$. It may be concluded that the singularity of the Green's function determines the value of the coefficient, and the singularity of the two Green's functions G_0 and G is of the same type. This result does not yet provide any assistance in the practical computation of $C(\mathbf{x}_i)$, but if a method can be found for computing $C_0(\mathbf{x}_i)$, then it may be used for computing $C(\mathbf{x}_i)$ as well. To this end, note that a constant potential of unity value, $\phi = 1$, is a solution of equation (3.34). The gradients of a constant potential disappear, and equation (3.37) reduces to

$$C_0(\mathbf{x}_i) = \oint_S \left[-\frac{\partial G_0}{\partial \eta} \right] dS \tag{3.39}$$

which also must be identical to $C(\mathbf{x}_i)$ by the above discussion, so the integral

$$C(\mathbf{x}_i) = -\oint_S \frac{\partial G_0}{\partial \eta} dS = -\oint_S \frac{\partial}{\partial \eta} \left[\frac{1}{R} \right] dS \tag{3.40}$$

provides a practical method of computing the value of $C(\mathbf{x}_i)$. The form of the Helmholtz integral formula that will be used for subsequent discussion is now

$$C(\mathbf{x}_i)\phi(\mathbf{x}_i) + \oint_S \phi \frac{\partial G}{\partial \eta} dS = \oint_S G \frac{\partial \phi}{\partial \eta} dS, \tag{3.41}$$

which holds for all points $\mathbf{x}_i$ on a piecewise smooth surface S bounding the domain V.

3.3 Axisymmetric Formulation

In an axisymmetric acoustic horn, the pressure and particle velocity are constant along the rotational coordinate. Because the field variables ϕ and $\partial\phi/\partial\eta$ are symmetric, the portion of the surface integration along the circumferential coordinate can be performed independently of the field values. This has been previously reported by Seybert et al. [160].

The cylindrical coordinate system and horn contour geometry are depicted in figure 3.3. The elements of differential surface area dS are obtained

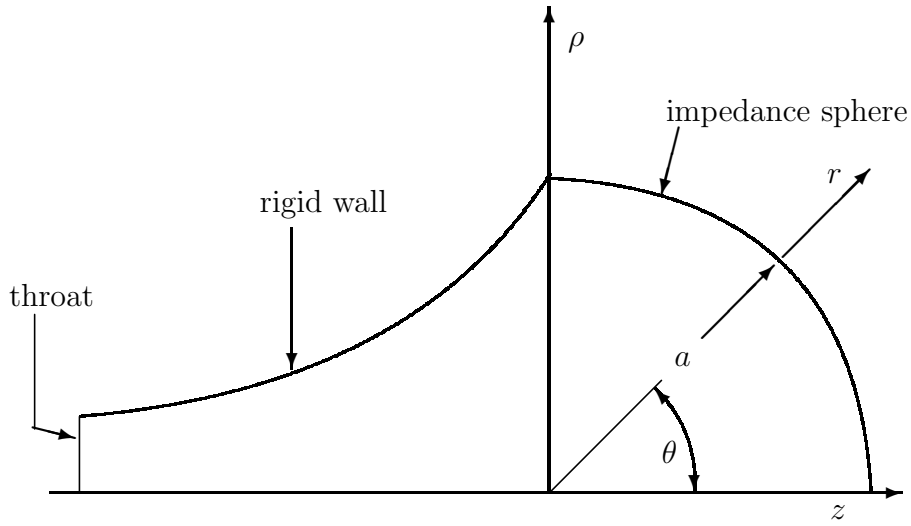

Figure 3.3: Coordinate systems defined in relation to the horn geometry. Note the cylindrical coordinates over the length of the horn and the use of spherical coordinates over the impedance sphere.

by taking a differential line segment of length dL along the contour, located at a radial distance ρ, and rotating the segment about the z axis. Letting the cylindrical angle coordinate be represented by φ, the differential area element dS is replaced by

$$dS = \rho \, d\varphi \, dL \tag{3.42}$$

which can be used to rewrite the surface integrations in equation (3.41) as

$$\oint_S \phi \frac{\partial G}{\partial \eta} dS = \int_L \phi \left[\int_0^{2\pi} \frac{\partial G}{\partial \eta} d\varphi \right] \rho dL = \int_L \phi \mathcal{B} \rho dL \tag{3.43}$$

where $\mathcal{B}$ has been defined as

$$\mathcal{B} \equiv \int_0^{2\pi} \frac{\partial G}{\partial \eta} d\varphi, \tag{3.44}$$

and

$$\oint_S G \frac{\partial \phi}{\partial \eta} dS = \int_L \frac{\partial \phi}{\partial \eta} \left[\int_0^{2\pi} G \, d\varphi \right] \rho dL = \int_L \frac{\partial \phi}{\partial \eta} \mathcal{A} \, \rho dL \tag{3.45}$$

where $\mathcal{A}$ has been defined as

$$\mathcal{A} \equiv \int_0^{2\pi} G \, d\varphi. \tag{3.46}$$

The integral $\mathcal{A}$ is of the simpler form so it will be handled first. The $1/R$ singularity in the integrand makes it difficult to numerically integrate G. A method for avoiding this difficulty is to add and subtract the singularity as follows:

$$\mathcal{A} = \int_0^{2\pi} G\, d\varphi = \int_0^{2\pi} \frac{e^{-jkR}}{R}\, d\varphi = \mathcal{A}_1 + \mathcal{A}_2 \tag{3.47}$$

where the integrals $\mathcal{A}_1$ and $\mathcal{A}_2$ have been defined as

$$\mathcal{A}_1 \equiv \int_0^{2\pi} \left[\frac{e^{-jkR} - 1}{R}\right] d\varphi \quad \text{and} \quad \mathcal{A}_2 \equiv \int_0^{2\pi} \frac{1}{R}\, d\varphi. \tag{3.48}$$

The first integral $\mathcal{A}_1$ is now nonsingular and may be integrated by an ordinary Gauss-Legendre quadrature scheme. The integral $\mathcal{A}_2$ may be evaluated by manipulating it into the form of a complete elliptic integral. Recall that

$$R \equiv |\mathbf{x} - \mathbf{x}_i| \tag{3.49}$$

which in cylindrical coordinates may be written

$$R^2 = \rho^2 + \rho_i^2 - 2\rho\rho_i \cos\varphi + [z - z_i]^2. \tag{3.50}$$

Define

$$\bar{R}^2 \equiv [\rho + \rho_i]^2 + [z - z_i]^2 \tag{3.51}$$

so that

$$R^2 = \bar{R}^2 - 2\rho\rho_i[1 + \cos\varphi]. \tag{3.52}$$

Now substitute

$$\varphi = \pi - 2\vartheta \tag{3.53}$$

and use the trigonometric property

$$\cos(\pi - 2\vartheta) = -\cos(2\vartheta) = 2\sin^2\vartheta - 1 \tag{3.54}$$

to get

$$R^2 = \bar{R}^2 \left[1 - \frac{4\rho\rho_i}{\bar{R}^2} \sin^2\vartheta\right]. \tag{3.55}$$

Now $\mathcal{A}_2$ can be written as

$$\mathcal{A}_2 = \frac{4}{\bar{R}} \int_0^{\pi/2} \frac{d\vartheta}{\sqrt{1 - p^2 \sin^2 \vartheta}} = \frac{4}{\bar{R}} K(p) \tag{3.56}$$

where

$$p^2 \equiv \frac{4\rho\rho_i}{\bar{R}^2} = \left\{ 1 - \left[\frac{R}{\bar{R}} \right]^2 \right\}_{\varphi=0} \tag{3.57}$$

has been defined as the square of the modulus of $K(p)$ which denotes the complete elliptic integral of the first kind [162, page 610]. Standard algorithms exist for accurately evaluating $K(p)$ [102, 190].

The integral $\mathcal{B}$ involves the gradient of the Green's function, which makes it slightly more involved. Just as was done with $\mathcal{A}$, first split the integral into two parts by subtracting and adding the singular portion of the integrand.

$$\mathcal{B} \equiv \int_0^{2\pi} \frac{\partial G}{\partial \eta} d\varphi = \int_0^{2\pi} \frac{\partial}{\partial \eta} \left[\frac{e^{-jkR}}{R} \right] d\varphi = \mathcal{B}_1 + \mathcal{B}_2 \tag{3.58}$$

where the integrals $\mathcal{B}_1$ and $\mathcal{B}_2$ have been defined as

$$\mathcal{B}_1 \equiv \int_0^{2\pi} \frac{\partial}{\partial \eta} \left[\frac{e^{-jkR} - 1}{R} \right] d\varphi \qquad \text{and} \qquad \mathcal{B}_2 = \int_0^{2\pi} \frac{\partial}{\partial \eta} \left[\frac{1}{R} \right] d\varphi. \tag{3.59}$$

The integral $\mathcal{B}_1$ can be expanded using the chain rule relation

$$\frac{\partial G(R)}{\partial \eta} = \frac{\partial G}{\partial R} \frac{\partial R}{\partial \eta}, \tag{3.60}$$

resulting in

$$\mathcal{B}_1 = \int_0^{2\pi} \left\{ \frac{1 - [1 + jkR] e^{-jkR}}{R^2} \right\} \frac{\partial R}{\partial \eta} d\varphi. \tag{3.61}$$

The quantity $\partial R / \partial \eta$ is finite and expressed as

$$\frac{\partial R}{\partial \eta} \equiv \nabla R \cdot \hat{\boldsymbol{\eta}} = \frac{\partial R}{\partial \rho} \eta_\rho + \frac{\partial R}{\partial z} \eta_z \tag{3.62}$$

where

$$\frac{\partial R}{\partial \rho} = \frac{\rho - \rho_i \cos \varphi}{R} \qquad \text{and} \qquad \frac{\partial R}{\partial z} = \frac{z - z_i}{R} \tag{3.63}$$

and η_ρ and η_z are the components of the unit normal $\hat{\boldsymbol{\eta}}$,

$$\hat{\boldsymbol{\eta}} = \eta_\rho \hat{\mathbf{a}}_\rho + \eta_\varphi \hat{\mathbf{a}}_\varphi + \eta_z \hat{\mathbf{a}}_z. \tag{3.64}$$

The portion of the integrand in equation (3.61) in curly brackets can now be seen to be finite as $R \to 0$ so $\mathcal{B}_1$ can be numerically integrated by the same method used to compute $\mathcal{A}_1$.

Because the unit normal to an axisymmetric surface has no $\hat{\mathbf{a}}_\varphi$ component, $\mathcal{B}_2$ can be expressed as

$$\mathcal{B}_2 = \int_0^{2\pi} \frac{\partial}{\partial \eta}\left(\frac{1}{R}\right) d\varphi = \frac{\partial}{\partial \eta}\int_0^{2\pi} \frac{1}{R} d\varphi = \frac{\partial}{\partial \eta}\left(\mathcal{A}_2\right) = \frac{\partial}{\partial \eta}\left(\frac{4}{\bar{R}} K(p)\right). \tag{3.65}$$

The quotient-rule relation,

$$\frac{\partial}{\partial \eta}\left(\frac{x}{y}\right) = \frac{1}{y^2}\left\{\frac{\partial x}{\partial \eta} y - x \frac{\partial y}{\partial \eta}\right\}, \tag{3.66}$$

and the chain-rule relation defined in equation (3.62), can be used to expand the differentiation in equation (3.65) as

$$\begin{aligned} \mathcal{B}_2 &= \frac{4}{\bar{R}^2}\left\{\bar{R}\frac{\partial K}{\partial \eta} - K\frac{\partial \bar{R}}{\partial \eta}\right\} \\ &= \frac{1}{\bar{R}}\left\{4\frac{\partial K}{\partial \eta} - \mathcal{A}_2 \frac{\partial \bar{R}}{\partial \eta}\right\}. \end{aligned} \tag{3.67}$$

The term $\partial \bar{R}/\partial \eta$ is analogous to equation (3.62) so,

$$\frac{\partial \bar{R}}{\partial \eta} \equiv \nabla \bar{R} \cdot \hat{\boldsymbol{\eta}} = \frac{\partial \bar{R}}{\partial \rho}\eta_\rho + \frac{\partial \bar{R}}{\partial z}\eta_z \tag{3.68}$$

where

$$\frac{\partial \bar{R}}{\partial \rho} = \frac{\rho + \rho_i}{\bar{R}} \qquad \text{and} \qquad \frac{\partial \bar{R}}{\partial z} = \frac{z - z_i}{\bar{R}}. \tag{3.69}$$

In a like manner,

$$\frac{\partial K}{\partial \eta} = \frac{\partial K}{\partial p}\frac{\partial p}{\partial \eta} \tag{3.70}$$

where

$$\frac{\partial p}{\partial \eta} = \frac{\partial p}{\partial \rho}\eta_\rho + \frac{\partial p}{\partial z}\eta_z, \tag{3.71}$$

and

$$\frac{\partial p}{\partial \rho} = \frac{p}{2\rho}\left[1 - \frac{2\rho}{\bar{R}}\frac{\partial \bar{R}}{\partial \rho}\right] \qquad \text{and} \qquad \frac{\partial p}{\partial z} = -\frac{p}{\bar{R}}\frac{\partial \bar{R}}{\partial z}. \tag{3.72}$$

The derivative $\partial K/\partial p$ can be further expanded [162, page 615] resulting in

$$\frac{\partial K}{\partial p} = \frac{E - q^2 K}{pq^2} \tag{3.73}$$

where

$$E(p) \equiv \int_0^{\pi/2} \sqrt{1 - p^2 \sin^2 \vartheta}\, d\vartheta \tag{3.74}$$

is the complete elliptic integral of the second kind of modulus p, and

$$q \equiv \sqrt{1 - p^2} \tag{3.75}$$

is known as the complementary modulus.

Equation (3.41) can now be written as

$$C(\mathbf{x}_i)\phi(\mathbf{x}_i) + \int_L \phi \mathcal{B} \rho dL = \int_L \frac{\partial \phi}{\partial \eta} \mathcal{A} \rho dL, \tag{3.76}$$

where from equation (3.40) and equation (3.59),

$$C(\mathbf{x}_i) = -\int_L \left[\int_0^{2\pi} \frac{\partial}{\partial \eta}\left[\frac{1}{R}\right] d\varphi\right] \rho dL = -\int_L \mathcal{B}_2 \rho dL. \tag{3.77}$$

Equation (3.77) is the desired result. Although portions of the axisymmetric integration must be implemented numerically, the problem formulation has been reduced from two-dimensional to one-dimensional.

3.4 Numerical Implementation

The Helmholtz integral formulation derived in section (3.2) was modified for axisymmetric geometries in section (3.3). In order to numerically implement the integrations in equation (3.76), the domain of integration is divided into subdomains commonly referred to as "elements" such as shown in figure 3.4.

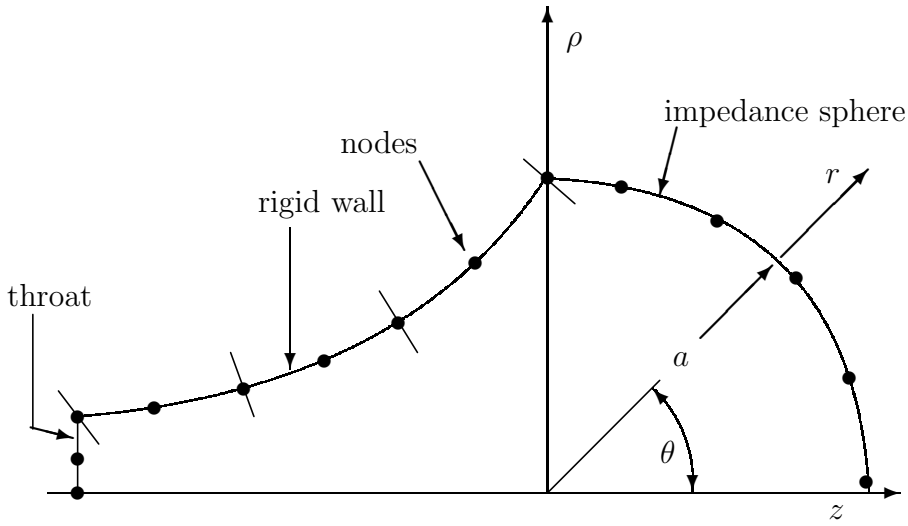

Figure 3.4: Discretization of the domain of integration.

To better approximate the curved geometries of most horns, three-noded quadratic elements are used to approximate both the surface of the throat and walls of the horn. These elements are separated by the lines passing through every second node on the horn wall and throat surfaces in figure 3.4. At the mouth of the horn, a single element is defined to be the surface of a fictitious hemisphere which will be referred to as an "impedance sphere," since an impedance relationship can be written using this surface in the external half space.

Discretizing integrals over one element at a time, equation (3.76) can now be written

$$C(\mathbf{x}_i)\phi(\mathbf{x}_i) + \sum_{m=1}^{N_\mathrm{Q}} \int_{L_m} \phi\mathcal{B}\rho dL + \int_{L_\Omega} \phi\mathcal{B}\rho dL = \sum_{m=1}^{N_\mathrm{Q}} \int_{L_m} \frac{\partial\phi}{\partial\eta}\mathcal{A}\rho dL + \int_{L_\Omega} \frac{\partial\phi}{\partial\eta}\mathcal{A}\rho dL, \tag{3.78}$$

where N_Q represents the number of quadratic elements and the added integration over L_Ω represents the impedance sphere. In the same manner, equation (3.77) can be written as

$$C(\mathbf{x}_i) = -\sum_{m=1}^{N_\mathrm{Q}} \int_{L_m} \mathcal{B}_2\rho dL - \int_{L_\Omega} \mathcal{B}_2\rho dL. \tag{3.79}$$

The integrations in the equations above are complicated by the singularity that exits as the path of integration passes through the evaluation point $\mathbf{x}_i$; for the case of quadratic elements, this occurs when $\xi = \xi_i$. This singularity is a weak singularity, so it is not necessary to evaluate the integral in a Cauchy principle value sense, but the integral will require special attention to achieve an accurate result *via* a numerical algorithm. The nature of the singularity is known and the result can be extracted analytically leaving the "well-behaved" remainder for numerical integration. The extraction process is dependent on the element type and will be included in the following sections. The quadratic elements are the more ordinary and will be handled first.

3.4.1 Quadratic Element Formulation

Both the geometry and the field variables are represented by quadratic polynomials over each element of the horn throat and wall. An example of using three-noded quadratic elements in this manner is shown in figure 3.4, where the individual elements are separated by short lines drawn through the boundary. One of these boundary elements, and the associated values of the field variable over the element, is illustrated in figure 3.5 where the three nodes of the element are enclosed by parentheses.

The variation in the field variables over a single element can be approximated by

$$\phi = \phi(\xi) = \phi_1 Q_1(\xi) + \phi_2 Q_2(\xi) + \phi_3 Q_3(\xi) \tag{3.80}$$

and

$$\frac{\partial \phi}{\partial \eta} \equiv \psi = \psi(\xi) = \psi_1 Q_1(\xi) + \psi_2 Q_2(\xi) + \psi_3 Q_3(\xi) \tag{3.81}$$

where the subscripts on the field variables are associated with the element node at which that value of the field exists, while the functions Q_1, Q_2, and Q_3 are the Lagrangian interpolation functions,

$$Q_1(\xi) \equiv \frac{1}{2}\xi[\xi - 1] = -\frac{1}{2}\xi + \frac{1}{2}\xi^2$$

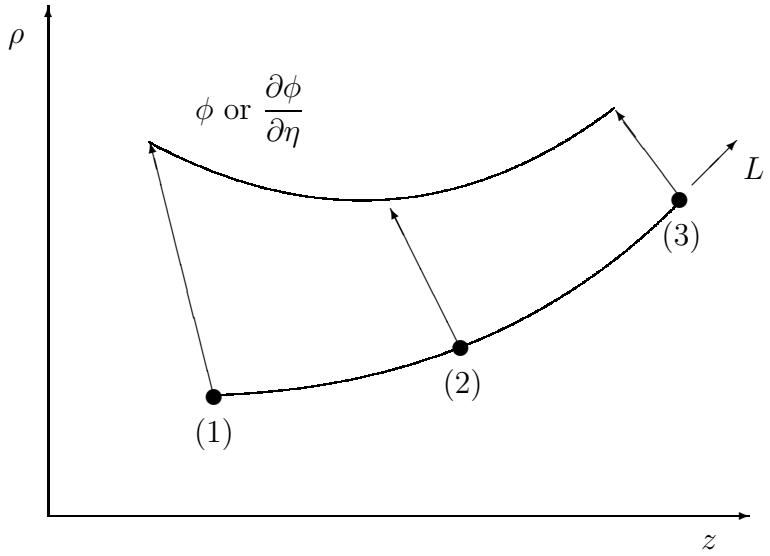

Figure 3.5: Quadratic element geometry showing the quadratic field variation over the element.

$$Q_2(\xi) \equiv [1-\xi][1+\xi] = 1-\xi^2$$
$$Q_3(\xi) \equiv \frac{1}{2}\xi[1+\xi] = \frac{1}{2}\xi + \frac{1}{2}\xi^2. \tag{3.82}$$

The three shape functions and the parameterizing variable ξ are shown graphically in figure 3.6.

Because these polynomials are equal to unity at one node and vanish at the others, the coefficients in equations (3.80) and (3.81) are identically the nodal values of the variable being interpolated.

The path of integration can be written in terms of the parameterizing coordinate ξ shown in figure 3.6 by expressing the global coordinates ρ and z as functions of the local coordinate ξ to give the coordinate mappings,

$$\rho = \rho(\xi) = \rho_1 Q_1 + \rho_2 Q_2 + \rho_3 Q_3 \tag{3.83}$$
$$= \frac{1}{2}\xi^2\left[\rho_1 - 2\rho_2 + \rho_3\right] + \frac{1}{2}\xi\left[\rho_3 - \rho_1\right] + \rho_2 \tag{3.84}$$

and

$$z = z(\xi) = z_1 Q_1 + z_2 Q_2 + z_3 Q_3 \tag{3.85}$$

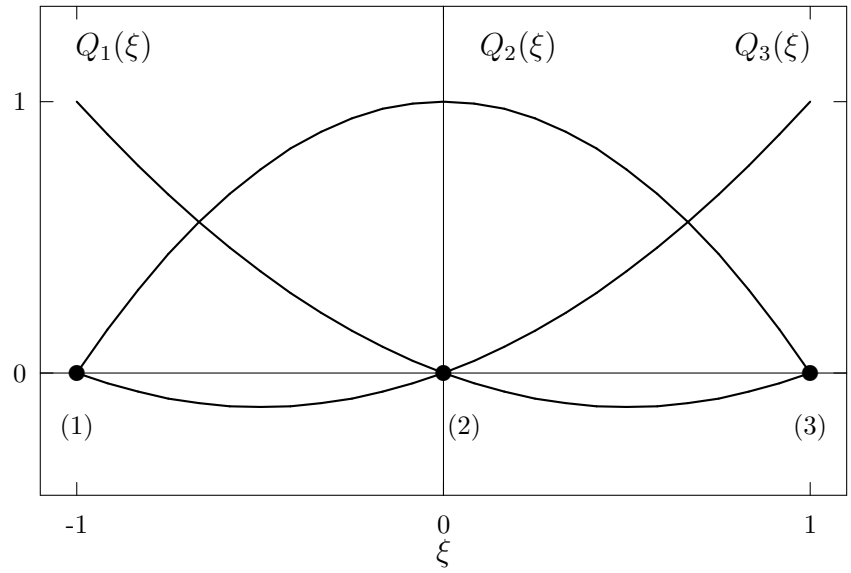

Figure 3.6: Quadratic shape functions and parameterizing variable ξ.

$$= \frac{1}{2}\xi^2 \left[z_1 - 2z_2 + z_3\right] + \frac{1}{2}\xi \left[z_3 - z_1\right] + z_2. \tag{3.86}$$

The outward normal to the contour of integration which is needed in equation (3.67) can now be found as follows. Begin by identifying the position vector for any point on a quadratic element which is shown in figure 3.7,

$$\mathbf{r} \equiv \rho(\xi)\hat{\mathbf{a}}_\rho + z(\xi)\hat{\mathbf{a}}_z \tag{3.87}$$

and the corresponding tangent vector,

$$\mathbf{r}_\mathrm{t} \equiv \frac{d\rho}{d\xi}\hat{\mathbf{a}}_\rho + \frac{dz}{d\xi}\hat{\mathbf{a}}_z \tag{3.88}$$

The outward normal vector is

$$\boldsymbol{\eta} = \hat{\mathbf{a}}_\varphi \times \mathbf{r}_\mathrm{t} = \frac{dz}{d_\xi}\hat{\mathbf{a}}_\rho - \frac{d\rho}{d_\xi}\hat{\mathbf{a}}_z \tag{3.89}$$

Normalizing this gives the outward unit normal,

$$\hat{\boldsymbol{\eta}} \equiv \frac{\boldsymbol{\eta}}{|\boldsymbol{\eta}|} = \eta_\rho\hat{\mathbf{a}}_\rho + \eta_z\hat{\mathbf{a}}_z \tag{3.90}$$

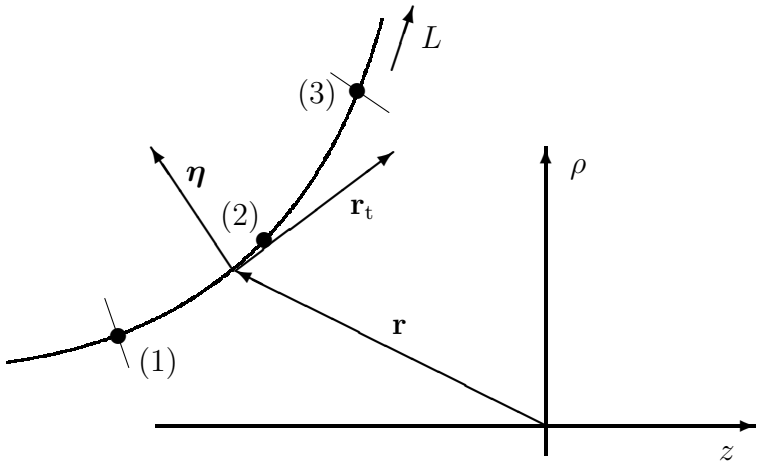

Figure 3.7: Outward normal vector for quadratic element.

where

$$\eta_\rho = \frac{dz/d\xi}{\sqrt{[d\rho/d\xi]^2 + [dz/d\xi]^2}} \qquad \text{and} \qquad \eta_z = \frac{-d\rho/d\xi}{\sqrt{[d\rho/d\xi]^2 + [dz/d\xi]^2}}. \tag{3.91}$$

Because the functions Q_1, Q_2, and Q_3 are used to approximate the geometry of the horn, they are known as "shape" functions. Because the shape functions are identical to the functions used to interpolate the field variables, the quadratic elements are referred to as "isoparametric" elements.

Using the parameterizations above, the integrals in equation (3.78) can be rewritten as

$$\int_{L_m} \phi \mathcal{B} \rho dL \Rightarrow \int_{-1}^{1} \left[\phi_1^{(m)} Q_1(\xi) + \phi_2^{(m)} Q_2(\xi) + \phi_3^{(m)} Q_3(\xi)\right] \mathcal{B} \rho J d\xi \tag{3.92}$$

where J has been introduced as the Jacobian of the transformation,

$$J \equiv \frac{dL}{d\xi} = \sqrt{\left[\frac{d\rho}{d\xi}\right]^2 + \left[\frac{dz}{d\xi}\right]^2}. \tag{3.93}$$

Because the nodal values of ϕ on element m are not a function of ξ, equation (3.92) can be rewritten as

$$\int_{L_m} \phi \mathcal{B} \rho dL \Rightarrow \sum_{\ell=1}^{3} \phi_\ell^{(m)} \mathcal{Y}_\ell^{(m)} \tag{3.94}$$

where

$$\mathcal{Y}_\ell^{(m)} \equiv \int_{-1}^{1} Q_\ell \mathcal{B} \rho J d\xi. \tag{3.95}$$

Parameterizing the remaining integrals results in

$$\int_{L_m} \psi \mathcal{A} \rho dL \Rightarrow \sum_{\ell=1}^{3} \psi_\ell^{(m)} \mathcal{X}_\ell^{(m)} \tag{3.96}$$

where $\mathcal{X}_\ell^{(m)}$ is defined as

$$\mathcal{X}_\ell^{(m)} \equiv \int_{-1}^{1} Q_\ell \mathcal{A} \rho J d\xi, \tag{3.97}$$

and

$$\int_{L_m} \mathcal{B}_2 \rho dL \Rightarrow C_i^{(m)}. \tag{3.98}$$

Summing these results over every quadratic element making up the horn throat and wall gives

$$\int_{L_\mathrm{Q}} \phi \mathcal{B} \rho dL \Rightarrow \sum_{m=1}^{N_\mathrm{Q}} \sum_{\ell=1}^{3} \phi_\ell^{(m)} \mathcal{Y}_\ell^{(m)}, \tag{3.99}$$

$$\int_{L_\mathrm{Q}} \psi \mathcal{A} \rho dL \Rightarrow \sum_{m=1}^{N_\mathrm{Q}} \sum_{\ell=1}^{3} \psi_\ell^{(m)} \mathcal{X}_\ell^{(m)}, \tag{3.100}$$

and

$$C_i^\mathrm{Q} = \sum_{m=1}^{N_\mathrm{Q}} C_i^{(m)}. \tag{3.101}$$

Each element node has a unique potential value so equation (3.99) requires assembly because adjacent element nodes are shared, as can be seen from figures 3.4 and 3.5. Expanding equation (3.99) gives

$$\begin{aligned} \sum_{m=1}^{N_\mathrm{Q}} \sum_{\ell=1}^{3} \phi_\ell^{(m)} \mathcal{Y}_\ell^{(m)} = \ldots &+ \phi_3^{(m-1)} \mathcal{Y}_3^{(m-1)} \\ &+ \phi_1^{(m)} \mathcal{Y}_1^{(m)} + \phi_2^{(m)} \mathcal{Y}_2^{(m)} + \phi_3^{(m)} \mathcal{Y}_3^{(m)} \\ &+ \phi_1^{(m+1)} \mathcal{Y}_1^{(m+1)} + \ldots \end{aligned} \tag{3.102}$$

where the integral associated with node (1) of the current element must be added to the integral associated with node (3) of the previous element. The

normal flux ψ must be allowed to be unique for each node since it is desirable to have discontinuities such as in corners or when the edge of a velocity source joins with a baffle. After assembly,

$$\int_{L_Q} \phi \mathcal{B} \rho dL \Rightarrow \sum_{n=1}^{2N_Q+1} Y_n \phi_n \tag{3.103}$$

$$\int_{L_Q} \psi \mathcal{A} \rho dL \Rightarrow \sum_{n=1}^{3N_Q} X_n \psi_n \tag{3.104}$$

where only one value of potential ϕ_n has been written for each global node n and Y_n represents the appropriate sum of the coefficients in equation (3.102). The integration over the flux in equation (3.100) was rewritten only with a change in indexing notation.

3.4.2 Singularity on the Quadratic Elements

As mentioned previously in this section, the integrands in equations (3.99) and (3.100) contain a singularity as the path of integration passes through the evaluation point $\mathbf{x}_i$. The singularity is a weak singularity so the values of the integrals exist and are unique, but need to be handled explicitly during numerical evaluation.

Begin with equation (3.97) and expand it to show

$$\mathcal{X}_\ell^{(m)} \equiv \int_{-1}^{1} Q_\ell \left[\mathcal{A}_1 + \mathcal{A}_2\right] \rho J d\xi. \tag{3.105}$$

The quantity $\mathcal{A}_1$ remains finite but $\mathcal{A}_2$ does not as the variable ξ of integration maps $\mathbf{x}$ through the point $\mathbf{x}_i$. The portion of the integral that needs special treatment can be written after referring to equation (3.56) as

$$\int_{-1}^{1} Q_\ell \mathcal{A}_2 \rho J d\xi = \int_{-1}^{1} Q_\ell \frac{4}{\bar{R}} K(p) \rho J d\xi = \int_{-1}^{1} \Gamma K(p) d\xi \tag{3.106}$$

where Γ has been defined as

$$\Gamma \equiv \frac{4}{\bar{R}} Q_\ell \rho J. \tag{3.107}$$

The behavior of the complete elliptic integral can be deduced from series expansions but it is known ([162], page 610) that

$$1.57 \approx \frac{\pi}{2} \geq K(p) + \log(q) \geq \log(4) \approx 1.39 \tag{3.108}$$

so rewrite the singular integral in equation (3.106) as

$$\int_{-1}^{1} \Gamma K(p) d\xi = \int_{-1}^{1} \left\{ \Gamma K(p) + \Gamma_i \log(q) \right\} d\xi - \Gamma_i \int_{-1}^{1} \log(q) d\xi \tag{3.109}$$

where Γ_i is defined as

$$\Gamma_i \equiv \lim_{\xi \to \xi_i} \Gamma(\xi) = 2 Q_\ell(\xi_i) J_i. \tag{3.110}$$

The first portion of this integral remains finite but the logarithmic portion does not so it must be evaluated analytically. To do this, the coordinates must be transformed so that the integral to evaluate is of the known form

$$\int_0^y \log(x) dx = y \left[\log(y) - 1 \right]. \tag{3.111}$$

To this end, introduce the Jacobian of transformation,

$$T \equiv \frac{d\xi}{dq} \tag{3.112}$$

which must be further investigated for vanishing points. Looking back to equations (3.57) and (3.75), it can be seen that

$$q = \frac{R}{\bar{R}} \tag{3.113}$$

where since the points $\mathbf{x}$ and $\mathbf{x}_i$ are in the same plane, $\varphi = 0$ resulting in

$$R^2 = [\rho - \rho_i]^2 + [z - z_i]^2 \tag{3.114}$$

and as before,

$$\bar{R}^2 = [\rho + \rho_i]^2 + [z - z_i]^2. \tag{3.115}$$

It can be seen from the above equations that q is always positive with the exception of when it vanishes at $\xi = \xi_i$, the value of ξ at which $\mathbf{x} = \mathbf{x}_i$.

The fact that q is always positive but vanishes necessitates a sign change in the Jacobian of transformation, which can be written

$$\frac{d\xi}{dq} = \frac{\bar{R}^2}{R'\bar{R} - R\bar{R}'} \tag{3.116}$$

where $\bar{R}'$ is

$$\bar{R}' = \frac{[\rho + \rho_i]\rho' + [z - z_i]z'}{\bar{R}} \tag{3.117}$$

and

$$R' = \frac{[\rho - \rho_i]\rho' + [z - z_i]z'}{R}. \tag{3.118}$$

The change in sign of the Jacobian requires that the logarithmic portion of the integration in equation (3.109) be split into the two intervals,

$$\int_{-1}^{1} \log(q) d\xi = \int_{q(-1)}^{q(\xi_i)=0} \log(q) T dq + \int_{q(\xi_i)=0}^{q(1)} \log(q) T dq. \tag{3.119}$$

Begin with the integration over the interval $-1 \leq \xi \leq \xi_i$ and rewrite it as

$$\int_{q(-1)}^{0} \log(q) T dq = \int_{q(-1)}^{0} \log(q)[T - T_{i-}] dq + T_{i-} \int_{q(-1)}^{0} \log(q) dq. \tag{3.120}$$

where T_{i-} has been defined as the value of the Jacobian at the singular point when approached from the left side. The first portion of the integration is now non-singular and can be transformed back into the ξ domain, while the second portion is the known form given previously in equation (3.111). Rewriting after these incorporations gives

$$\int_{q(-1)}^{0} \log(q) T dq = \int_{-1}^{\xi_i} \log(q) \left[1 - \frac{T_{i-}}{T}\right] d\xi - T_{i-} q(-1) \left\{\log q(-1) - 1\right\}. \tag{3.121}$$

In an analogous manner, the second integration over interval $\xi_i \leq \xi \leq 1$ in equation (3.119) can be written

$$\int_{0}^{q(1)} \log(q) T dq = \int_{\xi_i}^{1} \log(q) \left[1 - \frac{T_{i+}}{T}\right] d\xi + T_{i+} q(1) \left\{\log q(1) - 1\right\}. \tag{3.122}$$

The above equations require the limiting value of the Jacobian T when approached from the left and right side of the singularity. Begin with

$$\frac{1}{T_i} = \lim_{\xi \to \xi_i} \frac{dq}{d\xi} \tag{3.123}$$

where from equation (3.116),

$$\frac{dq}{d\xi} = \frac{R'}{\bar{R}} - \frac{R\bar{R}'}{\bar{R}^2}. \tag{3.124}$$

It can be seen after referring to equation (3.114), (3.115), and (3.117) that the second term of equation (3.124) vanishes as $\xi \to \xi_i$, but the first term needs manipulation before the limiting process gives a useful result. The limit of the denominator is

$$\lim_{\xi \to \xi_i} \bar{R} = 2\rho_i \tag{3.125}$$

but the numerator R' is indeterminant. As expressed in equation (3.118)

$$R' = \frac{[\rho - \rho_i]\rho' + [z - z_i]z'}{\sqrt{[\rho - \rho_i]^2 + [z - z_i]^2}}. \tag{3.126}$$

which can be written as

$$R' = \operatorname{sgn}(\xi - \xi_i) \frac{\left[\dfrac{\rho - \rho_i}{\xi - \xi_i}\right] \rho' + \left[\dfrac{z - z_i}{\xi - \xi_i}\right] z'}{\sqrt{\left[\dfrac{\rho - \rho_i}{\xi - \xi_i}\right]^2 + \left[\dfrac{z - z_i}{\xi - \xi_i}\right]^2}}. \tag{3.127}$$

As $\xi \to \xi_i$ the fractions become differentiation with respect to ξ, revealing that

$$\lim_{\xi \to \xi_i} R' = \begin{cases} -\sqrt{[\rho_i']^2 + [z_i']^2}, & \text{for } \xi \to \xi_{i-} \text{ and} \quad (3.128a) \\ \sqrt{[\rho_i']^2 + [z_i']^2}, & \text{for } \xi \to \xi_{i+}. \quad (3.128b) \end{cases}$$

Combining this with equation (3.125) gives the desired result,

$$T_{i+} = -T_{i-} = \frac{2\rho_i}{J_i} \tag{3.129}$$

where J_i is the Jacobian from equation (3.93) evaluated at ξ_i. Now equation (3.121) can be written as

$$\int_{-1}^{\xi_i} \log(q) \left[1 - \frac{T_{i+}}{|T|}\right] d\xi + T_{i+} q(-1) \left\{\log q(-1) - 1\right\} \tag{3.130}$$

where the absolute value of the Jacobian was taken since $T = -|T|$ over this interval. Combining this with equation (3.122) gives

$$\int_{-1}^{1} \log(q) d\xi = \int_{-1}^{1} \log(q) \left[1 - \frac{T_{i+}}{|T|}\right] d\xi + T_{i+} \left\{ \begin{array}{c} \text{singularity} \\ \text{extraction} \end{array} \right\}_{\text{Q}} \tag{3.131}$$

where

$$\left\{ \begin{array}{c} \text{singularity} \\ \text{extraction} \end{array} \right\}_{\text{Q}} \equiv \begin{cases} q(1) \left\{\log q(1) - 1\right\}, & \text{for } \xi_i = -1, \\ q(1) \left\{\log q(1) - 1\right\} + & \\ q(-1) \left\{\log q(-1) - 1\right\}, & \text{for } -1 \leq \xi_i \leq 1, \text{ and} \\ q(-1) \left\{\log q(-1) - 1\right\}, & \text{for } \xi_i = 1. \end{cases}$$

The complete solution can now be written by rejoining equation (3.131) with equation (3.109), resulting in

$$\int_{-1}^{1} \Gamma K(p) d\xi = \int_{-1}^{1} \left\{ \Gamma K(p) + \frac{\Gamma_i T_{i+}}{|T|} \log(q) \right\} d\xi - \Gamma_i T_{i+} \left\{ \begin{array}{c} \text{singularity} \\ \text{extraction} \end{array} \right\}_{\text{Q}}. \tag{3.132}$$

The desired integral yielding the value of $\mathcal{X}_\ell^{(m)}$ can be summarized by combining the above results with equation (3.105) to give

$$\mathcal{X}_\ell^{(m)} = \int_{-1}^{1} \left\{ Q_\ell \left[\mathcal{A}_1 + \mathcal{A}_2\right] \rho J + \frac{\Gamma_i T_{i+}}{|T|} \log(q) \right\} d\xi - \Gamma_i T_{i+} \left\{ \begin{array}{c} \text{singularity} \\ \text{extraction} \end{array} \right\}_{\text{Q}}. \tag{3.133}$$

Using this formulation relaxes the requirements for the numerical integration procedure when the evaluation point $\mathbf{x}_i$ lies on element (m).

There is one remaining singularity in the integral of equation (3.95) which needs special attention. Expand it as

$$\mathcal{Y}_\ell^{(m)} \equiv \int_{-1}^{1} Q_\ell [\mathcal{B}_1 + \mathcal{B}_2] \rho J d\xi. \tag{3.134}$$

The quantity $\mathcal{B}_1$ remains finite but $\mathcal{B}_2$ does not as $\xi \to \xi_i$. The nature of the singularity can be seen by returning to equation (3.67). The first term can be shown to be finite by expanding in a power series about $\xi = \xi_i$, while the second term can be written proportional to $\mathcal{A}_2$, which is a type of singularity that has already been extracted. Using equation (3.67), the part of equation (3.134) that needs further attention can be written

$$\begin{aligned}\int_{-1}^{1} Q_\ell \mathcal{B}_2 \rho J d\xi &= \int_{-1}^{1} Q_\ell \frac{4}{\bar{R}} \left\{ \frac{\partial K}{\partial \eta} - \frac{K}{\bar{R}} \frac{\partial \bar{R}}{\partial \eta} \right\} \rho J d\xi \\ &= \int_{-1}^{1} Q_\ell \frac{4}{\bar{R}} \frac{\partial K}{\partial \eta} \rho J d\xi - \int_{-1}^{1} \Lambda K(p) d\xi \end{aligned} \tag{3.135}$$

where

$$\Lambda \equiv Q_\ell \frac{4}{\bar{R}^2} \frac{\partial \bar{R}}{\partial \eta} \rho J. \tag{3.136}$$

The integral containing the singularity,

$$\int_{-1}^{1} \Lambda K(p) d\xi, \tag{3.137}$$

is of identical form to the previous result in equation (3.132). That result can be used to evaluate equation (3.137) simply by replacing Γ with Λ as defined in equation (3.136).

The complete integral yielding $\mathcal{Y}_\ell^{(m)}$ can now be summarized by combining the results above with equation (3.134) to give:

$$\mathcal{Y}_\ell^{(m)} = \int_{-1}^{1} \left\{ Q_\ell \left[\mathcal{B}_1 + \mathcal{B}_2 \right] \rho J - \frac{\Lambda_i T_{i+}}{|T|} \log(q) \right\} d\xi + \Lambda_i T_{i+} \left\{ \begin{array}{c} \text{singularity} \\ \text{extraction} \end{array} \right\}_{\text{Q}} \tag{3.138}$$

which must be used when element (m) contains the evaluation point $\mathbf{x}_i$ if accurate numerical integration is to be achieved. Because of the close relationship of $C(\mathbf{x}_i)$ to $\mathcal{Y}_\ell^{(m)}$, the above result can be used to express equation (3.98) as

$$C_i^{(m)} = \int_{-1}^{1} \left\{ \mathcal{B}_2 \rho J - \frac{\Lambda_i^\star T_{i+}}{|T|} \log(q) \right\} d\xi + \Lambda_i^\star T_{i+} \left\{ \begin{array}{c} \text{singularity} \\ \text{extraction} \end{array} \right\}_{\text{Q}} \tag{3.139}$$

where

$$\Lambda^\star \equiv \frac{4}{\bar{R}^2}\frac{\partial \bar{R}}{\partial \eta}\rho J \tag{3.140}$$

and $\Lambda_i^\star$ represents the value of $\Lambda^\star$ as $\xi \to \xi_i$.

3.4.3 Hemispherical Element Formulation

In the previous sections, the integrations over the horn wall and throat were subdivided into small domains over which the potential and flux were assumed to vary in a quadratic manner. The integration over the impedance sphere will be handled in a similar manner, but instead of using quadratic polynomials as interpolation functions over small, three-noded elements, the impedance sphere expands the acoustic field as a sum of Legendre polynomials on the spherical surface. Each term in this series is equivalent to a 'node' on the quadratic elements.

The parameterization of the circular contour at the mouth follows from reference to figure 3.4. The variable θ "sweeps out" the contour as θ ranges from $0 \to \pi/2$. The transformation between the spherical surface and the cylindrical coordinate values is given by

$$\rho = a\sin\theta \qquad \text{and} \qquad z = a\cos\theta. \tag{3.141}$$

The position vector $\mathbf{r}$ is also the normal vector on the impedance sphere so that the unit normal vector can be written

$$\hat{\boldsymbol{\eta}} \equiv \frac{\mathbf{r}}{|\mathbf{r}|} = \eta_\rho \hat{\mathbf{a}}_\rho + \eta_z \hat{\mathbf{a}}_z \tag{3.142}$$

where

$$\eta_\rho = \sin\theta \qquad \text{and} \qquad \eta_z = \cos\theta. \tag{3.143}$$

This impedance sphere separates the problem into two regions. The boundary element formulation of the horn can now be formulated as an "interior" problem, while in the half-space outside the impedance sphere the formulation is a "radiation" type problem. In the half-space exterior to the impedance

sphere, the problem is the same as that of a hemispherical source mounted in a rigid baffle, which has been solved analytically. This type of formulation has a distinct advantage over more traditional radiation-type formulations. In boundary elements, the radiation formulation is singular at the frequencies that correspond to the eigenfrequencies of the radiating body. This result is not physical, but a numerical side-effect of the formulation [107]. The interior formulation does not suffer from this singularity problem.

Modeling a source as an axisymmetric hemisphere in an infinite baffle, the potential in the external half-space can be written ([144], page 319)

$$\phi(r,\theta) = \sum_{n=0}^{\infty} D_n h_{2n}^{(2)}(kr) P_{2n}(\cos\theta), \tag{3.144}$$

where $h_{2n}^{(2)}(kr)$ are the spherical Hankel functions of the second kind of order $2n$ which correspond to outgoing radiation, $P_{2n}(\cos\theta)$ are Legendre polynomials of order $2n$, and D_n is a coefficient in the series. The superscript (2) in the Hankel functions will be implicitly assumed hereafter.

The flux in the radial direction can be found by differentiating equation (3.144) to get

$$\psi(r,\theta) = \frac{\partial \phi}{\partial r} = \sum_{n=0}^{\infty} D_n k\, h_{2n}'(kr) P_{2n}(\cos\theta) \tag{3.145}$$

where the prime $(\cdot)'$ denotes differentiation with respect to the argument. The number of terms in the infinite series representation of the potential must be truncated to a finite number N_Ω which can be chosen according to the free-space wavelengths excited by the velocity source.

Using equations (3.144) and (3.145), expand the potential and flux in equation (3.78) to give

$$\int_{L_\Omega} \phi \mathcal{B} \rho dL \Rightarrow \int_0^{\pi/2} \left[\sum_{n=0}^{N_\Omega - 1} D_n h_{2n}(ka) P_{2n}(\cos\theta) \right] \mathcal{B} \rho a d\theta$$

$$= \sum_{n=0}^{N_\Omega - 1} D_n h_{2n}(ka) \int_0^{\pi/2} P_{2n}(\cos\theta) \mathcal{B} \rho a d\theta$$
$$= \sum_{n=0}^{N_\Omega - 1} D_n \bar{Y}_n \tag{3.146}$$

where L_Ω denotes integration over the impedance sphere, and

$$\bar{Y}_n \equiv h_{2n}(ka) \int_0^{\pi/2} P_{2n}(\cos\theta) \mathcal{B} \rho a d\theta. \tag{3.147}$$

From the above it follows to define

$$C_i^\Omega \equiv \int_0^{\pi/2} \mathcal{B}_2 \rho a d\theta \tag{3.148}$$

as the fraction of C_i resulting from the integration over the hemispherical surface.

In a similar manner to that used to generate equation (3.146), the integration over the normal flux in equation (3.78) can be written

$$\int_{L_\Omega} \psi \mathcal{A} \rho dL \Rightarrow \int_0^{\pi/2} \left[\sum_{n=0}^{N_\Omega - 1} D_n k h'_{2n}(ka) P_{2n}(\cos\theta) \right] \mathcal{A} \rho a d\theta$$
$$= \sum_{n=0}^{N_\Omega - 1} D_n k h'_{2n}(ka) \int_0^{\pi/2} P_{2n}(\cos\theta) \mathcal{A} \rho a d\theta$$
$$= \sum_{n=0}^{N_\Omega - 1} D_n \bar{X}_n \tag{3.149}$$

where

$$\bar{X}_n \equiv k h'_{2n}(ka) \int_0^{\pi/2} P_{2n}(\cos\theta) \mathcal{A} \rho a d\theta. \tag{3.150}$$

3.4.4 Singularity on the Impedance Sphere

Although the form of equations (3.149) and (3.150) is slightly different from equations (3.103) and (3.104) due to different parameterizing variables, the same kind of singularity occurs in both formulations. During numerical integration, the singularity must be given special attention. For quadratic elements

it has been removed analytically in a previous section. This section follows a similar procedure to remove the singularity occurring when integrating over the hemispherical element. The first singularity can be exposed by expanding equation (3.150) to show

$$\bar{X}_n = kh'_{2n}(ka)\int_0^{\pi/2} P_{2n}(\cos\theta)\mathcal{A}\rho a d\theta = kh'_{2n}(ka)\int_0^{\pi/2} P_{2n}(\cos\theta)[\mathcal{A}_1+\mathcal{A}_2]\rho a d\theta \tag{3.151}$$

As stated before in the section on the quadratic singularity removal, $\mathcal{A}_1$ remains finite, but $\mathcal{A}_2$ is undefined when the path of integration passes through the evaluation point $\mathbf{x}_i$. Write the portion of the integration requiring further attention as

$$\int_0^{\pi/2} P_{2n}(\cos\theta)\mathcal{A}_2\rho a d\theta = \int_0^{\pi/2} P_{2n}(\cos\theta)\frac{4}{\bar{R}}K(p)\rho a d\theta = \int_0^{\pi/2}\Theta K(p)d\theta \tag{3.152}$$

where

$$\Theta \equiv \frac{4}{\bar{R}}P_{2n}(\cos\theta)\rho a. \tag{3.153}$$

The various required quantities can be expressed in spherical coordinates as

$$\left[\frac{R}{a}\right]^2 = 2[1-\cos(\theta-\theta_i)], \qquad \left[\frac{\bar{R}}{a}\right]^2 = 2[1-\cos(\theta+\theta_i)], \tag{3.154}$$

$$p^2 = \frac{2\sin\theta\sin\theta_i}{1-\cos(\theta+\theta_i)}, \qquad \text{and} \qquad q^2 = \frac{1-\cos(\theta-\theta_i)}{1-\cos(\theta+\theta_i)}. \tag{3.155}$$

Write equation (3.152) as

$$\int_0^{\pi/2}\Theta K(p)d\theta = \int_0^{\pi/2}\left[\Theta K(p)+\Theta_i\log(q)\right]d\theta - \Theta_i\int_0^{\pi/2}\log(q)d\theta \tag{3.156}$$

where

$$\Theta_i = \lim_{\theta\to\theta_i}\Theta(\theta) = 2aP_{2n}(\cos\theta_i). \tag{3.157}$$

The integrand of equation (3.156) is now finite, and the singularity has been moved to the second integral, which must be transformed to a coordinate system in the variable q for removal. To accomplish this, introduce[§] the Jacobian of transformation,

$$\bar{T} \equiv \frac{d\theta}{dq} = \frac{q[1-\cos(\theta+\theta_i)]^2}{\sin\theta_i[\cos\theta_i - \cos\theta]} = \frac{\sqrt{[1-\cos(\theta-\theta_i)][1-\cos(\theta+\theta_i)]^3}}{\sin\theta_i[\cos\theta_i - \cos\theta]}. \quad (3.158)$$

Since the Jacobian $\bar{T}$ changes sign as θ crosses θ_i, it is necessary to split the singular integral in equation (3.156) over two intervals as

$$\int_0^{\pi/2} \log(q)d\theta = \int_{q(0)=1}^{q(\theta_i)=0} \log(q)\bar{T}dq + \int_{q(\theta_i)=0}^{q(\pi/2)} \log(q)\bar{T}dq. \quad (3.159)$$

The final extraction can be accomplished by expanding this as

$$\int_0^{\pi/2} \log(q)d\theta = \int_1^0 \log(q)[\bar{T} - \bar{T}_{i-}]dq + \bar{T}_{i-}\underbrace{\int_1^0 \log(q)dq}_{1} \quad (3.160)$$

$$+ \int_0^{q(\pi/2)} \log(q)[\bar{T} - \bar{T}_{i+}]dq + \bar{T}_{i+}\underbrace{\int_0^{q(\pi/2)} \log(q)dq}_{q(\pi/2)[\log q(\pi/2)-1]} \quad (3.161)$$

where the rightmost integrals are known, as expressed in equation (3.111), while the others are nonsingular and can be returned to the θ domain for integration. Using the inverse of the Jacobian to return yields

$$\int_0^{\pi/2} \log(q)d\theta = \int_0^{\theta_i} \log(q)\left[1 - \frac{\bar{T}_{i-}}{\bar{T}}\right]d\theta + \bar{T}_{i-}$$

$$+ \int_{\theta_i}^{\pi/2} \log(q)\left[1 - \frac{\bar{T}_{i+}}{\bar{T}}\right]d\theta + \bar{T}_{i+}q(\pi/2)\left[\log q(\pi/2) - 1\right]. \quad (3.162)$$

The behavior of the Jacobian approaching the singularity is needed to further combine the above results. To do this, write q as a function that can be expanded in a series about zero. Define

$$\delta \equiv \theta - \theta_i \quad (3.163)$$

[§]For the sake of computational efficiency, the Jacobian can be expressed as $\bar{T} = \bar{R}^2/\left[R'\bar{R} - R\bar{R}'\right]$.

and rewrite equation (3.155) as

$$q = \sqrt{\frac{1-\cos\delta}{1-\cos(\delta+2\theta_i)}}. \tag{3.164}$$

Expanding the numerator in a power series for cosine yields

$$q = \sqrt{\frac{1-[1-\delta^2/2+\ldots]}{1-\cos(\delta+2\theta_i)}}, \tag{3.165}$$

which approaches

$$q = \sqrt{\frac{\delta^2/2-\ldots}{1-\cos(\delta+2\theta_i)}} = \frac{\delta}{\sqrt{2[1-\cos(2\theta_i)]}}+\ldots \tag{3.166}$$

as δ tends towards zero. This first term in the series expansion is the desired result (note that $dq/d\theta = dq/d\delta$),

$$\bar{T}_{i+} = -\bar{T}_{i-} = \sqrt{2[1-\cos(2\theta_i)]} = 2\sin\theta_i. \tag{3.167}$$

This relationship between $\bar{T}_{i+}$ and $\bar{T}_{i-}$ can be used to rewrite equation (3.162) as

$$\begin{aligned}\int_0^{\pi/2}\log(q)d\theta &= \int_0^{\theta_i}\log(q)\left[1-\frac{\bar{T}_{i+}}{|\bar{T}|}\right]d\theta - \bar{T}_{i+} \\ &\quad + \int_{\theta_i}^{\pi/2}\log(q)\left[1-\frac{\bar{T}_{i+}}{\bar{T}}\right]d\theta + \bar{T}_{i+}q(\pi/2)\left[\log q(\pi/2)-1\right] \\ &= \int_0^{\pi/2}\log(q)\left[1-\frac{\bar{T}_{i+}}{|\bar{T}|}\right]d\theta + \bar{T}_{i+}\left\{\begin{array}{c}\text{singularity}\\ \text{extraction}\end{array}\right\}_\Omega .\end{aligned} \tag{3.168}$$

where

$$\left\{\begin{array}{c}\text{singularity}\\ \text{extraction}\end{array}\right\}_\Omega \equiv q(\pi/2)\left[\log q(\pi/2)-1\right]-1. \tag{3.169}$$

Adding this back to equation (3.156) gives the desired result,

$$\begin{aligned}\int_0^{\pi/2}\Theta(\theta)K(p)d\theta &= \int_0^{\pi/2}\left\{\Theta(\theta)K(p)+\frac{\Theta_i\bar{T}_{i+}}{|\bar{T}|}\log(q)\right\}d\theta \\ &\quad -\Theta_i\bar{T}_{i+}\left\{\begin{array}{c}\text{singularity}\\ \text{extraction}\end{array}\right\}_\Omega .\end{aligned} \tag{3.170}$$

The complete integral yielding $\bar{X}_n$ can be summarized by combining the above results with equation (3.151) to give

$$\frac{\bar{X}_n}{kh'_{2n}(ka)} = \int_0^{\pi/2} \left\{ P_{2n}(\cos\theta) \left[\mathcal{A}_1 + \mathcal{A}_2\right] \rho a + \frac{\Theta_i \bar{T}_{i+}}{|\bar{T}|} \log(q) \right\} d\theta \\ -\Theta_i \bar{T}_{i+} \left\{ \begin{array}{c} \text{singularity} \\ \text{extraction} \end{array} \right\}_\Omega . \tag{3.171}$$

which should be used when the evaluation point $\mathbf{x}_i$ lies on the impedance sphere.

The remaining singularity can be exposed by expanding equation (3.147) to show

$$\bar{Y}_n \equiv h_{2n}(ka) \int_0^{\pi/2} P_{2n}(\cos\theta) \left[\mathcal{B}_1 + \mathcal{B}_2\right] \rho a d\theta. \tag{3.172}$$

The quantity $\mathcal{B}_1$ remains finite as $\theta \to \theta_i$, but $\mathcal{B}_2$ is undefined at that point as can be seen from investigating equation (3.67). With equation (3.67), the portion of equation (3.172) requiring further attention can be expressed

$$\int_0^{\pi/2} P_{2n}(\cos\theta) \mathcal{B}_2 \rho a d\theta = \int_0^{\pi/2} P_{2n}(\cos\theta) \frac{4}{\bar{R}} \left\{ \frac{\partial K}{\partial \eta} - \frac{K}{\bar{R}} \frac{\partial \bar{R}}{\partial \eta} \right\} \rho a d\theta \\ = \int_0^{\pi/2} P_{2n}(\cos\theta) \frac{4}{\bar{R}} \frac{\partial K}{\partial \eta} \rho a d\theta - \int_0^{\pi/2} \Upsilon K(p) d\theta, \tag{3.173}$$

where

$$\Upsilon \equiv P_{2n}(\cos\theta) \frac{4}{\bar{R}^2} \frac{\partial \bar{R}}{\partial \eta} \rho a. \tag{3.174}$$

The integral containing the singularity,

$$\int_0^{\pi/2} \Upsilon K(p) d\theta, \tag{3.175}$$

is of identical form to the previous result in equation (3.170). That result can be used to evaluate equation (3.175) simply by replacing Θ with Υ as defined in equation (3.174).

The complete integral yielding $\bar{Y}_n$ can now be summarized by combining the results above with equation (3.172) to give

$$\frac{\bar{Y}_n}{h_{2n}(ka)} = \int_0^{\pi/2} \left\{ P_{2n}(\cos\theta) \left[\mathcal{B}_1 + \mathcal{B}_2\right] \rho a - \frac{\Upsilon_i \bar{T}_{i+}}{|\bar{T}|} \log(q) \right\} d\theta \\ +\Upsilon_i \bar{T}_{i+} \left\{ \begin{array}{c} \text{singularity} \\ \text{extraction} \end{array} \right\}_\Omega \tag{3.176}$$

which should be used when the evaluation point $\mathbf{x}_i$ lies on the impedance sphere.

Following from the expression above, the geometry coefficient can be expressed

$$C_i^{\Omega} = \int_0^{\pi/2} \left\{ \mathcal{B}_2 \rho a - \frac{\Upsilon_i^{\star} \bar{T}_{i+}}{|\bar{T}|} \log(q) \right\} d\theta + \Upsilon_i^{\star} \bar{T}_{i+} \left\{ \begin{array}{c} \text{singularity} \\ \text{extraction} \end{array} \right\}_{\Omega} \tag{3.177}$$

where

$$\Upsilon^{\star} \equiv \frac{4}{\bar{R}^2} \frac{\partial \bar{R}}{\partial \eta} \rho a. \tag{3.178}$$

3.4.5 Construction of Discrete System Equations

Considerable effort has been expended evaluating the integrals of the Helmholtz integral theorem. These results can now be combined to yield a linear, simultaneous system of equations to be solved for the unknown values of surface potential, and coefficients in the series expansion of the potential over the mouth of the horn.

Combining the line integrals over the quadratic elements and the impedance sphere in the previous sections gives

$$C(\mathbf{x}_i)\phi(\mathbf{x}_i) + \sum_{n=1}^{2N_{\mathrm{Q}}+1} Y_n \phi_n + \sum_{n=0}^{N_{\Omega}-1} \bar{Y}_n D_n = \sum_{n=1}^{3N_{\mathrm{Q}}} X_n \psi_n + \sum_{n=0}^{N_{\Omega}-1} \bar{X}_n D_n. \tag{3.179}$$

The flux ψ is prescribed for the integrations over the quadratic elements, so ϕ_n and D_n comprise the $2N_{\mathrm{Q}} + 1 + N_{\Omega}$ unknowns in the above equation, which can be written as

$$C(\mathbf{x}_i)\phi(\mathbf{x}_i) + \sum_{n=1}^{2N_{\mathrm{Q}}+1} Y_n \phi_n + \sum_{n=0}^{N_{\Omega}-1} \left[\bar{Y}_n - \bar{X}_n \right] D_n = \sum_{n=1}^{3N_{\mathrm{Q}}} X_n \psi_n. \tag{3.180}$$

To obtain a linear system of $2N_{\mathrm{Q}} + 1 + N_{\Omega}$ equations needed to solve for ϕ_n and D_n, rewrite equation (3.180) for $2N_{\mathrm{Q}} + 1 + N_{\Omega}$ values of $\mathbf{x}_i$,

$$C_i \phi_i + \sum_{n=1}^{2N_{\mathrm{Q}}+1} Y_{in} \phi_n + \sum_{n=0}^{N_{\Omega}-1} \left[\bar{Y}_{in} - \bar{X}_{in} \right] D_n = \sum_{n=1}^{3N_{\mathrm{Q}}} X_{in} \psi_n. \tag{3.181}$$

For the $2N_{\mathrm{Q}}+1$ values of $\mathbf{x}_i$ that correspond to the nodal coordinates of the quadratic elements, this becomes

$$\sum_{n=1}^{2N_{\mathrm{Q}}+1}\left[Y_{in}+C_i\delta_{in}\right]\phi_n+\sum_{n=0}^{N_\Omega-1}\left[\bar{Y}_{in}-\bar{X}_{in}\right]D_n=\sum_{n=1}^{3N_{\mathrm{Q}}}X_{in}\psi_n \tag{3.182}$$

where δ_{in} is the Kronecker delta function,

$$\delta_{in}=\begin{cases}1, & \text{for } i=n \text{ and}\\ 0, & \text{for } i\neq n.\end{cases}$$

The N_Ω points remaining must be chosen on the surface of the impedance sphere where equation (3.144) has been used to expand the potential in the form

$$\phi_i=\sum_{n=0}^{N_\Omega-1}W_{in}D_n \tag{3.183}$$

where

$$W_{in}\equiv h_{2n}^{(2)}(ka)P_{2n}(\cos\theta_i). \tag{3.184}$$

This can be substituted for ϕ_i in equation (3.181) when the points of evaluation lie on the impedance sphere, resulting in

$$\sum_{n=1}^{2N_{\mathrm{Q}}+1}Y_{in}\phi_n+\sum_{n=0}^{N_\Omega-1}\left[\bar{Y}_{in}-\bar{X}_{in}+C_iW_{in}\right]D_n=\sum_{n=1}^{3N_{\mathrm{Q}}}X_{in}\psi_n. \tag{3.185}$$

The entire linear system of equations can be written for all values of $\mathbf{x}_i$ as

$$\sum_{n=1}^{2N_{\mathrm{Q}}+1}\left[Y_{in}+C_i\delta_{in}\right]\phi_n+\sum_{n=0}^{N_\Omega-1}\left[\bar{Y}_{in}-\bar{X}_{in}+C_iW_{in}H_{i-2N_{\mathrm{Q}}-2}\right]D_n=\sum_{n=1}^{3N_{\mathrm{Q}}}X_{in}\psi_n, \tag{3.186}$$

where H_i is the Heaviside step function,

$$H_i=\begin{cases}0, & \text{for } i<0 \text{ and}\\ 1, & \text{for } i\geq 0.\end{cases}$$

and the resulting system has the form

$$\left[\begin{array}{c|c}Y_{in}+C_i\delta_{in} & \bar{Y}_{in}-\bar{X}_{in}\\ \hline Y_{in} & Y_{in}-X_{in}+C_iW_{in}\end{array}\right]\left\{\begin{array}{c}\phi_n\\ \hline D_n\end{array}\right\}=\left[\begin{array}{c|c}X_{in}\end{array}\right]\left\{\begin{array}{c}\psi_n\end{array}\right\} \tag{3.187}$$

which can be solved yielding the values of ϕ_n and D_n. Once these values are known, it is possible to calculate any interior value of the potential by returning to equation (3.180) with $C(\mathbf{x}_i)=4\pi$ and $\mathbf{x}_i$ as the point of evaluation.

3.4.6 Alternative Hemispherical Formulation

In a previous section an impedance sphere was defined as a single element of the boundary of integration and the potential was replaced by the coefficients in the expansion series. This section briefly points out an alternative method which allows the entire surface to be composed of quadratic elements. The system of equations would be written as before but a matrix form of an impedance condition on the impedance sphere must be found to make the system of equations unique. To find this impedance matrix first recall the orthogonality relationship for Legendre polynomials,

$$\int_0^1 P_{2m}(x)P_{2n}(x)dx = \frac{1}{4n+1}\delta_{mn}. \tag{3.188}$$

Using the orthogonality property above, the coefficient in the series expansion of ϕ can be expressed

$$D_n = \frac{4n+1}{h_{2n}(ka)} \int_0^1 \phi(r, a\cos\bar{z}) P_{2n}(\cos\theta) d\bar{z}, \tag{3.189}$$

where $\bar{z} \equiv \cos\theta = z/a$. Equation (3.189) can be evaluated by an N point Gaussian quadrature to give

$$D_n \approx \frac{4n+1}{h_{2n}(ka)} \sum_{j=1}^{N} w_j \phi(r, a\cos\bar{z}_j) P_{2n}(\bar{z}_j). \tag{3.190}$$

where w_j are the weights and $\bar{z}_j$ are the abscissa values of the quadrature scheme. Substituting this into equation (3.145) gives

$$\frac{\partial\phi}{\partial\eta} \approx \sum_{j=1}^{N} \left[k \sum_{n=0}^{N} [4n+1] \frac{h'_{2n}(ka)}{h_{2n}(ka)} w_j P_{2n}(\bar{z}_j) P_{2n}(\cos\theta) \right] \phi(a, a\cos\bar{z}_j) \tag{3.191}$$

which can be written

$$\frac{\partial\phi_i}{\partial\eta} = Y_{ij}\phi_j \tag{3.192}$$

where

$$Y_{ij} \equiv k \sum_{n=0}^{N} [4n+1] \frac{h'_{2n}(ka)}{h_{2n}(ka)} w_j P_{2n}(\bar{z}_j) P_{2n}(\bar{z}). \tag{3.193}$$

The matrix Y_{ij} may be called an admittance matrix and its inverse would then be an impedance matrix. If the nodes on the impedance sphere are chosen to correspond to the abscissas of the quadrature formula, the admittance relation in equation (3.193) can be used to make the system of equations unique. This formulation does not seem as natural for the current problem as defining a single element composed of the hemispherical surface. It is therefore not used in this work, but may be more suitable in certain problems.

3.4.7 Radiation Solution

On and outside of the impedance sphere, the potential ϕ can be found by using equation (3.144) limited to a finite number of terms,

$$\phi(r,\theta) = \sum_{n=0}^{N_\Omega - 1} D_n h_{2n}^{(2)}(kr) P_{2n}(\cos\theta). \tag{3.194}$$

To compute the potential in the far-field, use the relation [81, page 1573]

$$\lim_{kr\to\infty} h_{2n}^{(2)}(kr) = [-1]^n \frac{e^{-jkr}}{-jkr} \tag{3.195}$$

in equation (3.194) to write the asymptotic value of ϕ,

$$\phi(r,\theta) \Rightarrow \left[\sum_{n=0}^{N_\Omega - 1} D_n [-1]^n P_{2n}(\cos\theta)\right] \frac{e^{-jkr}}{-jkr}. \tag{3.196}$$

3.5 Verification

A formulation of the boundary element method suitable for implementation on a digital computer has been developed in the previous sections. A program was written in FORTRAN to implement the method by using the actual sections contained in this dissertation. This limits the possibility of translational errors in the text. As a test of the accuracy of the computer program, a problem having a known analytical solution can be solved and the numerical solution compared with the analytical one. For this purpose, the source was chosen to

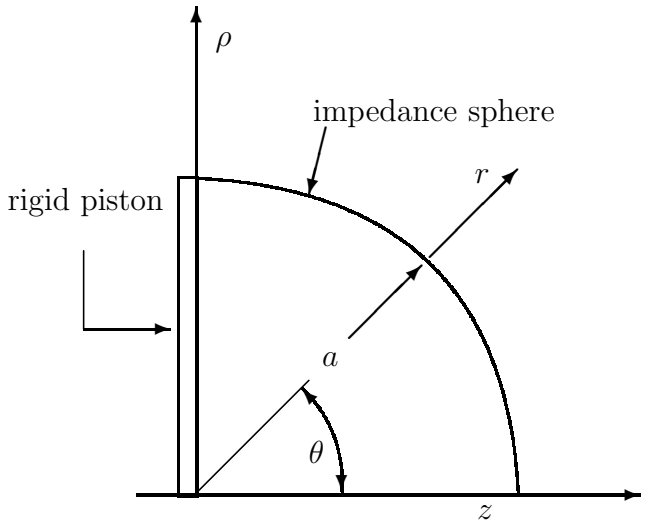

Figure 3.8: Coordinate system for the test problem of a rigid piston in an infinite baffle.

be a rigid piston such as seen in figure 3.8. For a rigid piston, the mechanical impedance and far-field directivity are both known [73]. From the far-field directivity solution, it is also known that the on-axis pressure in the far field is proportional to the frequency of the source. Numerically finding the far-field information is done just as described in the previous sections, but the program returns the pressure distribution on the surface of the piston rather than the mechanical driving impedance. This was remedied by adding a few lines of code to integrate the pressure over the surface of the piston. The program results are shown in figure 3.9 where the circles represent the numerical solution and the solid line is the exact solution.

The agreement between the exact solution and the computed one is good. It is readily possible to increase the precision by increasing the number of quadratic elements and the number of terms used in the series expansion for the pressure on the surface of the impedance sphere. The number of quadratic elements and series terms used for the generation of figure 3.9 was dynamically adjusted as a function of frequency. The algorithm for adjusting the program's

parameters is very dependent on the type of surface over which the integrations are performed. For the piston, it was found that approximately 6 elements per wavelength were sufficient to give very accurate results.

The number of terms needed in the series expansion of the pressure over the surface of the impedance sphere was adjusted to accurately predict the directivity of a piston. At small values of ka, 8 terms were used; this was linearly increased to 44 terms at $ka = 30$. An example of the match between the boundary element method and the exact solution is shown in figure 3.10. The directivity patterns were computed for many values of ka and figure 3.10 is very representative of the accuracy achieved.

Another simple check afforded by the rigid piston test problem is the on-axis pressure in the far-field, which should increase linearly with increasing frequency. The computer program was written to generate the far-field, on-axis pressure at the same time the driving point impedance is calculated. The results are shown in figure 3.11.

The on-axis pressure in the far-field agrees very well with the exact solution. At this point, the features of the program that will be used to analyze acoustic horns have been tested and found to be extremely accurate. In the next chapter, the program will be used to solve the wave equation in a boundary geometry for which there is no known exact solution, a tapered acoustic waveguide.

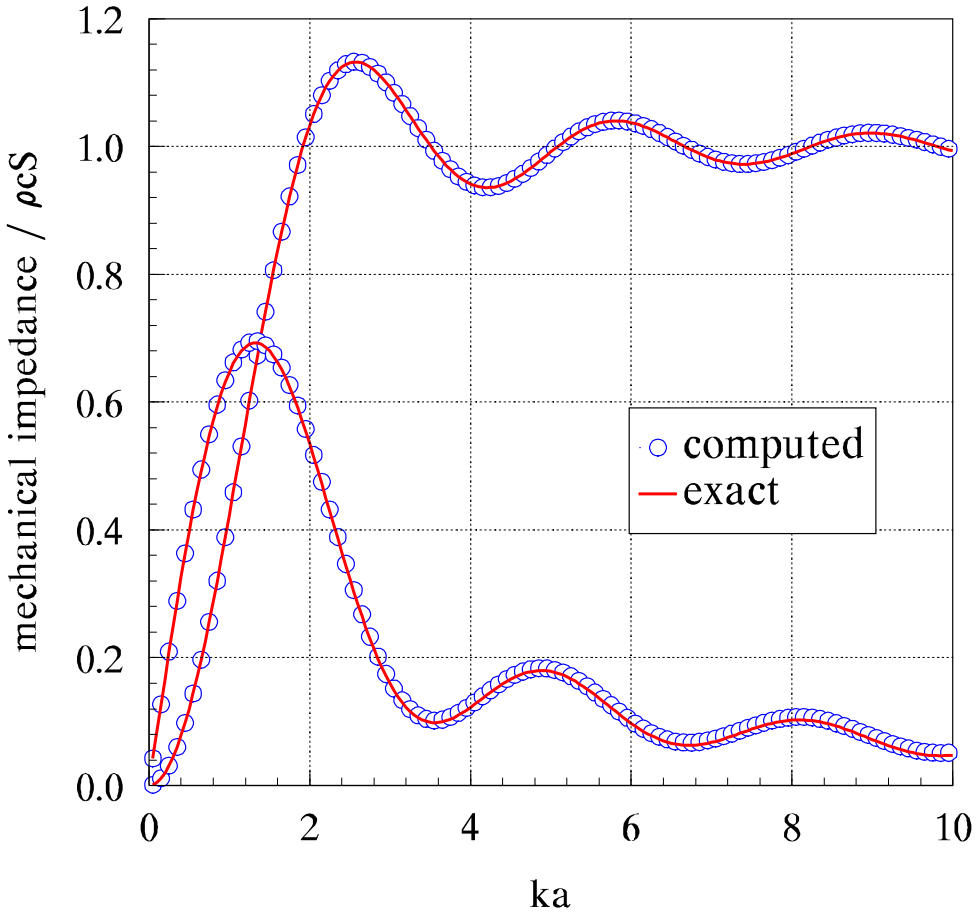

Figure 3.9: Normalized mechanical impedance of a piston in an infinite baffle. The numerical solution was obtained by the boundary element method. The program parameters were dynamically adjusted as a function of ka. Each of the 100 frequency points took approximately ka seconds for a total run time of 3.25 minutes on a 80486/33 MHz microcomputer.

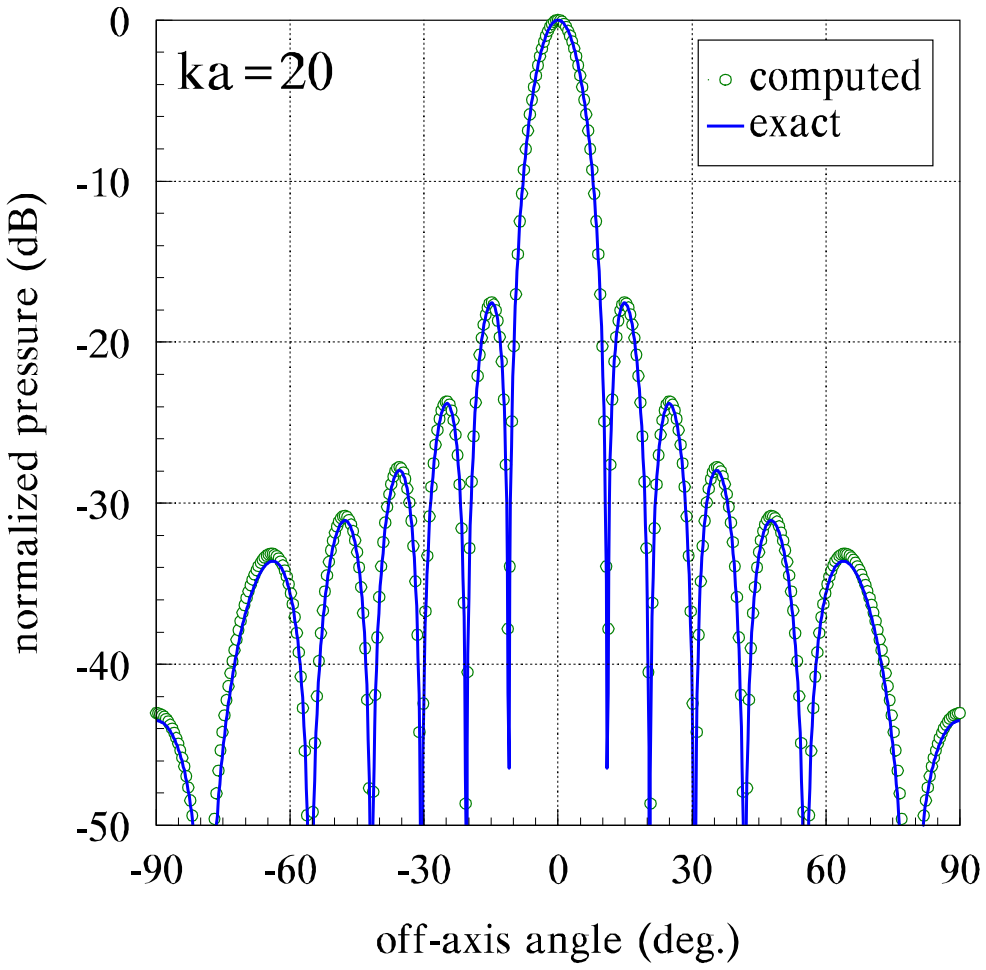

Figure 3.10: Directivity of a rigid piston in an infinite baffle at $ka = 20$. The circles represent the solution obtained by the boundary element method and the solid line represents the exact solution. The pressure is normalized to the on-axis value. The program parameters: 24 quadratic elements with 12 point Gauss integration rule, 36 terms in series expansion on impedance sphere with 37 point Gauss integration rule. Computation time: 48.8 seconds on an 80486/33 MHz microcomputer.

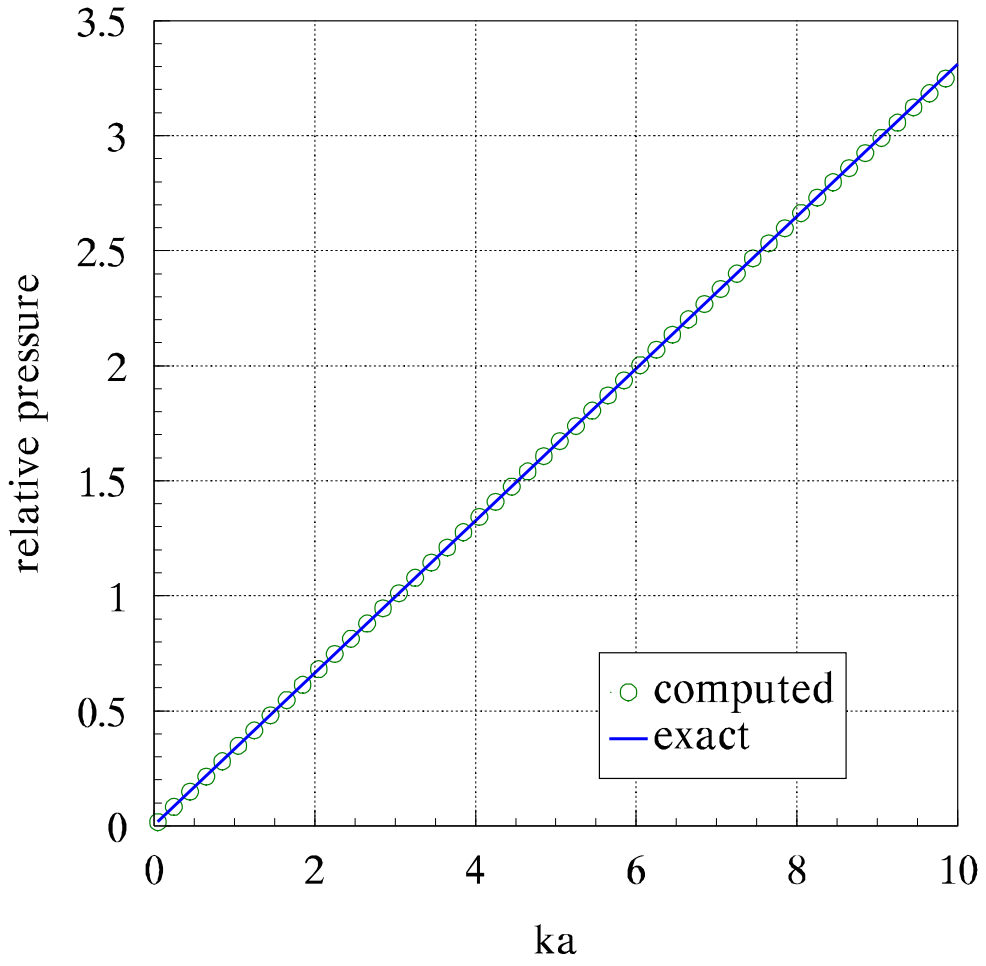

Figure 3.11: On-axis, far-field pressure of a rigid piston in an infinite baffle. The program parameters were dynamically adjusted as a function of ka. Each of the 50 frequency points took approximately ka seconds for a total run time of 1 minute, 53 seconds on a 80486/33 MHz microcomputer.

Chapter 4

Acoustic Impedance and Radiation Pattern Measurements

In the previous chapter, a numerical technique has been established that is suitable for the study of acoustic horns. Two axisymmetric horns were constructed for testing, each with a different taper. The contour of the first horn was chosen to be exponential, while the second horn was constructed with a tractrix contour. Both the exponential and tractrix tapers have been known for a very long time, but the tractrix is not often used in application, probably because of its more complicated mathematical formula. The cross-sectional area of the exponential horn expands exponentially, while the cross-sectional area of the tractrix horn expands in such a way that a spherical wave of constant radius always contacts the walls normally. This definition can be used to derive [145] the tractrix equation. Referring to figure 4.1, the slope of the taper at any point can be written,

$$\frac{dy}{dx} = \frac{-y}{\sqrt{a^2 - y^2}} \tag{4.1}$$

which can be integrated with the use of standard integral tables to yield

$$x = a \log\left(\frac{a - \sqrt{a^2 - y^2}}{y}\right) - \sqrt{a^2 - y^2}. \tag{4.2}$$

Written in the same coordinate system, the exponential contour is expressed as

$$x = \frac{1}{k_c} \log(a/y) \tag{4.3}$$

where k_c is known as the "cutoff" wave number.

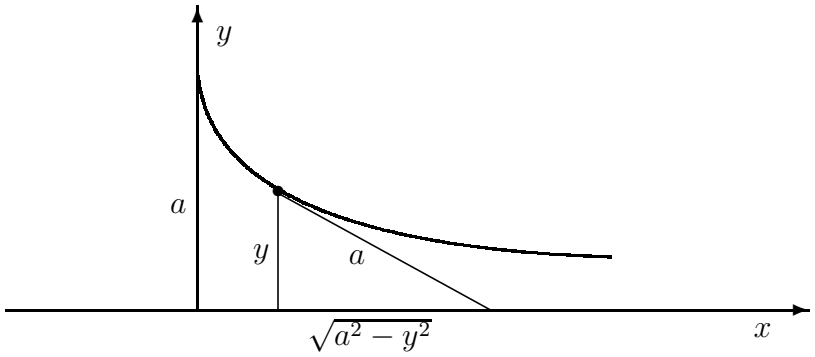

Figure 4.1: Geometry and coordinate system used for deriving the equation for the tractrix horn contour.

4.1 Designing the Horns

In choosing the appropriate dimensions of the horns to be tested, several factors were considered. The overall length and mouth diameter and frequency range of operation were chosen to be compatible with the physical dimensions and absorption bandwidth of the anechoic chamber testing facility. The hollow space beneath the floor of the chamber will accommodate a horn of 69 cm (27 in.) in length.

To compare the tractrix and exponential horns on an equal basis, it seems reasonable that the horns perform an equivalent task, that is going from a specified throat area to a specified mouth area with the same allowed length. This is contrary to the manner in which the horns are designed in practice. Typically, the throat and mouth areas are required to be the same, but the slope at the throat of the horns is chosen to be equal rather than the length, which results in a tractrix horn that is shorter than the "equivalent" exponential horn. The equal slope at the throat of the two horns allows a "cutoff" frequency to be defined for the tractrix horn based on the flare-rate of the initial portion of the taper, which is very nearly the same as the initial flare-rate of the exponential horn.

To find horns of equal areas and length, equate and rearrange equa-

tions (4.3) and (4.2) to give

$$\frac{1}{k_c a} = \left\{ \log\left(a/y_0 + \sqrt{[a/y_0]^2 - 1} \right) - \sqrt{1 - [y_0/a]^2} \right\} / \log(a/y_0). \qquad (4.4)$$

Examining the expression above, it is apparent that once the mouth and throat areas are set, and the lengths chosen to be equal, there is no freedom left in the choice of cutoff wave number k_c. It is standard practice [43, 118] in industry to choose $k_c a = 1$, but this choice does not satisfy equation (4.4). This explains why it is generally thought to be impossible to construct equivalent exponential and tractrix horns. This dilemma is resolved by relaxing the requirement that $k_c a = 1$, and letting it be slightly greater than unity. This is not a serious compromise however, because the requirement that $k_c a \not> 1$ has never been established experimentally in the literature, and very likely has no physical basis. The custom of choosing $k_c a$ to be *at least* unity is probably good practice, based on impedance matching between the expanding transmission line and a sphere or piston at the mouth of the horn. Because these approximations are only appropriate at low frequency, setting $k_c a = 1$ describes the necessary *minimum* mouth size.

Choosing $k_c a = 1.147$ results in a mouth-to-throat radius ratio of $y_0/a = 10.67$, which is typical of horns used for high quality sound reproduction. With the throat radius set to 25.4 mm (1 in.) to match available compression horn drivers, the remaining parameters follow as shown in figure 4.2. The actual horns used in the experiments are of fiberglass construction and are shown in figure 4.3 where they are standing on end in the anechoic chamber testing facility.

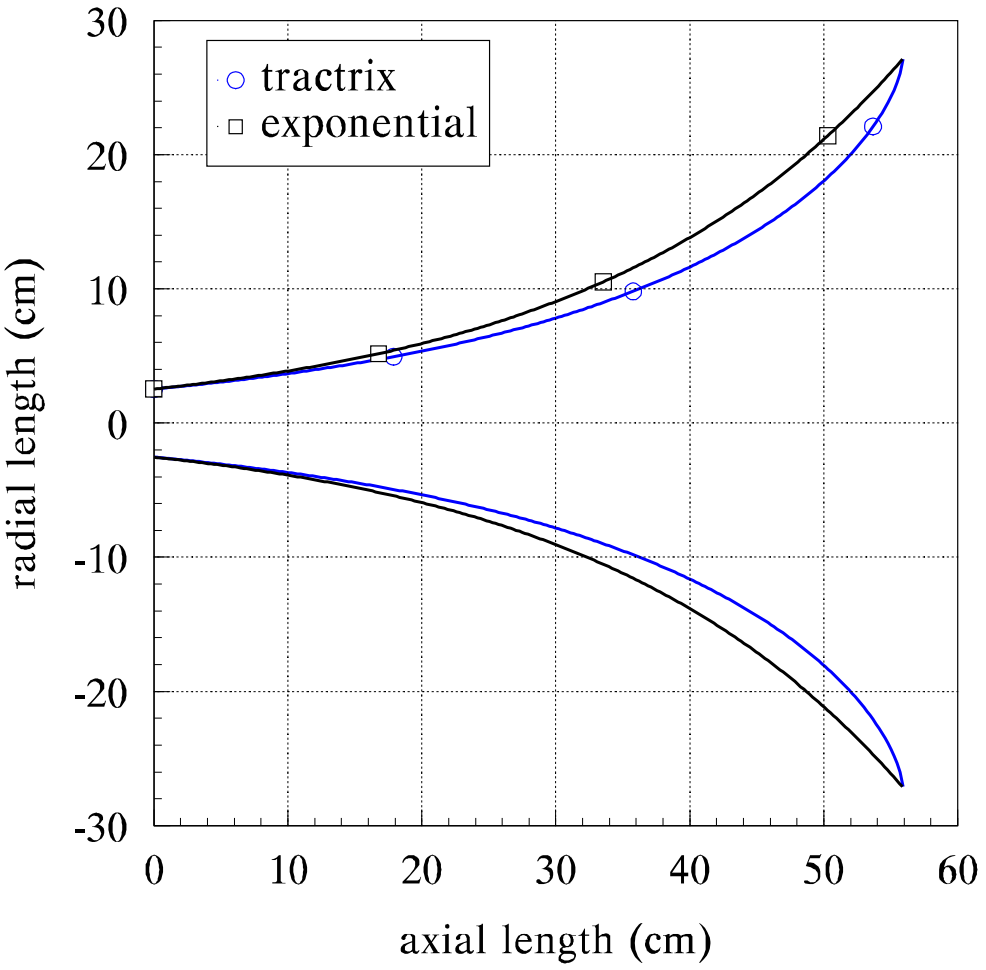

Figure 4.2: Contours of the exponential and tractrix horns used in the experiments. Dimensions: throat radius: 25.4 mm (1 in.), mouth radius: 271 mm (10.67 in.), axial length: 559 mm (22 in.), cutoff frequency: 232.5 Hz, exponential contour wall length: 627 mm (24.7 in.), tractrix contour wall length: 642 mm (25.3 in.)

Figure 4.3: Photograph of the tractrix and exponential horns constructed for experiments. The tractrix horn is on the left and the exponential horn is on the right. Note the larger diameter of the area profile for the exponential horn. Dimensions: throat radius: 25.4 mm (1 in.), mouth radius: 271 mm (10.67 in.), axial length: 559 mm (22 in.), cutoff frequency: 232.5 Hz, exponential contour wall length: 627 mm (24.7 in.), tractrix contour wall length: 642 mm (25.3 in.)

4.2 The Measurement Facility

Because an infinite baffle was assumed in all of the previous theoretical developments, it was necessary to place the horns in an effectively infinite baffle for the impedance and directivity measurements. For this purpose, a floor constructed of standard, medium-density fiberboard (commonly used in home construction) of 3/4 in. thickness was placed in the anechoic chamber on top of the existing floor.* The horns were placed in the floor and a boom was designed and constructed to rotate a microphone over the mouth of the horn at a fixed radius of 16 in. (40.64 cm) as seen in figure 4.4. The microphone boom is constructed of 3/8 in. stainless steel tubing. A linear, 10-turn potentiometer was attached to the gearbox which extended beneath the floor, and was used to determine the position of the boom. Two microphones were used in the experimental work: a Larson-Davis Laboratories† 1/4 in. condenser microphone model 2520, and a Brüel and Kjær‡ 1/4 in. condenser microphone type 4135. The Larson-Davis microphone was exclusively used to measure directivity while mounted to the rotating boom. The B&K microphone was used in all remaining measurements. The transfer functions were measured using a computer-controlled data acquisition system, the Tektronix 2630 Fourier Analyzer, which is beneath the video monitor in figure 4.5. Once measured, the data were downloaded to a microcomputer for post processing.

The exponential and tractrix horns used in the measurements were custom manufactured by Klipsch Professional.§ The compression horn driver used is the model DH1A-16, which is a 16 Ohm, 2 in. exit diameter driver, manufactured by Electro-Voice.¶

*The existing floor is made of 2 ft by 4 ft steel grating.
†Larson-Davis Laboratories, 1681 West 820 North, Provo, Utah 84601.
‡Brüel and Kjær, DK-2850, Nærum, Denmark.
§Klipsch Professional, P. O. Box 688, Hope, Arkansas 71801.
¶Electro-Voice Inc., 600 Cecil St., Buchanan, Michigan 49107

4.3 Measuring Acoustic Impedance

Accurate measurements of acoustic impedance are difficult but very important when comparing the relative performance of two horns as smooth and similar as the exponential and tractrix horns shown in figure 4.2. The smooth taper and wide mouth area result in very small reflections which are difficult for a measurement system to resolve. Two different methods for measuring acoustic impedance were implemented and compared. The first method is a modern implementation of the "reaction on the source" method [167] and has been reported previously by McLean, Post and Hixson [191]. The second method is a variation of the classical standing wave tube apparatus using two fixed microphone locations.

4.3.1 "Reaction on the Source" Method

The "reaction on the source" method is based on the linearity and reciprocity of an electromechanical transducer. This type of transducer can be represented by an equivalent two-port network. Referring to the compression horn driver in figure 4.6, a two-port representation using a transmission matrix can be expressed as

$$\left\{ \begin{array}{c} e \\ i \end{array} \right\} = \left[\begin{array}{cc} A & B \\ C & D \end{array} \right] \left\{ \begin{array}{c} p \\ U \end{array} \right\} \tag{4.5}$$

where e denotes the potential across, and i the current into, the electrical port, U denotes the volume velocity flowing from the acoustic port, and p the pressure at the acoustic port. Taking the ratio of the two equations above results in

$$Z_{\mathrm{e}} = \frac{AZ_{\mathrm{a}} + B}{CZ_{\mathrm{a}} + D} \tag{4.6}$$

where Z_{e} and Z_{a} have been defined as the electrical and acoustic impedance respectively. If the electrical impedance is known, equation (4.6) can be solved for the acoustical impedance,

$$Z_{\mathrm{a}} = \frac{B - DZ_{\mathrm{e}}}{CZ_{\mathrm{e}} - A}, \tag{4.7}$$

but before this step can be completed, the model parameters for the compression horn driver must be measured. The transmission matrix can be written

$$\begin{aligned} A &= \left.\frac{e}{p}\right|_{U=0} \quad B = \left.\frac{e}{U}\right|_{p=0} \\ C &= \left.\frac{i}{p}\right|_{U=0} \quad D = \left.\frac{i}{U}\right|_{p=0} \end{aligned}, \tag{4.8}$$

so the parameters A and C can be found by blocking the acoustic terminal as shown in figures 4.7 and 4.8 and measuring the transfer functions in equation (4.8).

The measurement of parameters B and D is complicated by the difficulty of enforcing a pressure release surface in air without using a vacuum which would modify the two-port parameters by removing the air from the driver. The additional parameters can be indirectly measured by applying a known acoustic load which is traditionally [167] chosen to be a closed tube, 1/8 wavelength long at the frequency being measured. This load is purely compliant and highly accurate, but its frequency dependence restricts the measurement to a single frequency, after which the length of the tube must be changed, resulting in a long and arduous measurement. The entire process can be done at all frequencies using an anechoic termination, which has a purely resistive impedance $Z_0 = \rho_0 c_0 / S$, so is independent of frequency. The anechoic termination used in the measurements was constructed by placing a slowly tapering strand of fiberglass inside an aluminum tube. The tubing has an internal diameter of 2 in. to match the compression horn driver and throat diameter of the horns, is 10 ft. in length, and has a 1/4 in. wall thickness.

Equation (4.5) can be manipulated to yield

$$B = (A' - A)Z_0 \qquad \text{and} \tag{4.9}$$

$$D = (C' - C)Z_0, \tag{4.10}$$

where

$$A' \equiv \left.\frac{e}{p}\right|_{Z_0} = A + B/Z_0, \qquad \text{and} \tag{4.11}$$

$$C' \equiv \left.\frac{i}{p}\right|_{Z_0} = C + D/Z_0. \tag{4.12}$$

The parameters A' and C' are measured with the anechoic termination attached as shown in figures 4.9 and 4.10.

The implementation of the above technique is straightforward. After the data for the transfer functions were gathered, a microcomputer was used to perform the necessary calculations. The results for the exponential horn are shown in figure 4.11.

When the impedance of the exponential horn in figure 4.11 was first plotted, the normalized resistive component did not reach the expected value of unity as the frequency was increased. Upon investigation, the throat area of the exponential horn was found to be significantly larger than the anechoic termination tubing which was used for normalization of the impedance. The throat of the horn was measured, curve fitted and, after integration of the resulting curve fit, found to have an area 2.5% larger than the reference termination. This slight increase in area does not cause significant reflections over the measured bandwidth so the impedance data could be scaled to the larger area, and it is the scaled result which is shown in figure 4.11. A similar problem occurred with the tractrix horn, which was found to have a throat area 4.45% smaller than the reference termination. The impedance of the tractrix horn in figure 4.12 has been normalized to the measured throat area.

The low frequency portions of the measured data display a noisy behavior as a result of the loss in horn loading at these frequencies. As the acoustic loading vanishes, there is insufficient "reaction on the source" for an accurate measurement. The loss of wall stiffness is also apparent in the data which

show the mechanical vibrations are especially pronounced in the $6 < ka < 8$ range. At the classical cutoff frequency ($ka = 1.15$), the impedance of both the exponential and tractrix horn are dominantly reactive.

With an abundance of patience on the part of the experimenter, the repeatability of these measurements can be made good, but repeatable measurements are certainly difficult with this system. It seems that all parameters of the two-port transmission matrix and the electrical impedance of the driver must be measured over a relatively small time interval to achieve good results. This might be the result of extreme sensitivity of the measurement to changes in the system caused by temperature drifts but a sensitivity analysis of this method has not been attempted.

The choice of compression horn driver used is also crucial to the success of the method. Because the acoustic impedance is "sensed" through the driver, the electromechanical coupling coefficient ($B\ell$) of the driver should be large, resulting in greater sensitivity for the measurement. Because other factors are also important, compression horn drivers are not optimized for the largest possible value of $B\ell$, but it should be possible to construct a driver optimized for this type of measurement, yielding greatly increased sensitivity.

4.3.2 Two-Microphone Method

Measuring the pressure minima and maxima in a standing wave tube has long since been the mainstay of acoustic impedance measurements. The classical measurement is performed by probing the standing wave field at each frequency, a technique that is impractical for obtaining large amounts of frequency data. It is possible to define and measure transfer functions to rapidly determine the impedance of the load. To derive the necessary formula, place a length of tube (to serve as a standing wave tube) between the driver and the horn as shown in figure 4.13 and begin with the solution (plane-wave) to the wave equation

within the standing wave tube,

$$p = K_1 \cos(kx) + K_2 \sin(kx). \tag{4.13}$$

The constants K_1 and K_2 depend on the boundary conditions. Combining this equation with the momentum equation,

$$jkZ_0U + \frac{dp}{dx} = 0, \tag{4.14}$$

gives the acoustic impedance at the throat of the horn,

$$Z = \frac{p}{U}\bigg|_{x=0} = -jZ_0\frac{K_1}{K_2}. \tag{4.15}$$

The constants K_1 and K_2 can be exchanged for two measurement positions ℓ_1 and ℓ_2 by writing equation (4.13) for $x = \ell_1$ and $x = \ell_2$ resulting in p_1 and p_2. Eliminating K_1 and K_2 from the two equations yields the desired relation,

$$\frac{Z}{Z_0} = j\frac{\sin(k\ell_2) - p_2/p_1 \sin(k\ell_1)}{p_2/p_1 \cos(k\ell_1) - \cos(k\ell_2)}. \tag{4.16}$$

This equation allows the impedance of the horn to be calculated if the pressure transfer function between the two microphone locations is known. This method is much more rapid than single frequency measurements and was first reported by Fahy [153] in 1984 and has been recently used by Holland, Fahy, and Morfey [185] to measure throat impedance of acoustic horns. However, additional improvement is possible by abandoning the traditional equipment, which suffers from the poor sensitivity and frequency response of a probe tube microphone, and the physically awkward dimensions of a standing wave tube. Consider the arrangement displayed in figure 4.14, which shows an added length of only several inches between the compression horn driver and the horn. The added length is effectively a standing wave tube. Instead of using a probe microphone, the microphone is mounted in the wall of the added length. Figures 4.14 and 4.15 show the microphone in the first measurement position. The second

measurement position was arrived at by simply inverting the position of the three elements making up the minimized standing wave tube and is shown in figure 4.16.

Because only one microphone was used in the measurements, a reference signal is needed to arrive at the desired transfer function. For this purpose, the pressure at the microphone location can be measured relative to the electric potential e applied to the compression horn driver. After the transfer functions at both microphone locations is measured, the desired transfer function is found by taking the ratio

$$\frac{p_2}{p_1} = \frac{p_2/e}{p_1/e}, \tag{4.17}$$

which is used in equation (4.16) to get the acoustic impedance of the horn. This technique is very robust and the figures presented here are from the first data set taken by the author. Additional data sets were gathered with no significant change in the measured results. Figure 4.17 shows the measured throat impedance of the exponential horn while figure 4.18 is the measured throat impedance of the tractrix horn.

A feature of the data curves that stands out is the low-frequency sensitivity of the measurement, which extends to $ka = 0.3$ in a very smooth manner. A normalized frequency of $ka = 0.3$ corresponds to 61 Hz, at which the 2.5 in. microphone spacing is only 1% of a wavelength. The sensitivity could be increased further by increasing the spacing between the two microphone measurement locations.

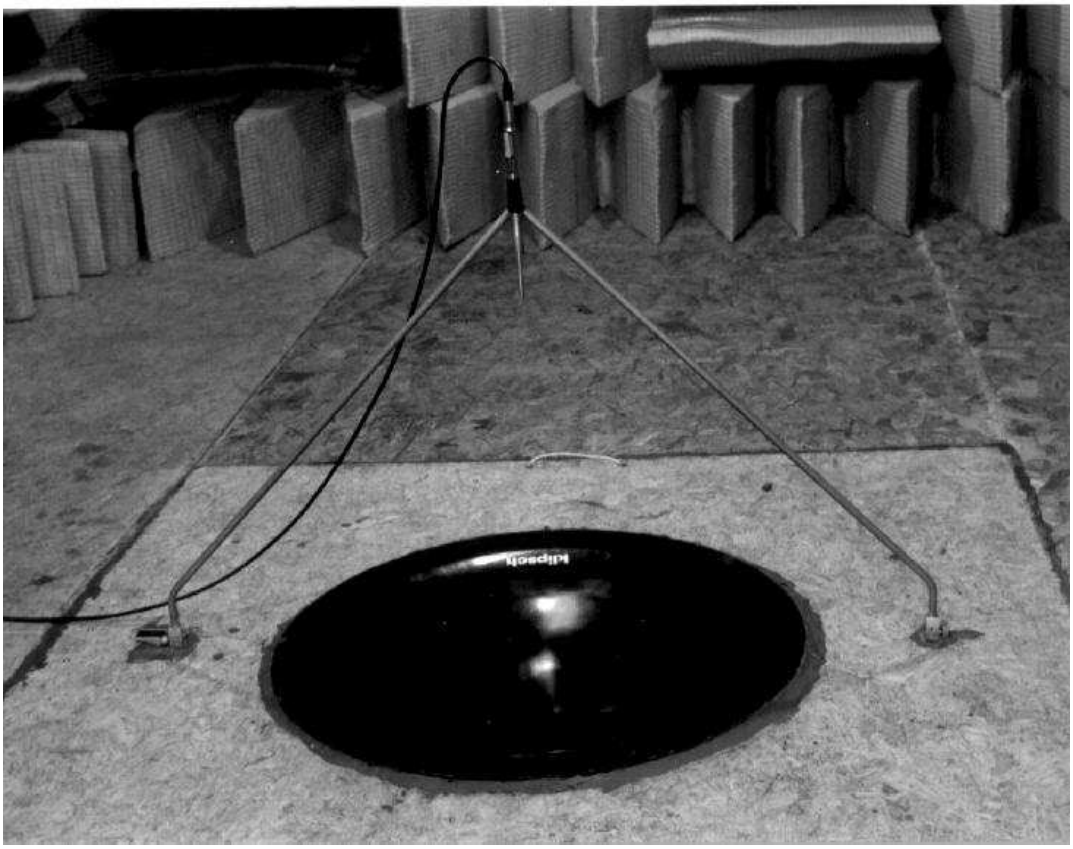

Figure 4.4: Hemi-anechoic chamber showing placement of horn to be tested and boom for rotating a microphone across the mouth of the horn. The boom itself is constructed of 3/8 in. stainless steel tubing. The microphone is 16 in. from the mouth of the horn, which is 24 in. in diameter including the mounting lip. The base of the boom is approximately 34 in. across.

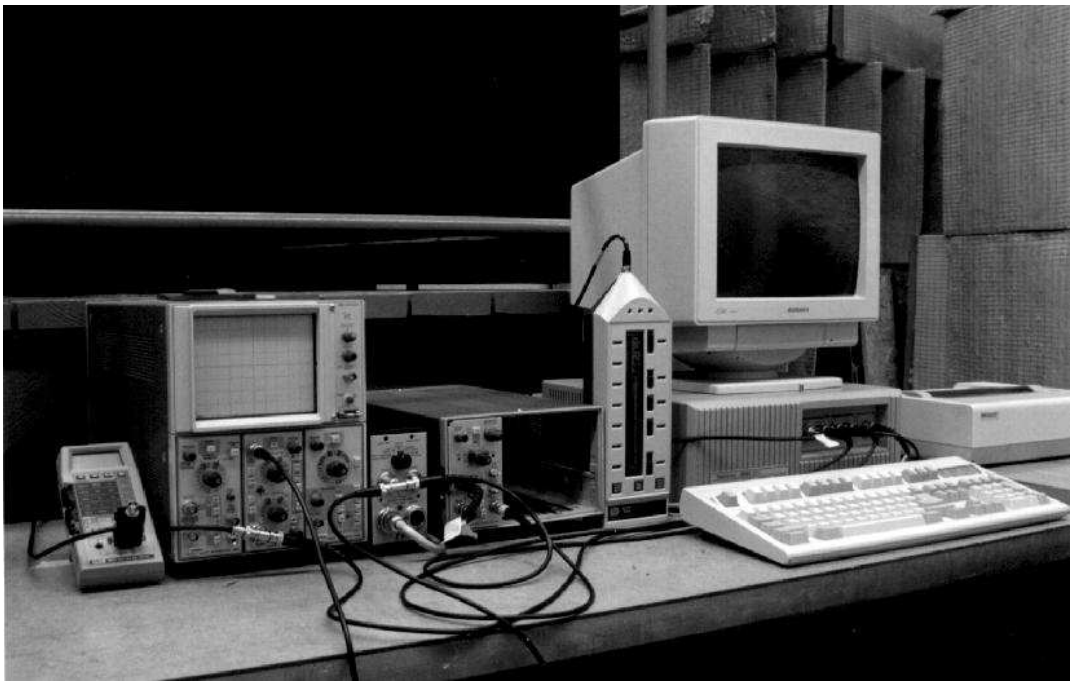

Figure 4.5: Electronic equipment used in measurement system. From left: Fluke 8060 multimeter, Tektronix 5110 oscilloscope, B&K 2807 microphone power supply, Tektronix AM502 differential amplifier, Larson-Davis 800B sound level meter, Tektronix 2630 Fourier analyzer.

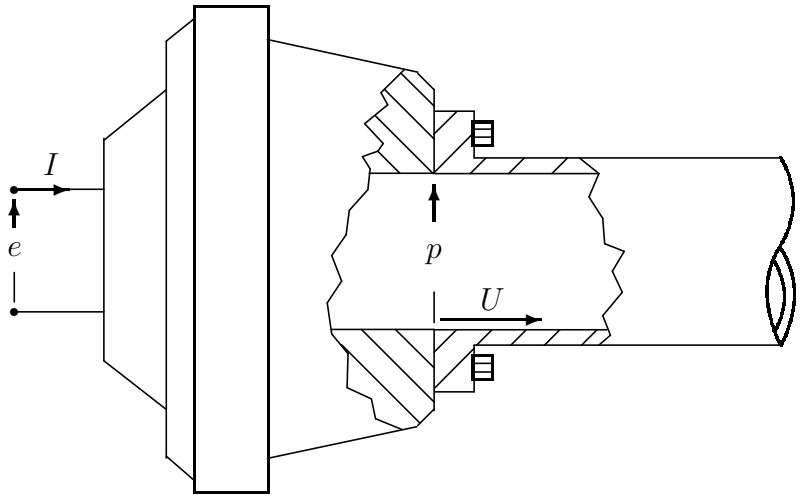

Figure 4.6: Description of the terminal planes used in definition of two-port transmission matrix representation of the compression horn driver.

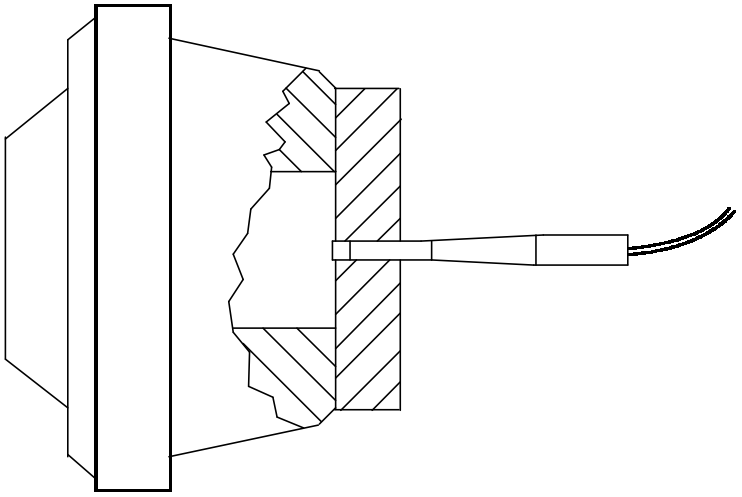

Figure 4.7: Acoustic terminal plane of the compression horn driver blocked for two-port parameter measurements. The aluminum blocking plate is 9.525 mm (3/8 in.) thick.

Figure 4.8: Photograph of the compression horn driver blocked for two-port parameter measurements. The B&K 1/4 in. microphone is mounted in a nylon sleeve. The aluminum blocking plate is 9.525 mm (3/8 in.) thick.

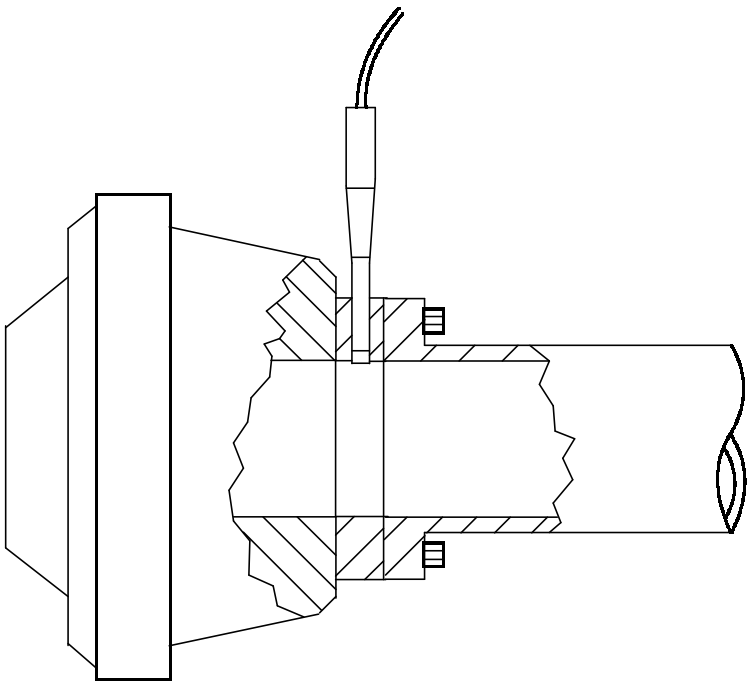

Figure 4.9: Anechoic termination and microphone location used for measurement of two-port parameters, A' and C'.

Figure 4.10: Photograph of anechoic termination used for two-port parameter measurements, A' and C'. The compression horn driver is the Electro-Voice DH1A-16. The anechoic termination is constructed from a linear taper of fiberglass in a 10 ft length of aluminum tubing. Note the horn mounted in the floor to the right of the anechoic termination.

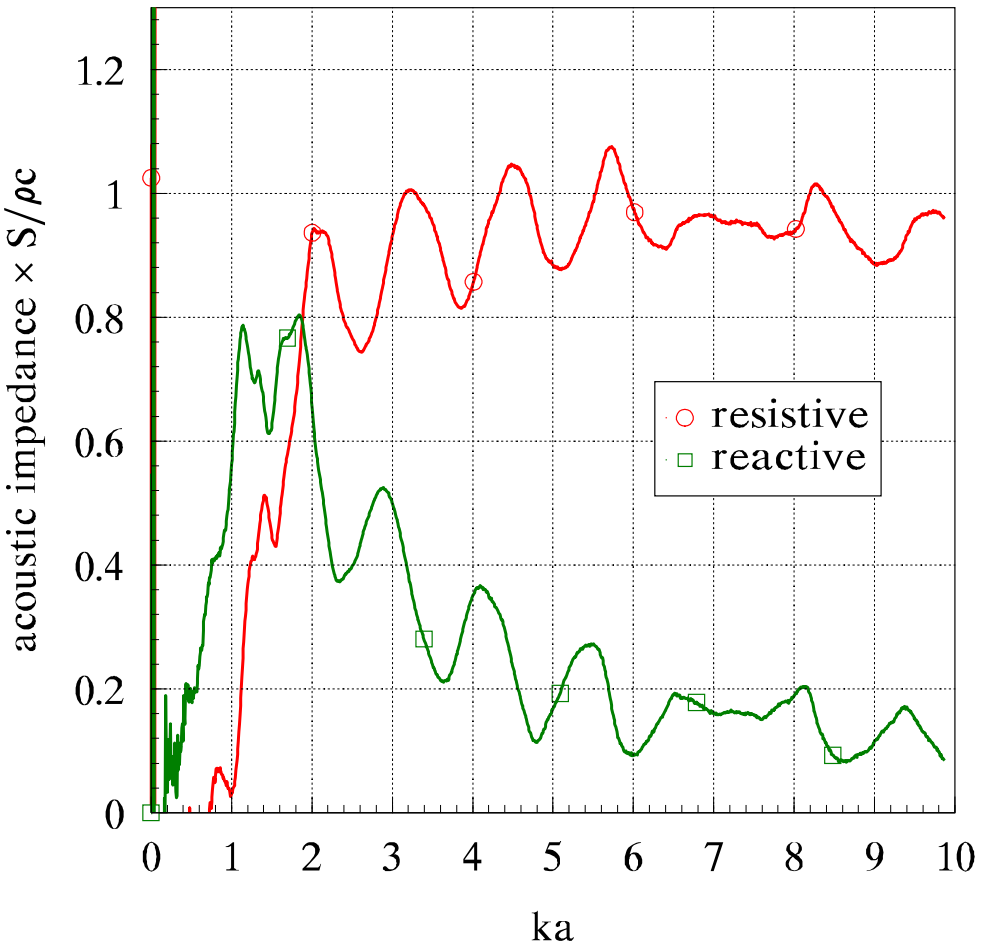

Figure 4.11: Measured acoustic impedance of the exponential horn using the "reaction on the source" method. The impedance is normalized by $\rho_0 c_0/S$, and the mouth radius a of the horn is used in the normalized frequency ka. The actual frequency range spans 0–2 kHz. The impedance has been scaled by 1.025 to compensate for the mismatch between the area of the calibration load (anechoic tube) and the area of the exponential horn throat. Analyzer settings: 0–2 kHz bandlimited random noise source, 200 averages, 4096 point data frames resulting in 1601 frequency points.

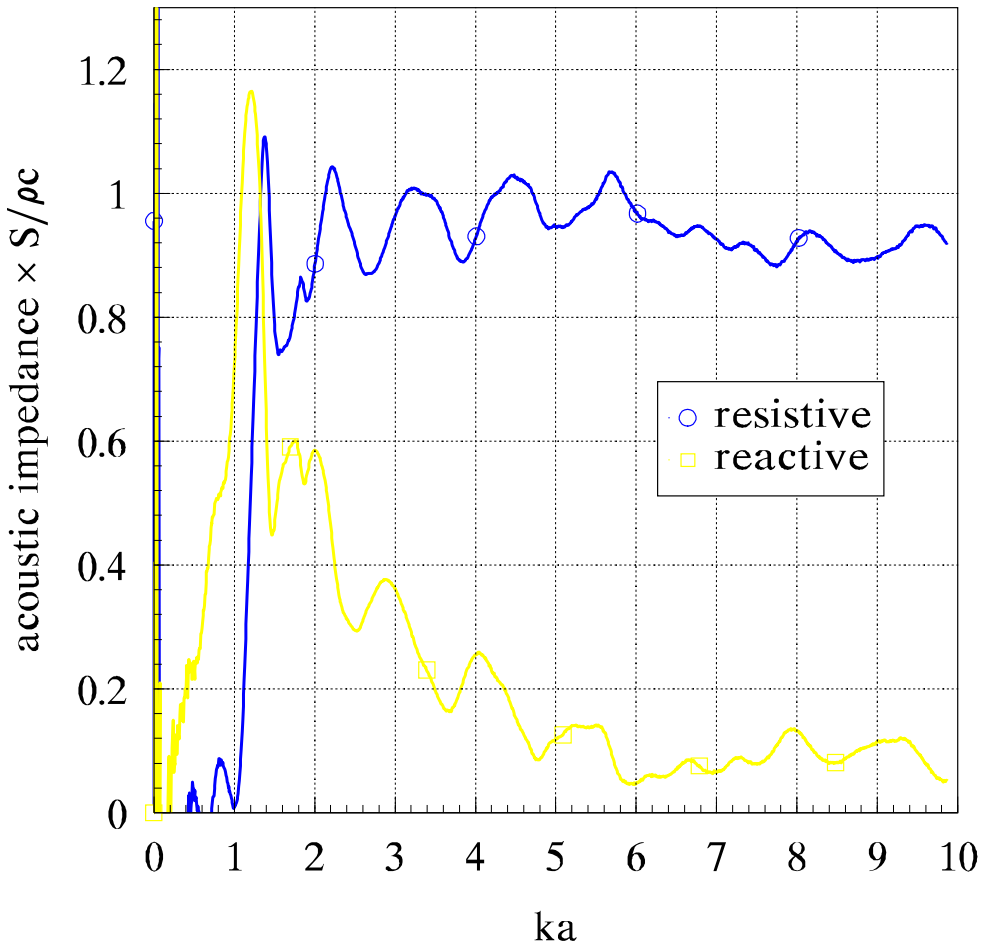

Figure 4.12: Measured acoustic impedance of the tractrix horn using the "reaction on the source" method. The impedance is normalized by $\rho_0 c_0/S$, and the mouth radius a of the horn is used in the normalized frequency ka. The actual frequency range of the data spans 0–2 kHz. The impedance has been scaled by 0.9555 to compensate for the mismatch between the area of the calibration load (anechoic tube) and the area of the tractrix horn throat. Analyzer settings: 0–2 kHz bandlimited random noise source, 200 averages, 4096 point data frames resulting in 1601 frequency points.

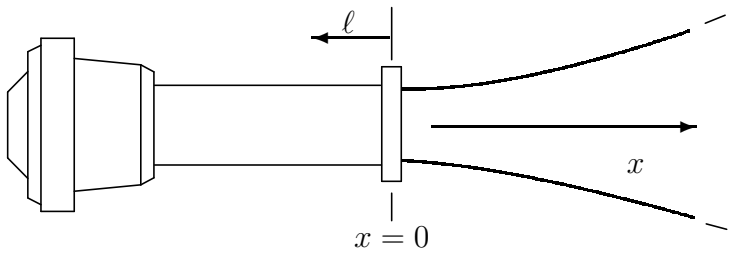

Figure 4.13: Section of standing wave tube placed between the compression horn driver and horn shown with the associated coordinate system used for derivations of the two-microphone method equations.

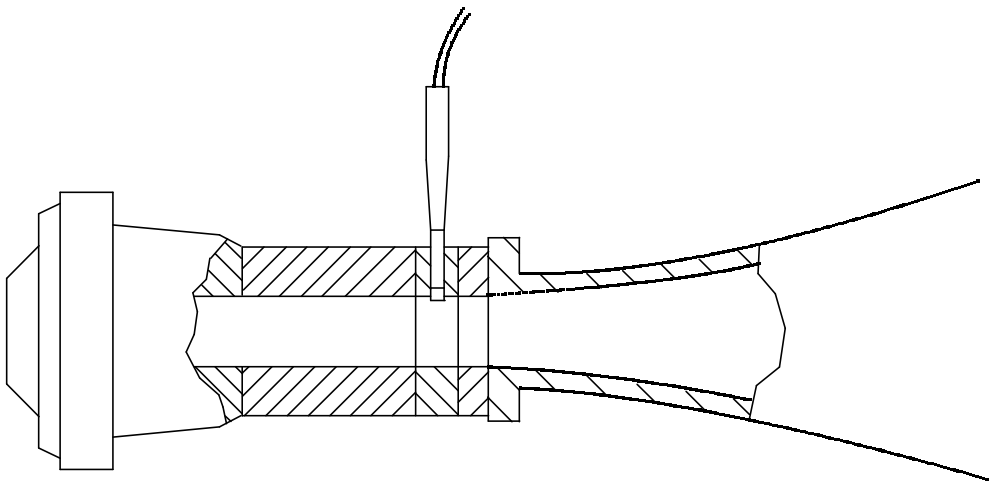

Figure 4.14: Two-microphone measurement system showing minimal length section of standing wave tube inserted between the compression horn driver and the throat of the horn. The microphone is shown in the first of two measurement locations. The spacer between microphone and horn throat is 3/8 in. thick, the plate containing the microphone is 1/2 in. thick, and the remaining section between the microphone and compression horn driver is 2 7/8 in. thick.

Figure 4.15: Photograph of the two-microphone measurement system showing minimal length section of standing wave tube inserted between the compression horn driver and the throat of the horn. The microphone is shown in the first of two measurement locations. The spacer between microphone and horn throat is 3/8 in. thick, the plate containing the microphone is 1/2 in. thick, the remaining section between the microphone and compression horn driver is 2 7/8 in. thick.

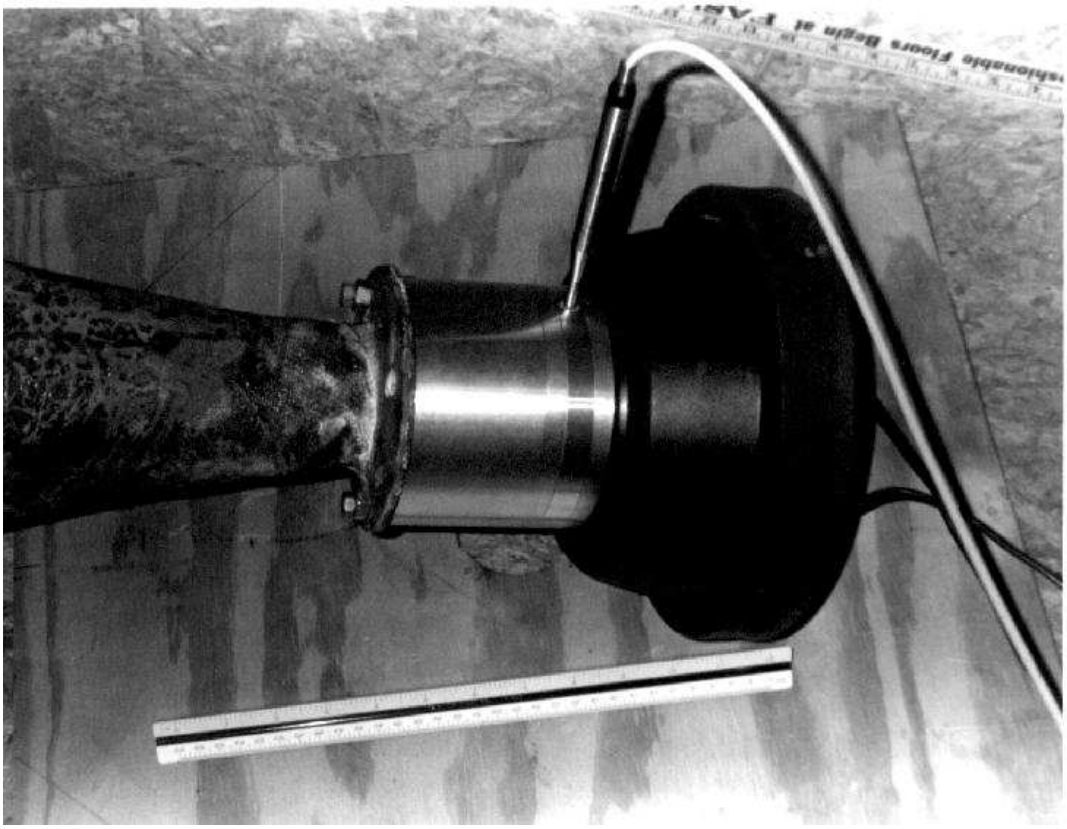

Figure 4.16: Photograph of the two-microphone measurement system showing minimal length section of standing wave tube inserted between the compression horn driver and the throat of the horn. The microphone is shown in the second of two measurement locations. The spacer between microphone and horn throat is 2 7/8 in. thick, the plate containing the microphone is 1/2 in. thick, the remaining section between the microphone and compression horn driver is 3/8 in. thick.

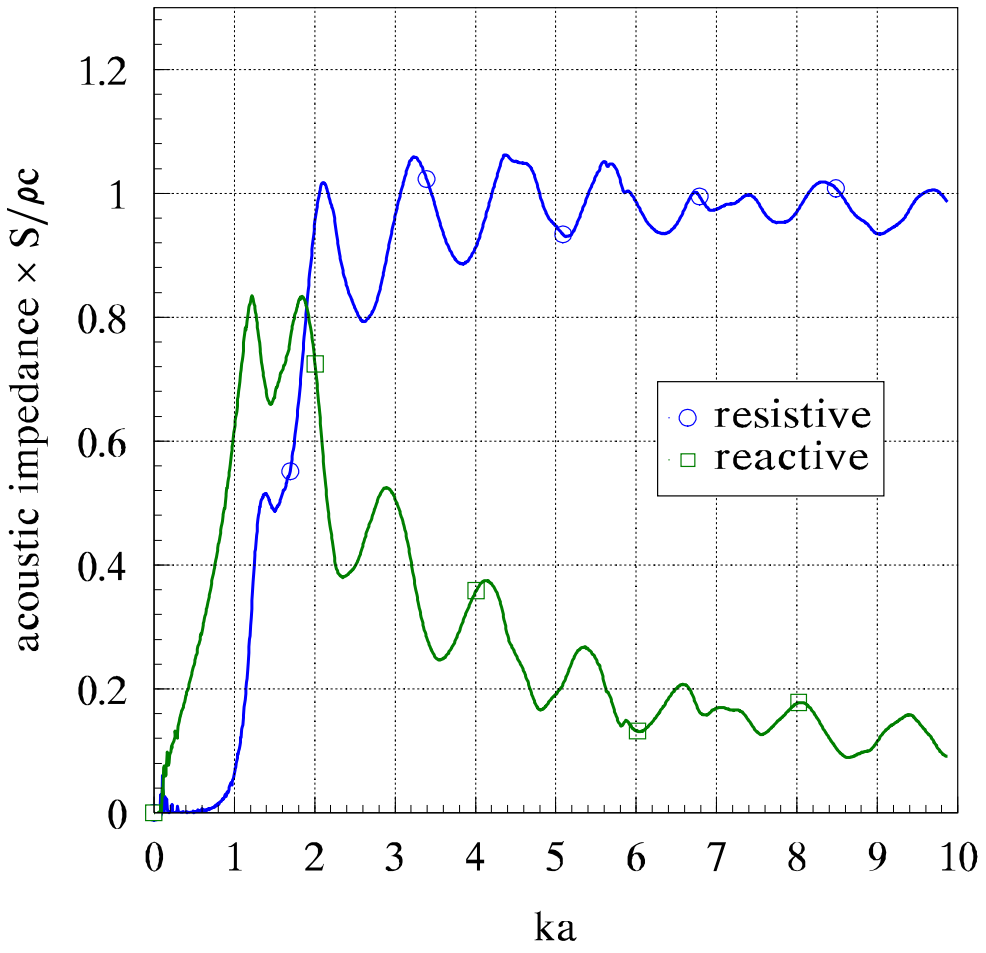

Figure 4.17: Measured acoustic impedance of the exponential horn using the two-microphone method. The impedance is normalized by $\rho_0 c_0/S$, and the mouth radius a of the horn is used in the normalized frequency ka. The actual frequency range spans from 0–2 kHz. The impedance has been scaled by 1.025 to compensate for the mismatch between the area of the minimized standing wave tube and the area of the exponential horn throat. Analyzer settings: 0–2 kHz bandlimited random noise source, 200 averages, 4096 point data frames resulting in 1601 frequency points.

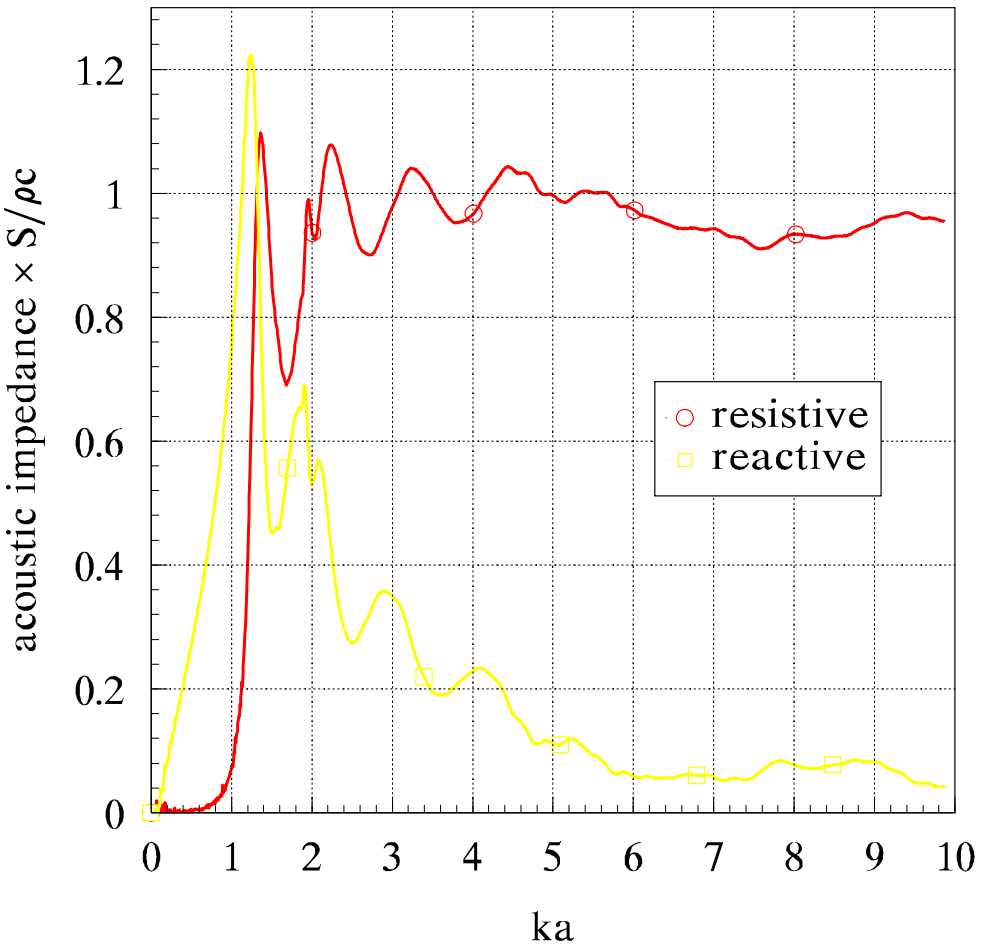

Figure 4.18: Measured acoustic impedance of the tractrix horn using the two-microphone method. The impedance is normalized by $\rho_0 c_0/S$, and the mouth radius a of the horn is used in the normalized frequency ka. The actual frequency range spans from 0–2 kHz. The impedance has been scaled by 0.9555 to compensate for the mismatch between the area of the minimized standing wave tube and the area of the tractrix horn throat. Analyzer settings: 0–2 kHz bandlimited random noise source, 200 averages, 4096 point data frames resulting in 1601 frequency points.

4.4 Comparison of Impedance Measurement Methods

To facilitate a comparison of the two methods used to measure the acoustic impedance, the results in the previous sections are plotted on the same graph. To increase the legibility of the graphs, the resistive and reactive components of the impedance have been separated.

Figures 4.19 and 4.20 show the comparison for the exponential horn. The agreement is good, especially so for the reactive portion of the impedance. The resistive component seems to be different by a constant scaling factor. The cause of the discrepancy is not clear, but could be the characteristics of the compression horn driver varying over the range of measurements performed. The low frequency range of the data shows more rapid changes in impedance for the "reaction on the source" method, which probably results from the anechoic termination used for calibration not behaving in a completely anechoic manner. Because the two-microphone method finds impedance directly, it was used to check the quality of the anechoic termination used to calibrate the "reaction on the source" method. Figure 4.21 shows that the anechoic termination is effectively anechoic above $ka = 0.5$ which corresponds to approximately 100 Hz. Although the deviations from purely resistive are small, the errors in the "reaction on the source" method are directly proportional to these deviations.

Figures 4.22 and 4.23 compare the two impedance measurement methods for the tractrix horn. The agreement is good, but just as in the case of the exponential horn, the reactive component agrees more closely than the resistive component of the impedance. Because the discrepancy between the two methods is similar for both horns, it can probably be calibrated out of the experiment if it is necessary to refine the "reaction on the source" technique.

Because the two-microphone method directly delivers the impedance data over a greater bandwidth than the "reaction on the source" method, it will be used for future comparisons in this work between experimental results

and numerical predictions. The "reaction on the source" method has certainly been shown to be a viable technique, and could be improved further by using a specially manufactured driver with a large electromechanical coupling coefficient ($B\ell$), and producing a calibration load that is more "anechoic."

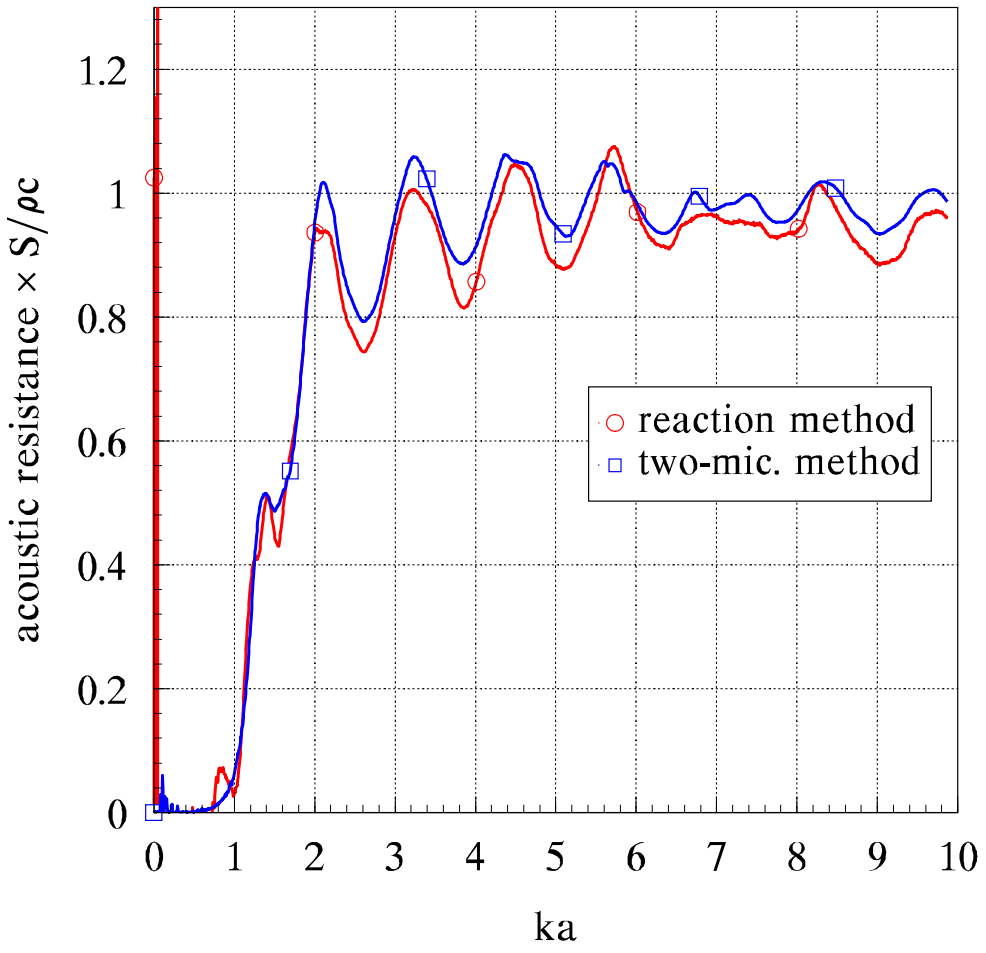

Figure 4.19: Comparison of the acoustic resistance of the exponential horn measured by both the "reaction on the source" method and the two-microphone method. The impedance is normalized by $\rho_0 c_0/S$ where S is the area of the throat of the horn; the mouth radius a is used in the normalized frequency ka. The actual frequency range of the measurement spans 0–2 kHz. The impedance has been scaled by 1.025 to compensate for the mismatch between the area of the minimized standing wave tube and the area of the horn throat. Analyzer settings: 0–2 kHz bandlimited random noise source, 200 averages, 4096 point data frames resulting in 1601 frequency points.

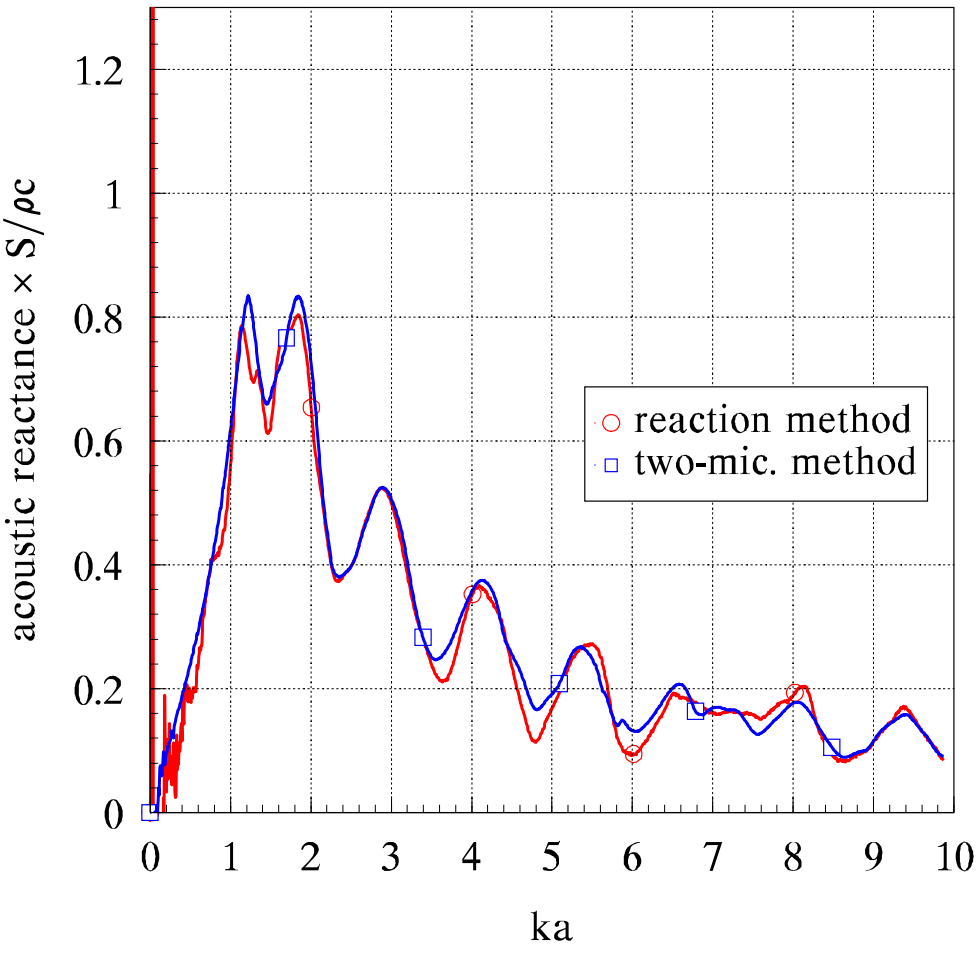

Figure 4.20: Comparison of the acoustic reactance of the exponential horn measured by both the "reaction on the source" method and the two-microphone method. The impedance is normalized by $\rho_0 c_0/S$ where S is the area of the throat of the horn; the mouth radius a is used in the normalized frequency ka. The actual frequency range of the measurement spans 0–2 kHz. The impedance has been scaled by 1.025 to compensate for the mismatch between the area of the minimized standing wave tube and the area of the horn throat. Analyzer settings: 0–2 kHz bandlimited random noise source, 200 averages, 4096 point data frames resulting in 1601 frequency points.

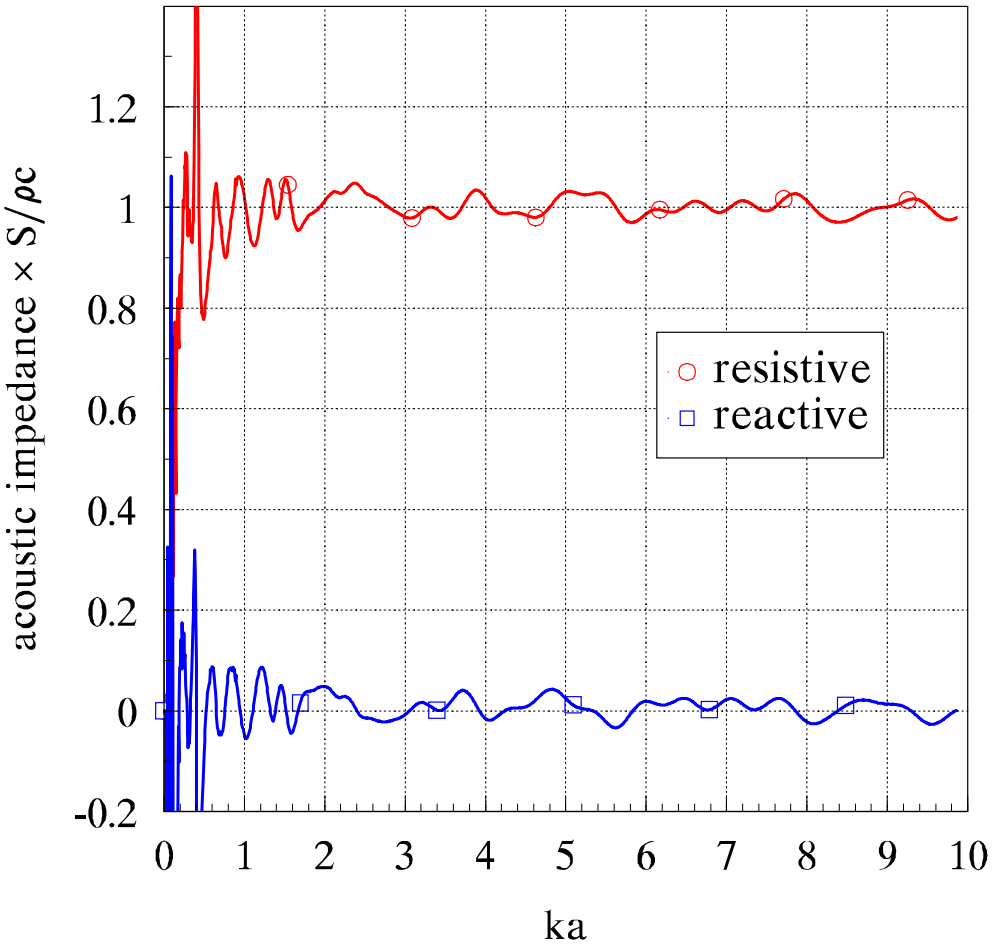

Figure 4.21: Acoustic impedance of "anechoic" termination, used for a calibration in the "reaction on the source" method. Measured using the two-microphone method. The mouth radius a of the horns is used to normalize the frequency ka for comparison. The actual frequency range of the measurement spans 0–2 kHz. Analyzer settings: 0–2 kHz bandlimited random noise source, 200 averages, 4096 point data frames resulting in 1601 frequency points.

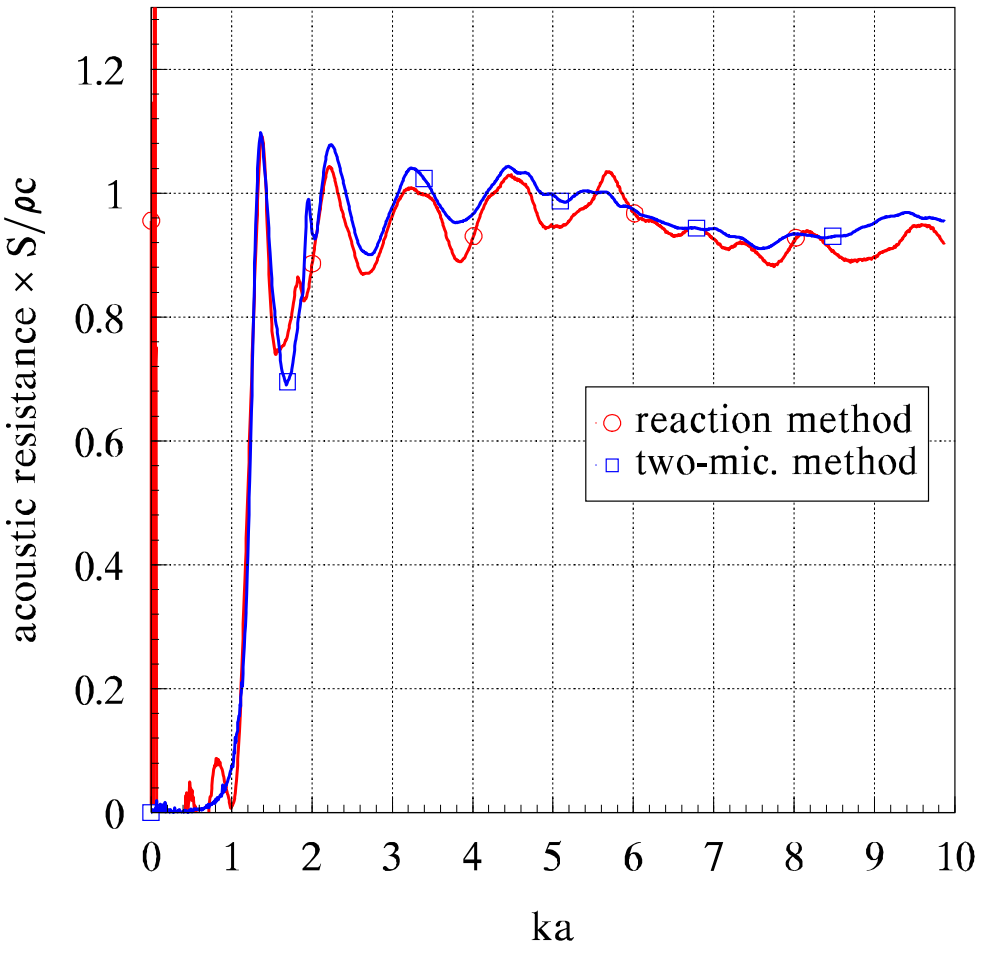

Figure 4.22: Comparison of the acoustic resistance of the tractrix horn measured by both the "reaction on the source" method and the two-microphone method. The impedance is normalized by $\rho_0 c_0/S$ where S is the area of the throat of the horn; the mouth radius a is used in the normalized frequency ka. The actual frequency range of the measurement spans 0–2 kHz. The impedance has been scaled by 0.9555 to compensate for the mismatch between the area of the minimized standing wave tube and the area of the horn throat. Analyzer settings: 0–2 kHz bandlimited random noise source, 200 averages, 4096 point data frames resulting in 1601 frequency points.

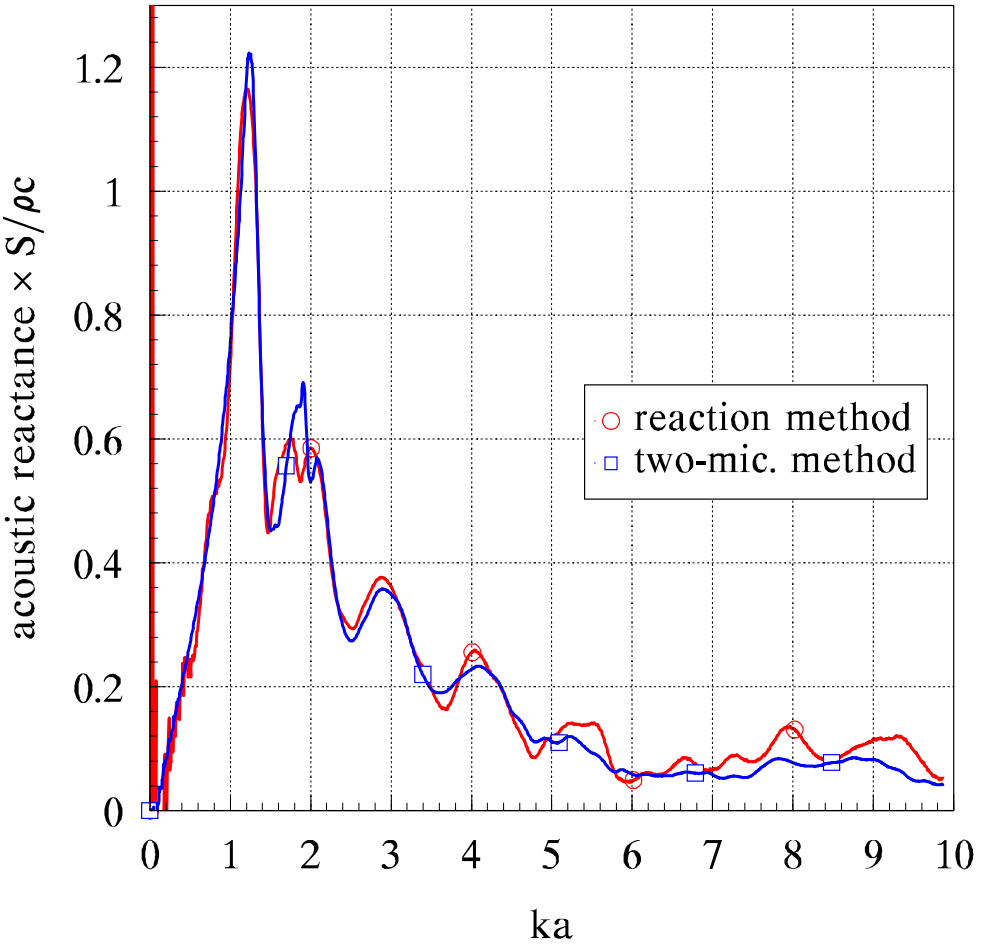

Figure 4.23: Comparison of the acoustic reactance of the tractrix horn measured by both the "reaction on the source" method and the two-microphone method. The impedance is normalized by $\rho_0 c_0/S$ where S is the area of the throat of the horn; the mouth radius a is used in the normalized frequency ka. The actual frequency range of the measurement spans 0–2 kHz. The impedance has been scaled by 0.9555 to compensate for the mismatch between the area of the minimized standing wave tube and the area of the horn throat. Analyzer settings: 0–2 kHz bandlimited random noise source, 200 averages, 4096 point data frames resulting in 1601 frequency points.

4.4.1 Comparison of Numerical Model with Measurement

The performance of the boundary element model has been previously evaluated in Chapter 3 by solving the problem of a rigid piston in an infinite baffle, which has a known analytical solution. The usefulness of such a tool is, of course, in finding numerical solutions to problems which do not have a known analytical solution. The exponential and tractrix horns are two examples which must be solved numerically. Both horns were modeled by discretizing the surface of the rigid walls of the horn with quadratic elements, as shown in figure 3.4. Because no exact solution exists for comparison, the number of quadratic elements was gradually increased until the numerical results ceased to change in any significant way. This limit was reached by using 180 elements. An additional increase in quadratic elements to 350 resulted in only subtle changes in the impedance results or the directivity patterns, so the numerical method is said to be "converged" in the sense that additional refinement of the model gridding will not result in significant changes in the results. The computed impedance of the exponential horn is shown in figure 4.24. It is interesting to note that the resistive component of the impedance remains significant at the cutoff frequency, $ka = 1.15$, where it has the value of 0.21 while the reactive component dominates at 0.79 but not to the degree expected. The computed impedance of the tractrix horn is shown in figure 4.25. At the cutoff frequency, the resistive component at 0.27 is slightly greater than that of the exponential horn. The reactance is also increased at a value of 1.02 compared to the value of 0.79 for the exponential horn.

Figures 4.26 and 4.27 display the measured and computed impedance of the exponential horn. The resistive and reactive components have been separated to improve the legibility of the results. The measured and computed data show a marked agreement. Mechanical resonances in the horn cause some deviation in the range $ka > 6$, but these could in principle be removed by stiff-

ening the walls of the horn. The other discrepancies can easily be attributed to the lack of mechanical tolerance in the dimensions of the horn, which was constructed by hand. Figures 4.28 and 4.29 display the measured and computed impedance of the tractrix horn, again with the resistive and reactive components separated to improve legibility. The agreement is good, but not nearly as good as for the exponential horn. This lack of agreement was the motivation for increasing the number of quadratic elements in the numerical model from 180 to 350, but no significant change resulted in the computed value of the impedance. At this point, the dimensions of the actual horn tested became suspect; unfortunately it is difficult to make accurate measurements of the interior dimensions of a horn. The error in the throat diameter has been previously accounted for, and the dimension of the mouth was accurate to within 2 mm. The remaining dimension of the horn that is easily measured is the length of the wall contour, which was measured and found to be 1.25 cm (2%) longer than designed. This may not seem to be an error of appreciable magnitude, but note that the difference between the arc lengths of the tractrix and exponential horns shown in figure 4.2 is only 2%, and the measured impedance of the two horns is quite different. Viewed in this manner, it is surprising that the measured impedance does not vary even more from the computed value.

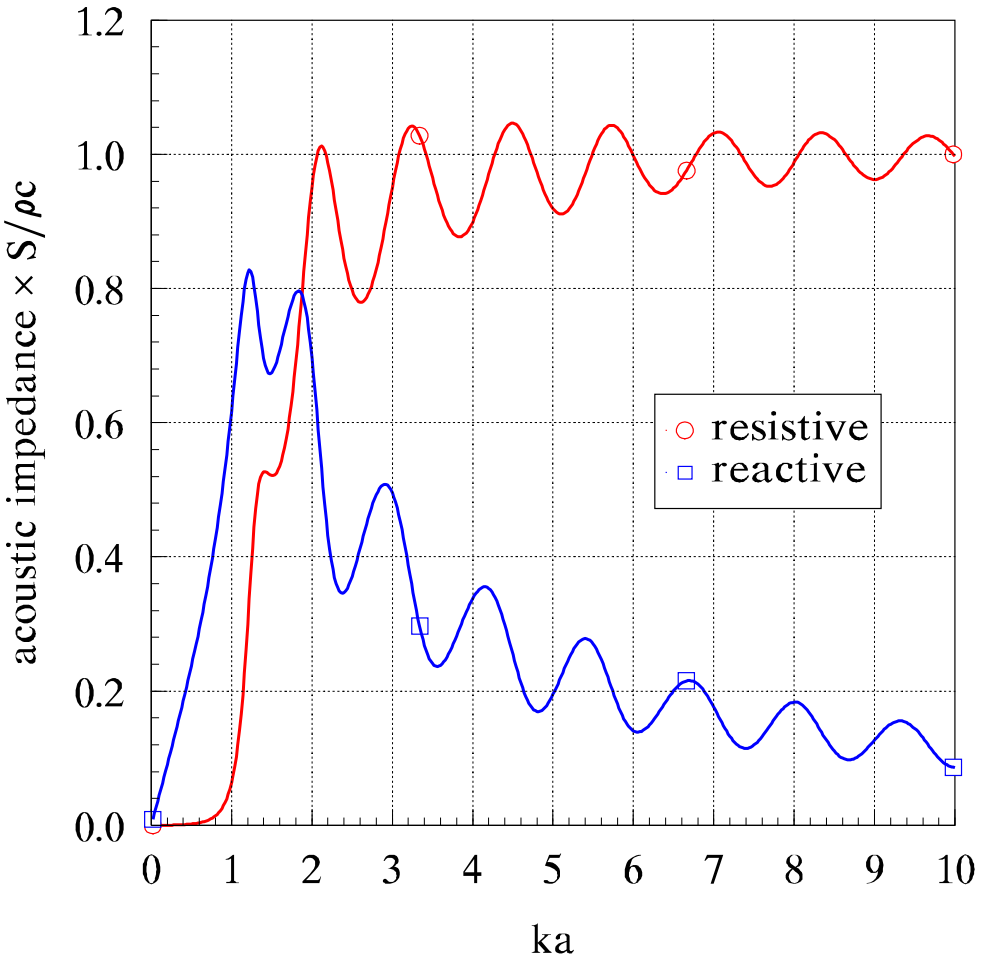

Figure 4.24: Acoustical impedance of the exponential horn computed by the boundary element method. The impedance is normalized by $\rho_0 c_0/S$ where S is the area of the throat of the horn; the mouth radius a is used in the normalized frequency ka. Program parameters: 350 quadratic elements with 12 point Gaussian quadrature rule per element. Number of terms in series expansion of the potential on impedance sphere was dynamically chosen based on values used for rigid, baffled piston. Computation time: 79.6 hours on a Convex C-220 for 500 frequency points. Note: 180 quadratic element model gives essentially identical results in 22.4 hours for 200 points on a 80486/66 MHz microcomputer.

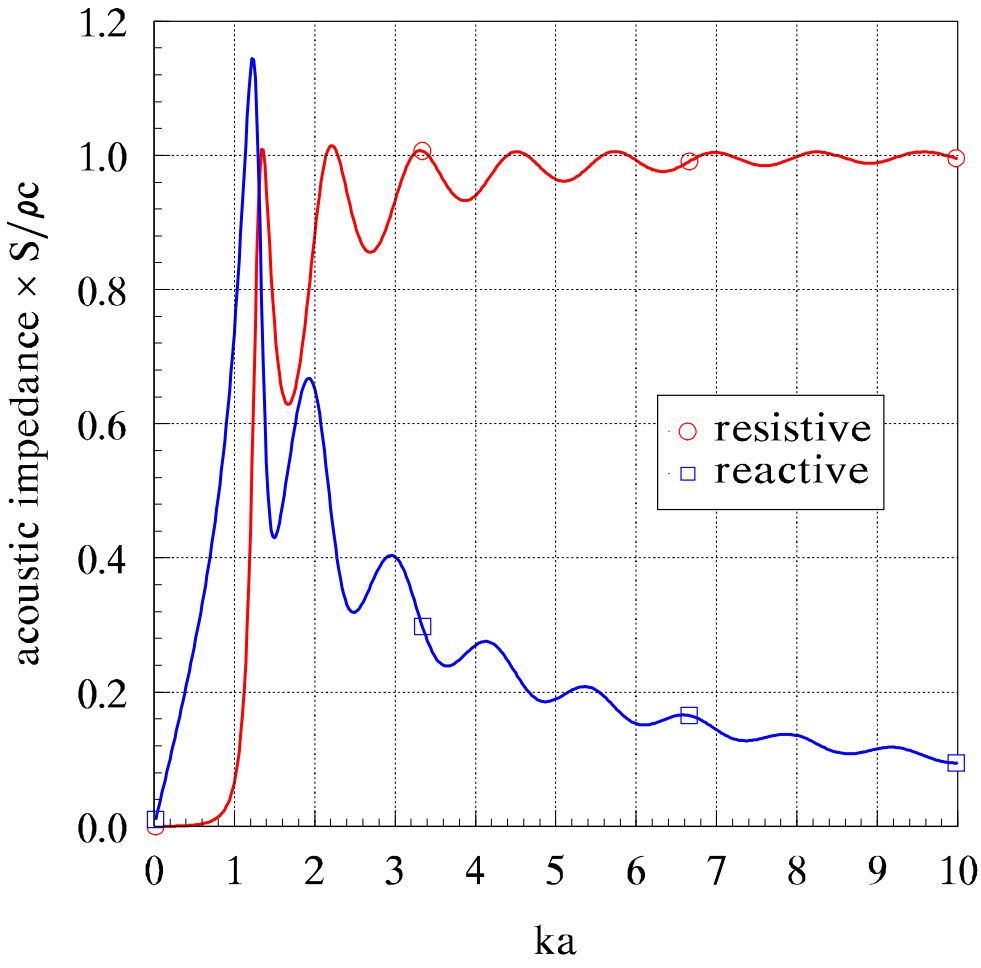

Figure 4.25: Acoustical impedance of the tractrix horn computed by the boundary element method. The impedance is normalized by $\rho_0 c_0/S$ where S is the area of the throat of the horn; the mouth radius a is used in the normalized frequency ka. Program parameters: 350 quadratic elements with 12 point Gaussian quadrature rule per element. Number of terms in series expansion of the potential on the impedance sphere were dynamically chosen based on values used for rigid, baffled piston. Computation time: 79.6 hours on a Convex C-220 for 500 frequency points. Note: 180 quadratic element model gives essentially identical results in 22.4 hours for 200 points on a 80486/66 MHz microcomputer.

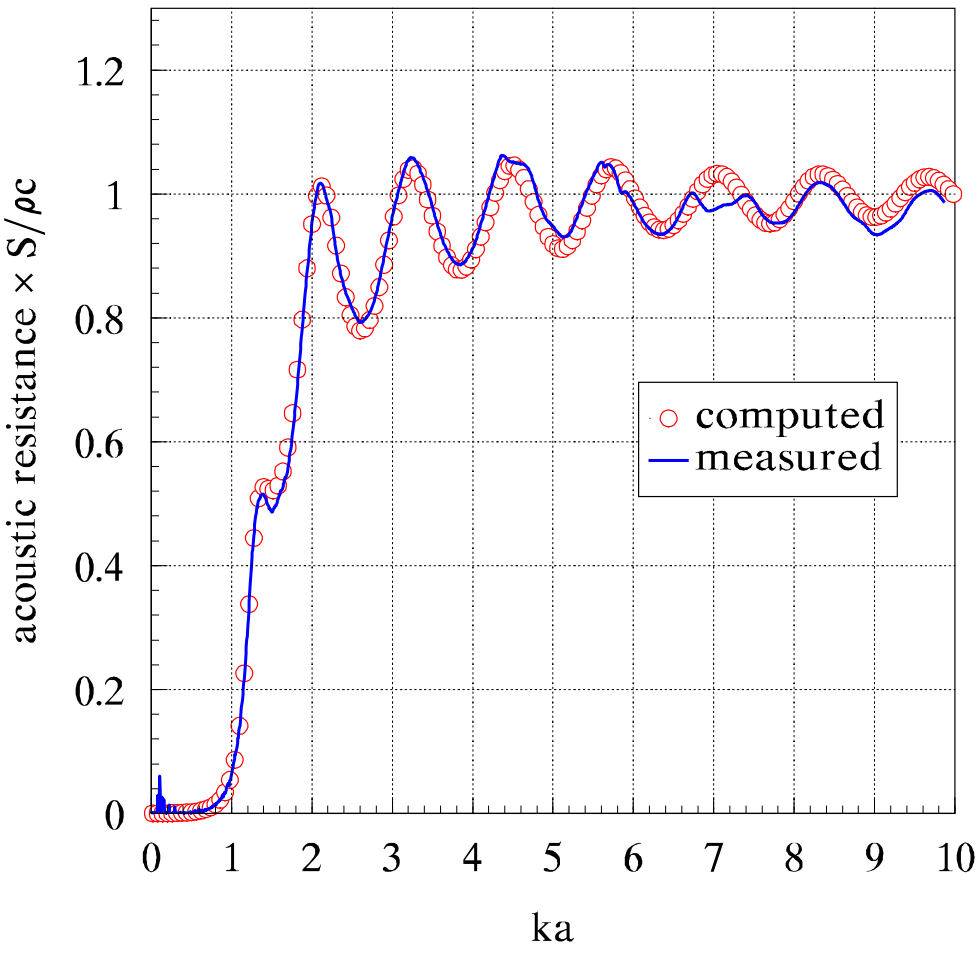

Figure 4.26: Comparison of the measured and computed acoustic resistance of the exponential horn. The two-microphone technique was used in the measurement. Analyzer settings: 0–2 kHz bandlimited random noise source, 200 averages, 4096 point data frames resulting in 1601 frequency points. Program parameters: 350 quadratic elements with 12 point Gaussian quadrature rule per element. Number of terms in series expansion of the potential on the impedance sphere were dynamically chosen based on values used for rigid, baffled piston. Computation time: 26.6 hours on a Convex C-220 for 166 frequency points. Note: 180 quadratic element model gives essentially identical results in 18.6 hours on a 80486/66 MHz microcomputer.

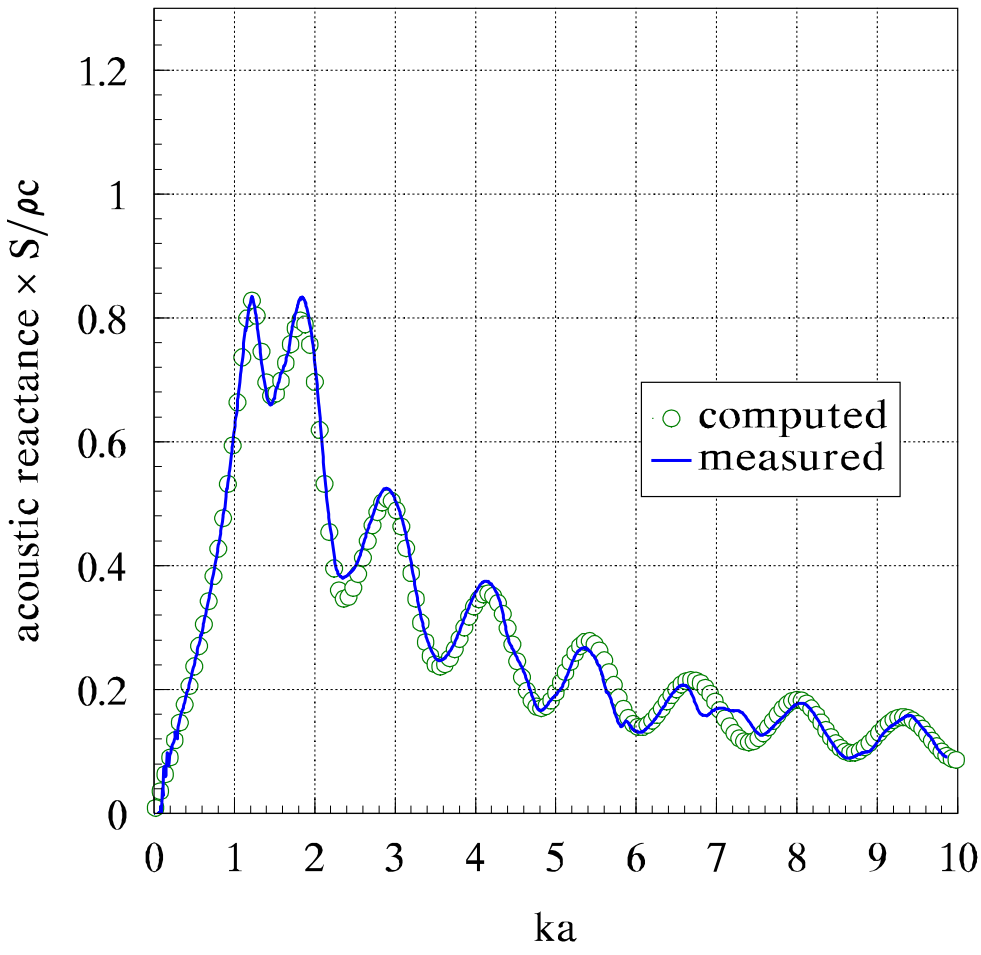

Figure 4.27: Comparison of the measured and computed acoustic reactance of the exponential horn. The two-microphone technique was used in the measurement. Analyzer settings: 0–2 kHz bandlimited random noise source, 200 averages, 4096 point data frames resulting in 1601 frequency points. Program parameters: 350 quadratic elements with 12 point Gaussian quadrature rule per element. Number of terms in series expansion of the potential on the impedance sphere were dynamically chosen based on values used for rigid, baffled piston. Computation time: 26.6 hours on a Convex C-220 for 166 frequency points. Note: 180 quadratic element model gives essentially identical results in 18.6 hours on a 80486/66 MHz microcomputer.

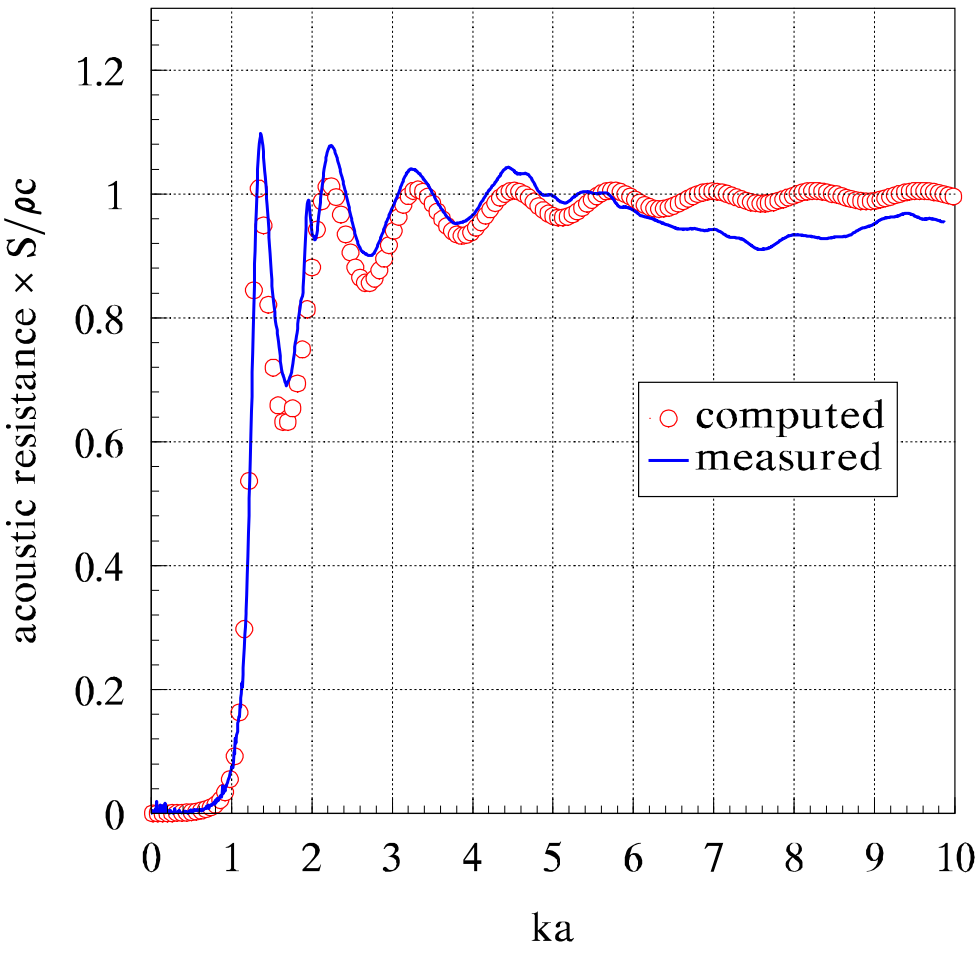

Figure 4.28: Comparison of the measured and computed acoustic resistance of the tractrix horn. The two-microphone technique was used in the measurement. Analyzer settings: 0–2 kHz bandlimited random noise source, 200 averages, 4096 point data frames resulting in 1601 frequency points. Program parameters: 350 quadratic elements with 12 point Gaussian quadrature rule per element. Number of terms in series expansion of the potential on the impedance sphere were dynamically chosen based on values used for rigid, baffled piston. Computation time: 26.6 hours on a Convex C-220 for 166 frequency points. Note: 180 quadratic element model gives essentially identical results in 18.6 hours on a 80486/66 MHz microcomputer.

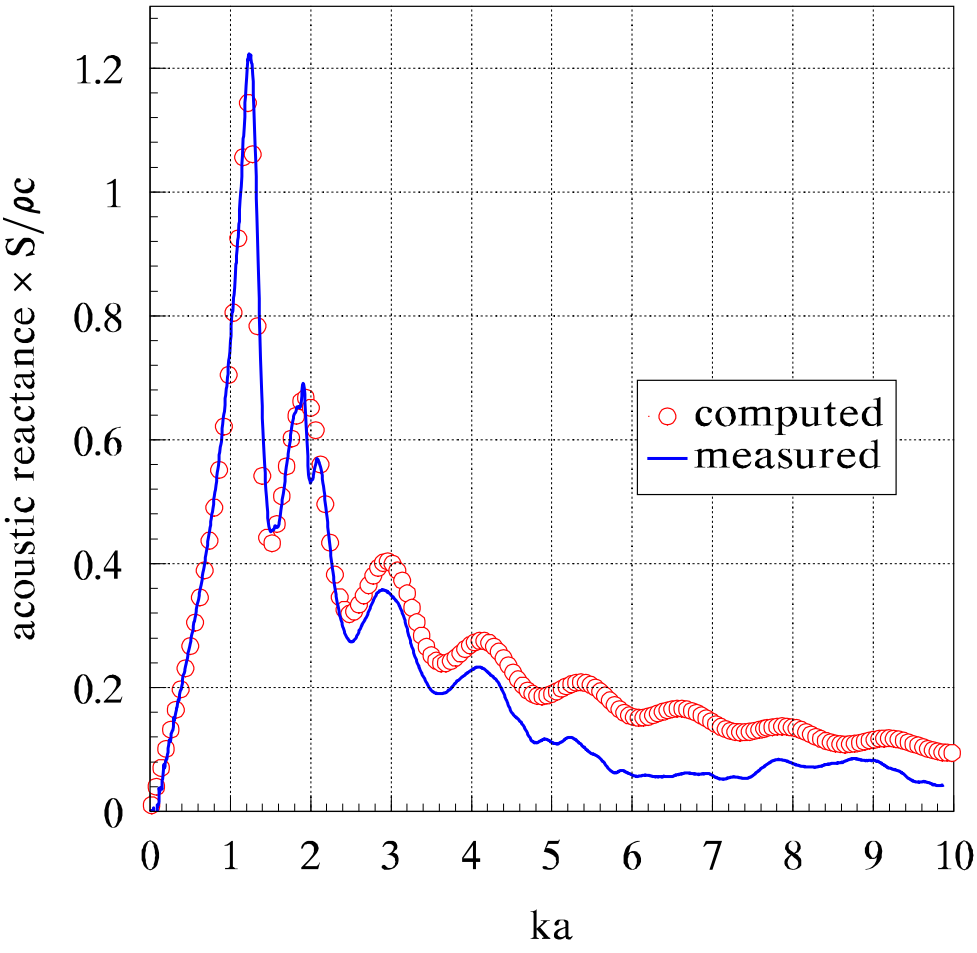

Figure 4.29: Comparison of the measured and computed acoustic reactance of the tractrix horn. The two-microphone technique was used in the measurement. Analyzer settings: 0–2 kHz bandlimited random noise source, 200 averages, 4096 point data frames resulting in 1601 frequency points. Program parameters: 350 quadratic elements with 12 point Gaussian quadrature rule per element. Number of terms in series expansion of the potential on the impedance sphere were dynamically chosen based on values used for rigid, baffled piston. Computation time: 26.6 hours on a Convex C-220 for 166 frequency points. Note: 180 quadratic element model gives essentially identical results in 18.6 hours on a 80486/66 MHz microcomputer.

4.4.2 Plane-Wave Results

This dissertation is meant to extend the current methods of horn analysis, but those readers who are familiar with plane-wave horn theory may be curious how plane-wave results compare to those of the boundary element method, which are practically exact. While plane-wave theory cannot predict the directivity of a horn, it can predict the throat impedance with negligible effort relative to that required by the boundary element method. Because the efficiency is so great, it is of interest to understand what loss in accuracy results from using a plane-wave model. The loss in accuracy may be acceptable in many applications considering the high cost of improving the solution *via* the boundary element method.

Webster's equation admits an exact solution in the case of an exponential horn, so the throat impedance of the exponential horn will be used in the following comparisons rather than the throat impedance of the tractrix horn. The throat impedance of an exponential horn is [35]

$$Z_1 = \frac{\rho_0 c_0}{S_1}\left[\frac{Z_2\cos(k\ell-\theta)+j\sin(k\ell)}{jZ_2\sin(k\ell)+[\rho_0 c_0/S_2]\cos(k\ell+\theta)}\right] \tag{4.18}$$

where ℓ is the length of the horn, $\theta \equiv \text{atan}(\alpha/k)$, S_1 the throat area, and S_2 the area of the mouth. The flare-rate α is defined in the expression for the cross-sectional area of the exponential horn, $S(x) = S_1 e^{2\alpha x}$. The wave number is represented by k. The terminating impedance Z_2 can be approximated by the lumped-element piston impedance model given by Beranek [85, page 121],

$$Z_2 = \left\{[j\omega M_{\text{A1}}]^{-1} + \left[R_{\text{A2}} + \left\{R_{\text{A1}}^{-1} + j\omega C_{\text{A1}}\right\}^{-1}\right]^{-1}\right\}^{-1} \tag{4.19}$$

where $R_{\text{A1}} = .1404\rho_0 c_0/a^2$, $R_{\text{A2}} = \rho_0 c_0/\pi a^2$, $C_{\text{A1}} = 5.94a^3/\rho_0 c_0^2$, and $M_{\text{A1}} = 8\rho_0/3\pi^2 a$. The radius of the mouth of the horn is taken to be the radius a used in the piston impedance function above.

The resistive and reactive components of the throat impedance computed by the plane-wave model are plotted in figures 4.30 and 4.31 respectively, along with the results from the boundary element model. Qualitatively, the agreement is surprising considering the crudeness of the approximations involved in the plane-wave model. Olson [53] found that the directivity of exponential horns is roughly equivalent to that of a piston for a frequency range extending to the frequency at which the circumference of the horn mouth is equal to a wavelength. This condition occurs when $ka = 1.15$ in figures 4.30 and 4.31. Indeed the plane-wave approximation is in close agreement for frequencies up to $ka = 1.2$ as Olson predicts. In the frequency range $1 < ka < 2$, the behavior of the terminating impedance at the mouth of the horn is more complicated than that predicted by a piston impedance model. The complicated behavior in this region is probably a result of the horn being relatively short with a rapid flare.

For $ka > 2$, the primary difference between the plane-wave results and the boundary element results is the spacing of the ripples in the impedance data. Webster's model underestimates the effective length of the horn, which causes the spacing in the ripples to increase. The effective length of the horn can be increased by considering the expanding wavefront area to be curved rather than planer. The type of modifications necessary to Webster's model have been described by Holland, Fahy, and Morfey [185], but further work with one-dimensional models in this dissertation would be too great of a digression, and will not be pursued.

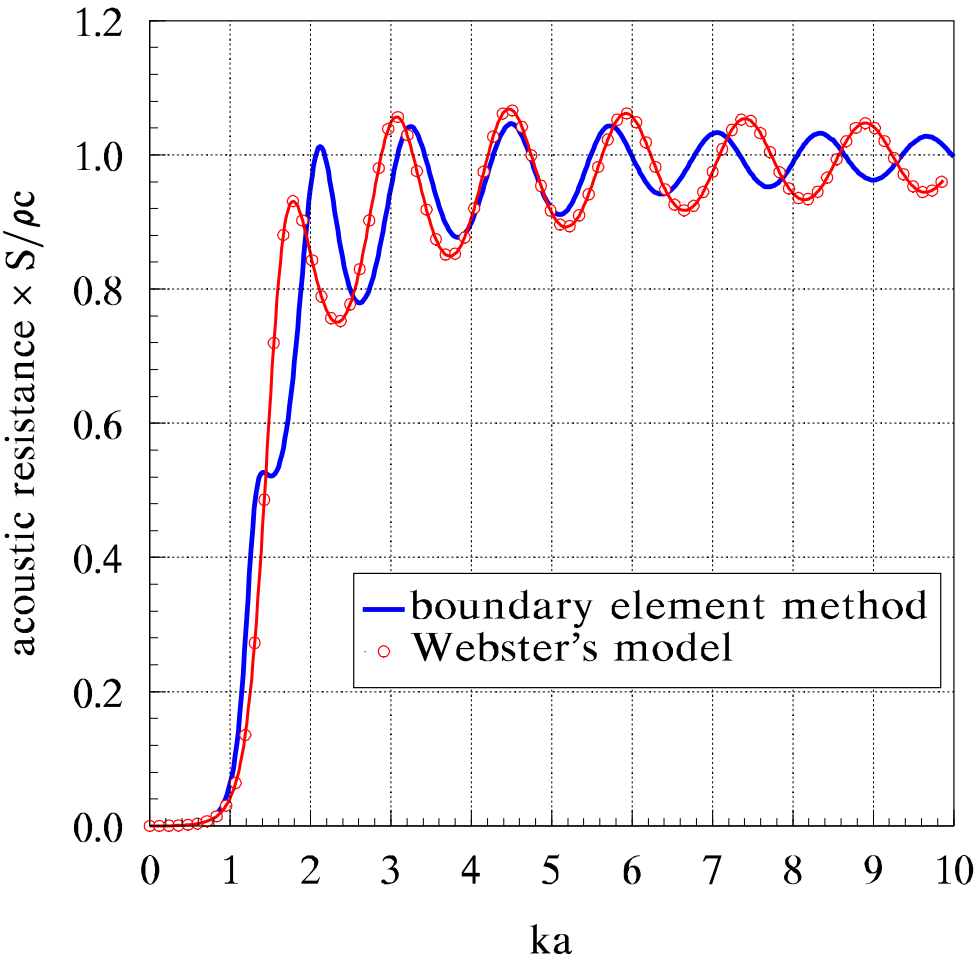

Figure 4.30: Acoustic resistance at the throat of the exponential horn as computed from Webster's plane-wave model and by the boundary element method. The plane-wave model approximates the terminating impedance at the horn mouth by a simplified (lumped-element) piston impedance function.

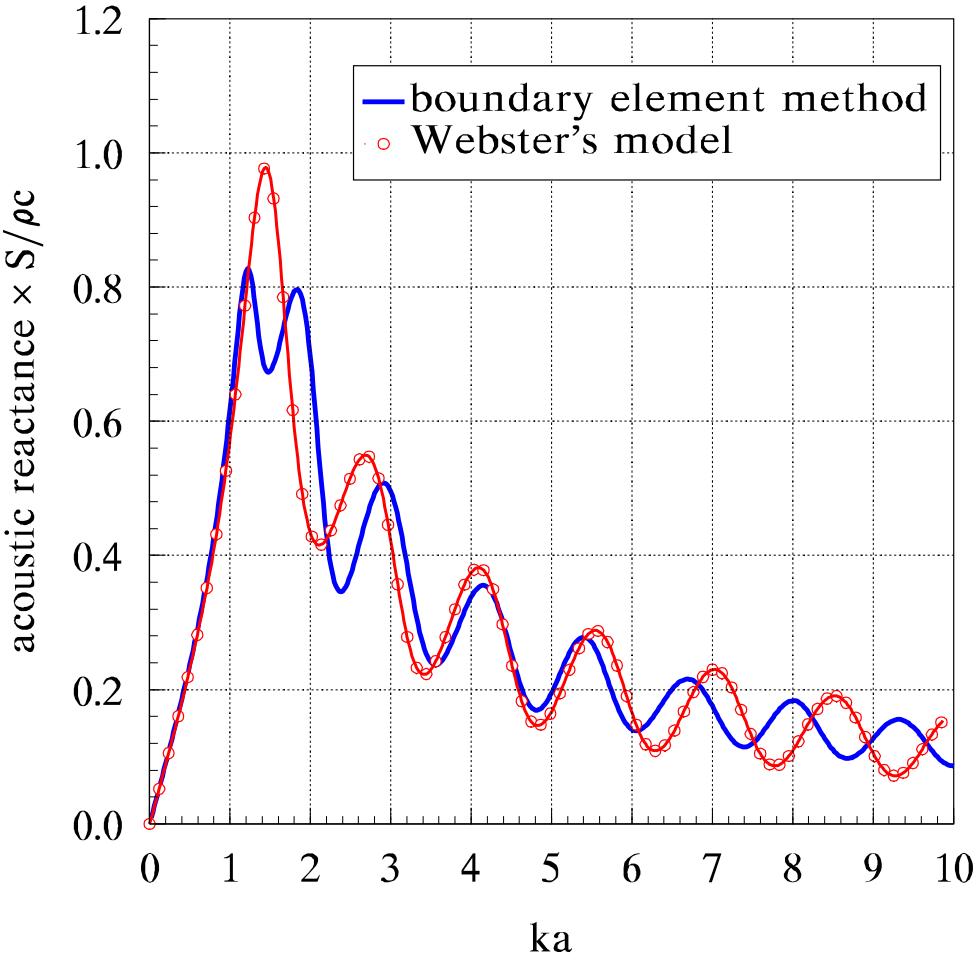

Figure 4.31: Acoustic reactance at the throat of the exponential horn as computed from Webster's plane-wave model and by the boundary element method. The plane-wave model approximates the terminating impedance at the horn mouth by a simplified (lumped-element) piston impedance function.

4.5 Predicting the Far-Field Radiation Pattern

The driving point impedance of acoustic horns is an important design criterion, but the far-field directivity is probably of greater importance. The current generation of horns has been largely designed using empirical data, which is difficult to gather, and leads to design rules which do not extend well to other types of horns. Clearly it would be a great advantage in the design process to have the ability to accurately predict the directivity of a particular horn without the actual construction and testing of a prototype.

In this section, the far-field directivity of the exponential and tractrix horns will be measured, and the results compared to those computed *via* the boundary element method. Measuring the directivity of an acoustic horn is inconvenient because of the large distance required between the horn and the microphone element before the "far field" is actually reached. The measurements are traditionally taken on outdoor ranges, but these suffer from exposure to the natural elements, and external sources of noise. To avoid the problems associated with an outdoor range, details for calculating the far-field directivity from measurements in the near-field are described in this section. Calculating the far-field directivity from near-field measurements is not new in the area of microwave antennas, where the technique has been in use since the early 1970's [177].

The first step in the near-field measurement technique is to place over the mouth of the horn a fictitious hemisphere. The pressure in the half-space external to this hemisphere can be written ([144], page 319)

$$p(r,\theta) = \sum_{n=0}^{\infty} B_n h_{2n}^{(2)}(kr) P_{2n}(\cos\theta), \tag{4.20}$$

where $h_{2n}^{(2)}(kr)$ is the spherical Hankel function of the second kind of order $2n$ (corresponding to outgoing radiation for $e^{j\omega t}$ time convention), $P_{2n}(\cos\theta)$ the

Legendre polynomial of order $2n$, and B_n a coefficient in the series. The superscript (2) in the Hankel functions will be implicitly assumed hereafter. To find the coefficients in the series expansion for the pressure, multiply equation (4.20) by P_{2m} and integrate over the interval $0 \leq x \leq 1$ (where $x = \cos\theta$) using the orthogonality relationship,

$$\int_0^1 P_{2m}(x)P_{2n}(x)dx = \begin{cases} 0 & \text{for } m \neq n, \\ \dfrac{1}{4n+1}, & \text{for } m = n. \end{cases} \tag{4.21}$$

This yields

$$B_n = \frac{4n+1}{h_{2n}(ka)} \int_0^1 p(a, \text{acos}x)P_{2n}(x)dx \tag{4.22}$$

which can be substituted into equation (4.20) to give the pressure at any location outside the fictitious hemisphere. To compute the pressure in the far field, use the relation ([81], page 1573)

$$\lim_{kr\to\infty} h_{2n}^{(2)}(kr) = [-1]^n \frac{e^{-jkr}}{-jkr} \tag{4.23}$$

in equation (4.20) to write the asymptotic value of p,

$$p(r,\theta) \Rightarrow \left[\sum_{n=0}^{\infty} B_n[-1]^n P_{2n}(\cos\theta)\right] \frac{e^{-jkr}}{-jkr}. \tag{4.24}$$

In practice the number of terms in the series is limited to that necessary for a sufficiently accurate representation of the pressure.

The on-axis, far-field frequency response of the horns is shown in figures 4.32 and 4.33. Although both compare quite well with the computed values, the tractrix does less so than the exponential horn. Below $ka = 4$, the ripples in the frequency response from diffraction at the mouth of the exponential horn can be seen in both prediction and measurement. The response of the tractrix horn is notably smoother in this region because the taper at the mouth meets the baffle without making an edge. This decrease in diffraction has been previously documented in measurements of a high-frequency tractrix

horn [171]. The ripples in the measured responses above $ka = 4$ are likely to be caused by the structural resonances in the horn walls.

The far-field directivity is plotted for several values of ka in figures 4.34–4.41. The fact that the exponential horn agrees more closely with numerical predictions can once again be attributed to closer tolerances in the mechanical construction. At a normalized frequency of $ka = 24$, resonances in the horn cause noticeable ripples in the pressure at the extreme, off-axis angles.

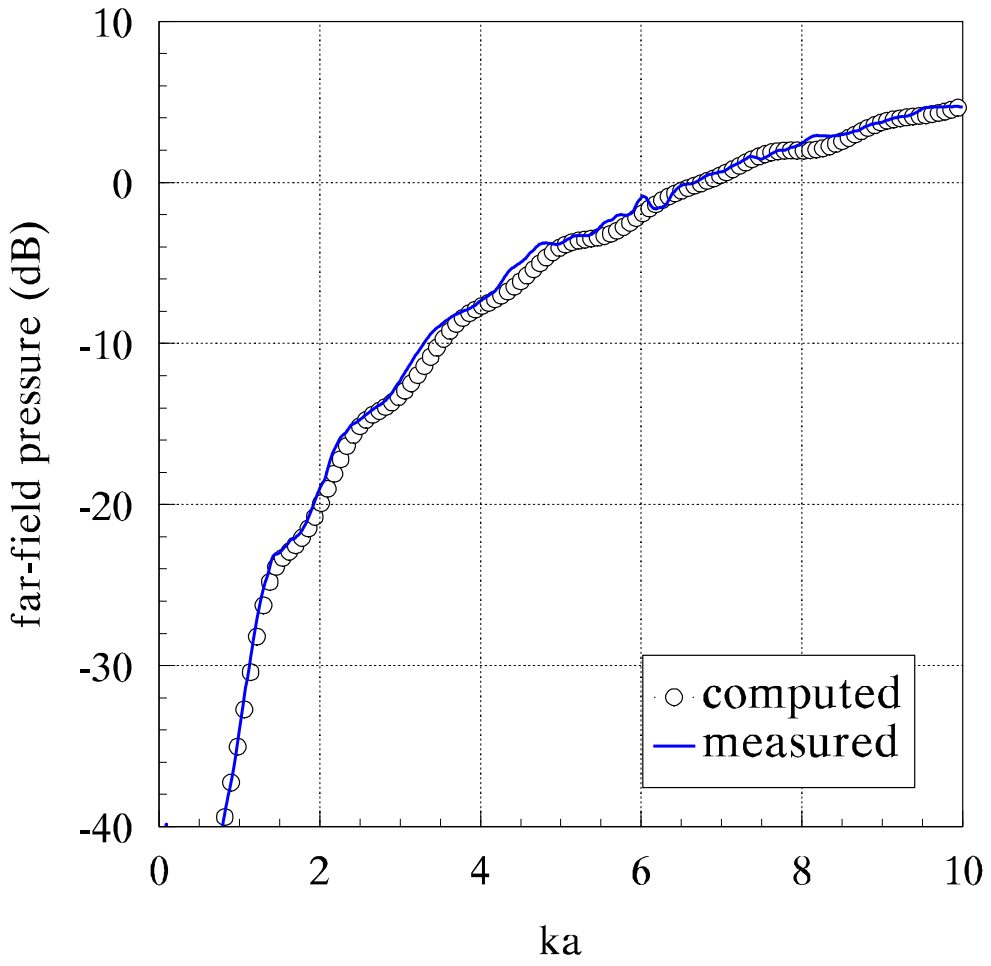

Figure 4.32: Far-field, on-axis frequency response of the exponential horn with respect to pressure at the throat of the horn. Measured far-field response calculated from near-field data. The mouth radius a is used in the normalized frequency ka. Actual frequency range of measurement: 0–2 kHz. Analyzer settings: 0–2 kHz bandlimited random noise source, 30 averages, 4096 point data frames resulting in 1601 frequency points. Program parameters: 350 quadratic elements with 12 point quadrature rule per element. Number of terms in series expansion of the potential on the impedance sphere were dynamically chosen based on values used for rigid, baffled piston. Computation time: 20.0 hours on a Convex C-220 for 125 frequency points. Note: 180 quadratic element model gives essentially identical results in 14.0 hours on a 80486/66 MHz microcomputer.

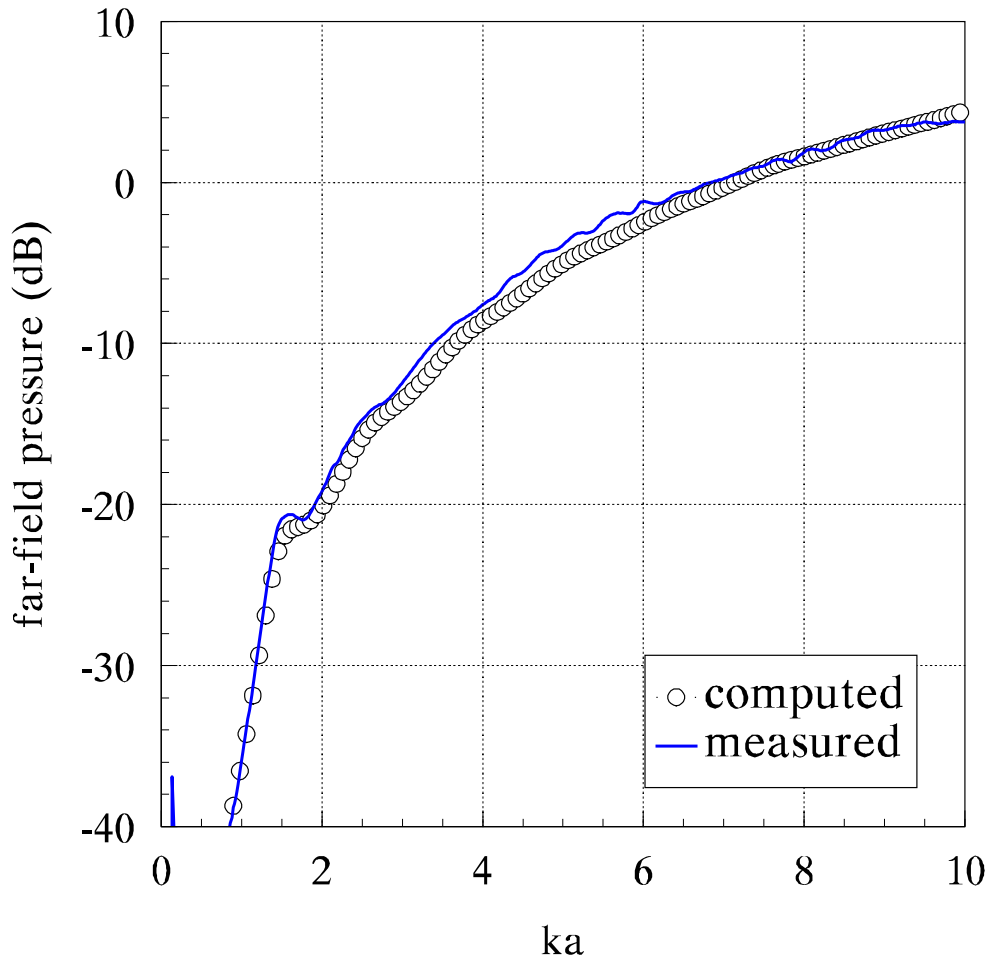

Figure 4.33: Far-field, on-axis frequency response of the tractrix horn with respect to pressure at the throat of the horn. Measured far-field response calculated from near-field data. The mouth radius a is used in the normalized frequency ka. Actual frequency range of measurement: 0–2 kHz. Analyzer settings: 0–2 kHz bandlimited random noise source, 30 averages, 4096 point data frames resulting in 1601 frequency points. Program parameters: 350 quadratic elements with 12 point quadrature rule per element. Number of terms in series expansion of the potential on the impedance sphere were dynamically chosen based on values used for rigid, baffled piston. Computation time: 20.0 hours on a Convex C-220 for 125 frequency points. Note: 180 quadratic element model gives essentially identical results in 14.0 hours on a 80486/66 MHz microcomputer.

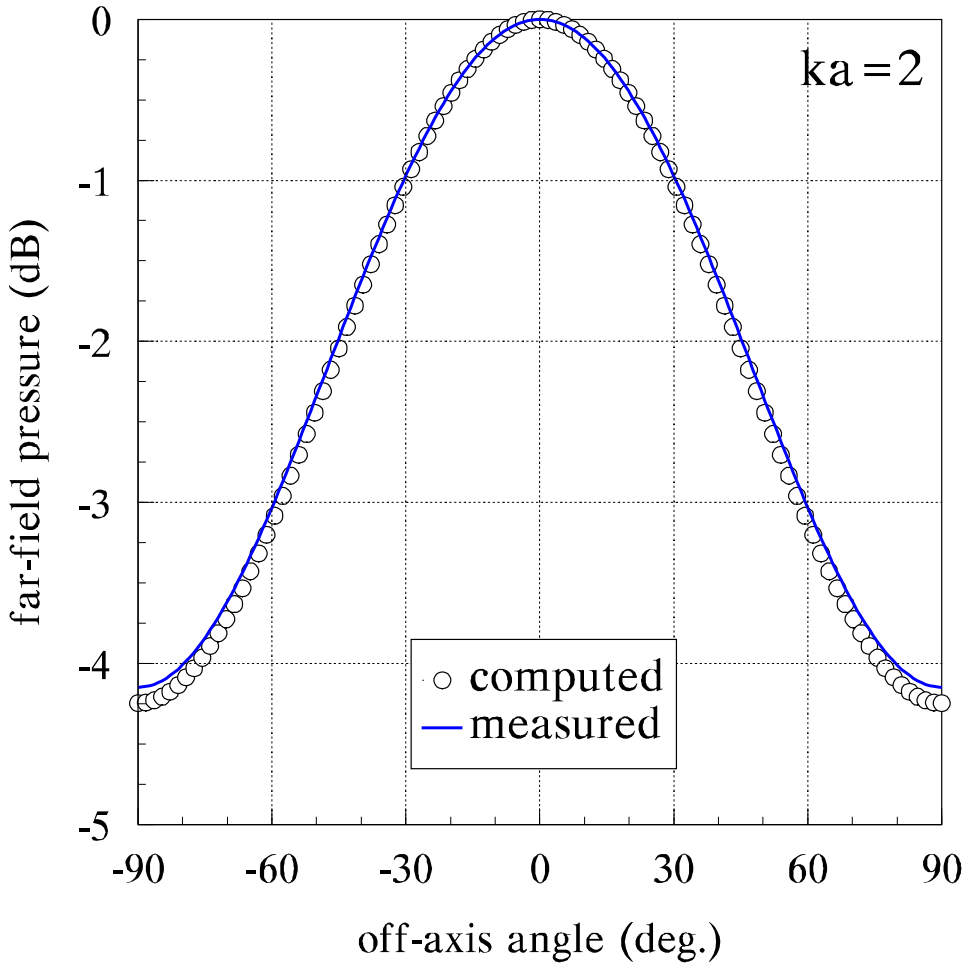

Figure 4.34: Far-field directivity of the exponential horn at $ka = 2$. The measured far-field directivity was calculated from near-field data. The mouth radius a is used in the normalized frequency ka. The actual frequency of the measurement is 405 Hz. Analyzer settings: 0–2 kHz bandlimited random noise source, 30 averages, 4096 point data frames resulting in 1601 frequency points. Program parameters: 180 quadratic elements with 12 point Gaussian quadrature rule per element, 11 terms in series expansion of potential on the impedance sphere with 12 point Gaussian quadrature rule. Computation time: 10.5 minutes on a 80486/33 MHz microcomputer.

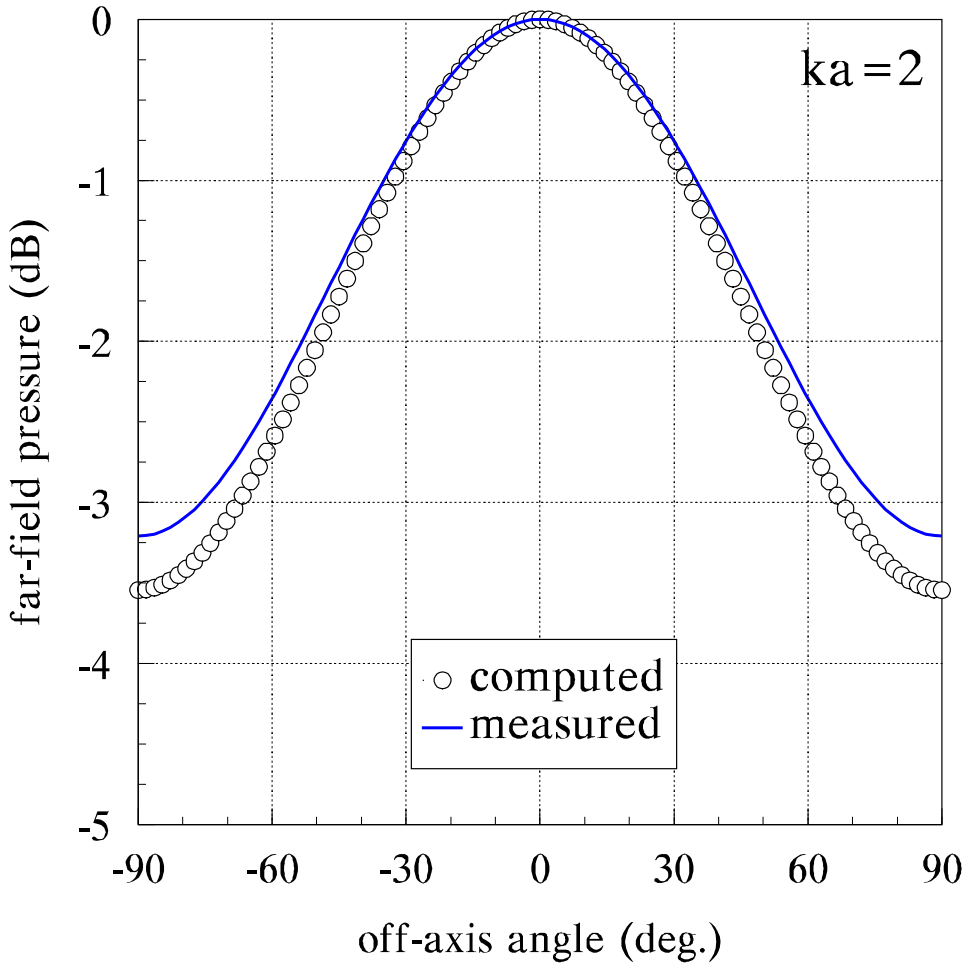

Figure 4.35: Far-field directivity of the tractrix horn at $ka = 2$. The measured far-field directivity was calculated from near-field data. The mouth radius a is used in the normalized frequency ka. The actual frequency of the measurement is 405 Hz. Analyzer settings: 0–2 kHz bandlimited random noise source, 30 averages, 4096 point data frames resulting in 1601 frequency points. Program parameters: 180 quadratic elements with 12 point Gaussian quadrature rule per element, 11 terms in series expansion of potential on the impedance sphere with 12 point Gaussian quadrature rule. Computation time: 10.5 minutes on a 80486/33 MHz microcomputer.

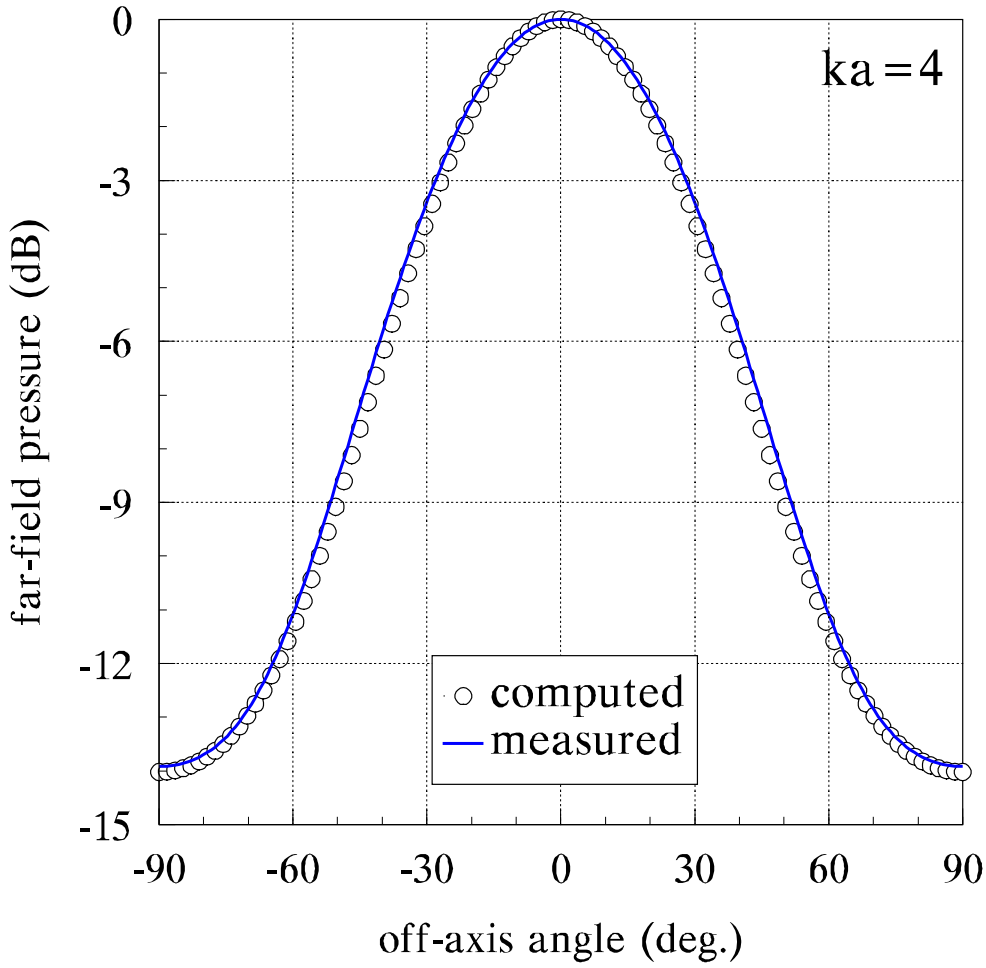

Figure 4.36: Far-field directivity of the exponential horn at $ka = 4$. The measured far-field directivity was calculated from near-field data. The mouth radius a is used in the normalized frequency ka. The actual frequency of the measurement is 810 Hz. Analyzer settings: 0–2 kHz bandlimited random noise source, 30 averages, 4096 point data frames resulting in 1601 frequency points. Program parameters: 180 quadratic elements with 12 point Gaussian quadrature rule per element, 14 terms in series expansion of potential on the impedance sphere with 15 point Gaussian quadrature rule. Computation time: 13.0 minutes on a 80486/33 MHz microcomputer.

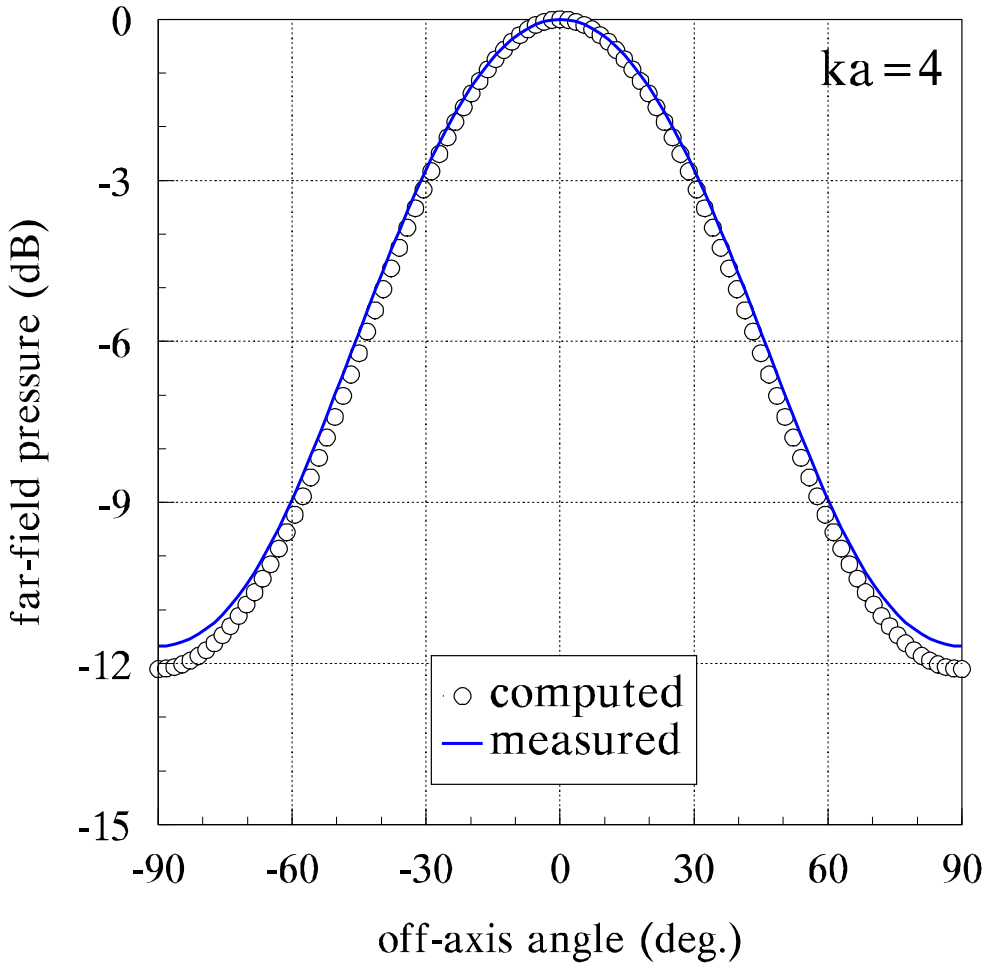

Figure 4.37: Far-field directivity of the tractrix horn at $ka = 4$. The measured far-field directivity was calculated from near-field data. The mouth radius a is used in the normalized frequency ka. The actual frequency of the measurement is 810 Hz. Analyzer settings: 0–2 kHz bandlimited random noise source, 30 averages, 4096 point data frames resulting in 1601 frequency points. Program parameters: 180 quadratic elements with 12 point Gaussian quadrature rule per element, 14 terms in series expansion of potential on the impedance sphere with 15 point Gaussian quadrature rule. Computation time: 13.0 minutes on a 80486/33 MHz microcomputer.

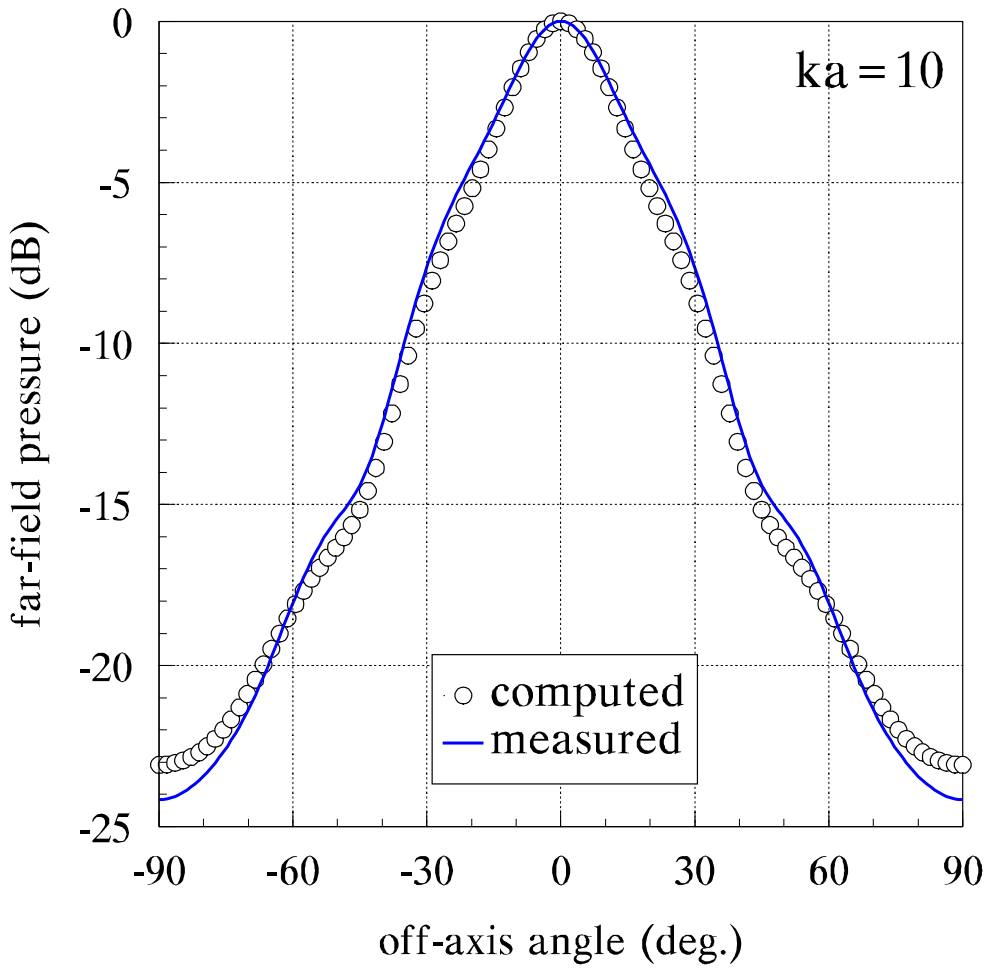

Figure 4.38: Far-field directivity of the exponential horn at $ka = 10$. The measured far-field directivity was calculated from near-field data. The mouth radius a is used in the normalized frequency ka. The actual frequency of the measurement is 2026 Hz. Analyzer settings: 0–2 kHz bandlimited random noise source, 30 averages, 4096 point data frames resulting in 1601 frequency points. Program parameters: 180 quadratic elements with 12 point Gaussian quadrature rule per element, 19 terms in series expansion of potential on the impedance sphere with 20 point Gaussian quadrature rule. Computation time: 17.9 minutes on a 80486/33 MHz microcomputer.

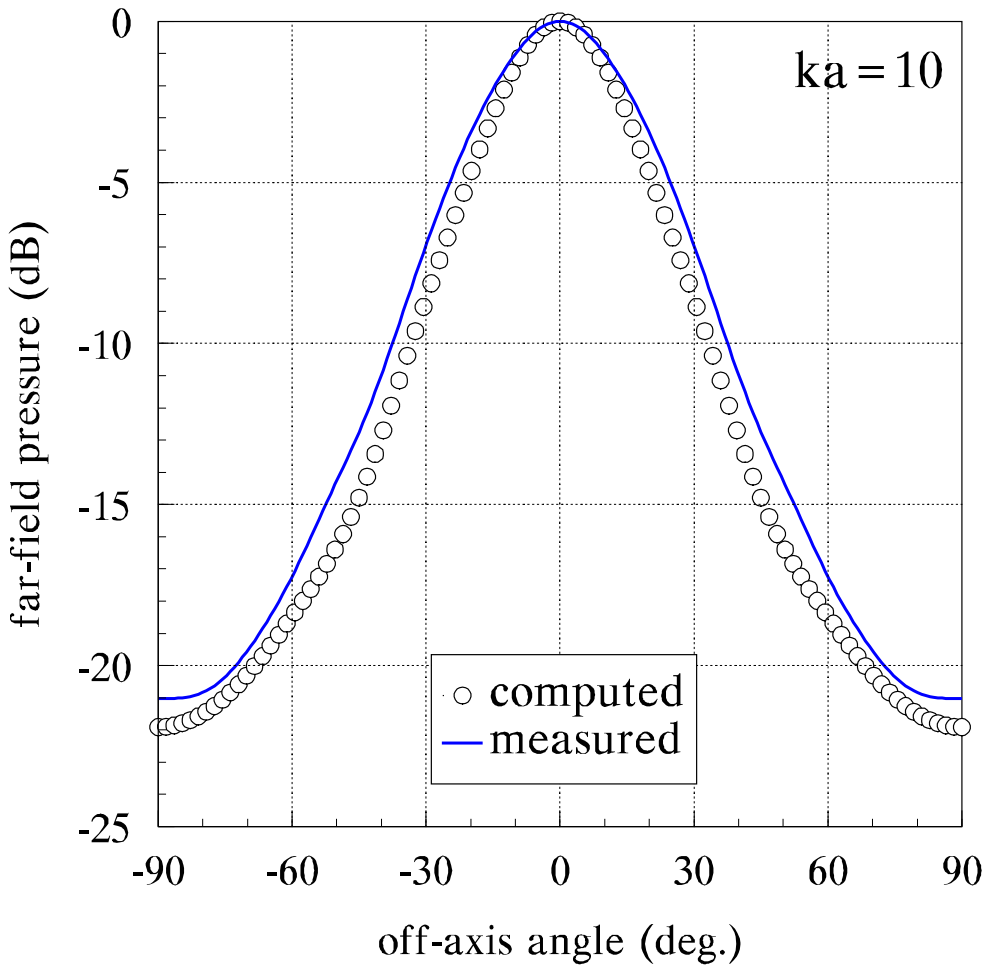

Figure 4.39: Far-field directivity of the tractrix horn at $ka = 10$. The measured far-field directivity was calculated from near-field data. The mouth radius a is used in the normalized frequency ka. The actual frequency of the measurement is 2026 Hz. Analyzer settings: 0–2 kHz bandlimited random noise source, 30 averages, 4096 point data frames resulting in 1601 frequency points. Program parameters: 180 quadratic elements with 12 point Gaussian quadrature rule per element, 19 terms in series expansion of potential on the impedance sphere with 20 point Gaussian quadrature rule. Computation time: 17.9 minutes on a 80486/33 MHz microcomputer.

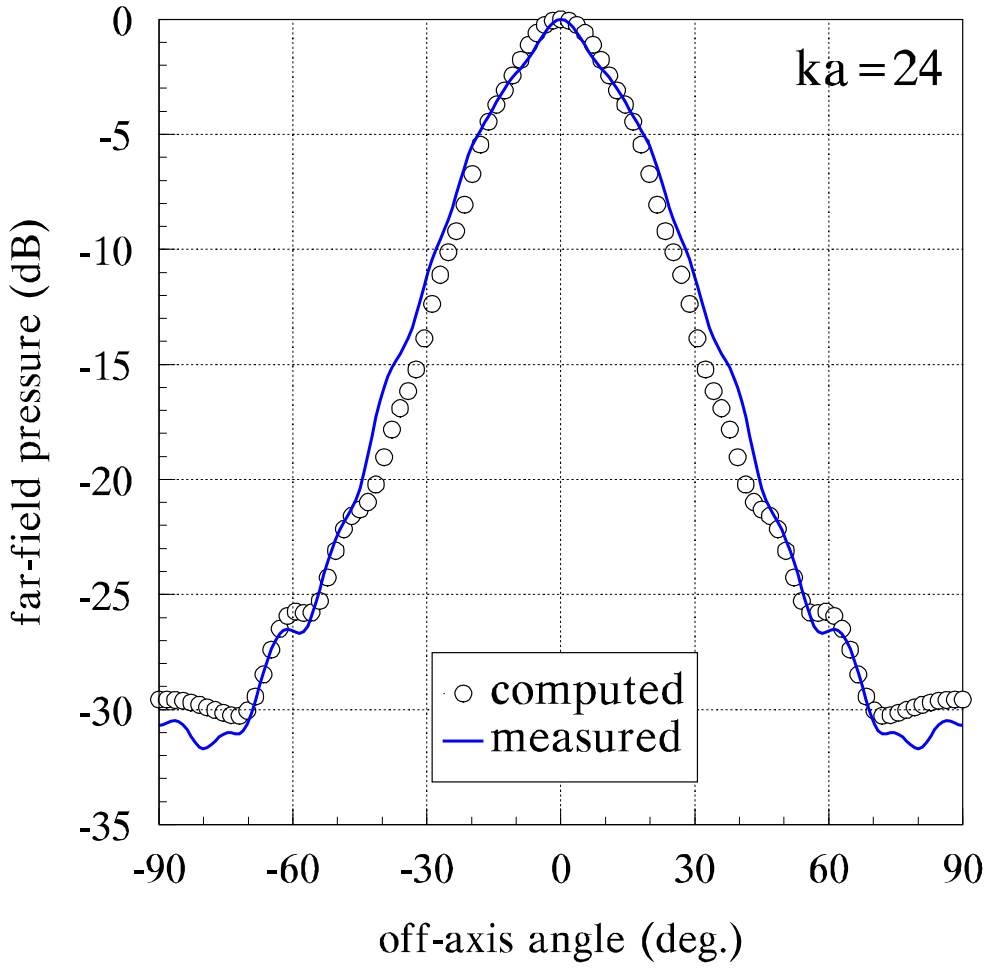

Figure 4.40: Far-field directivity of the exponential horn at $ka = 24$. The measured far-field directivity was calculated from near-field data. The mouth radius a is used in the normalized frequency ka. The actual frequency of the measurement is 4863 Hz. Analyzer settings: 0–2 kHz bandlimited random noise source, 30 averages, 4096 point data frames resulting in 1601 frequency points. Program parameters: 180 quadratic elements with 12 point Gaussian quadrature rule per element, 35 terms in series expansion of potential on the impedance sphere with 36 point Gaussian quadrature rule. Computation time: 28.1 minutes on a 80486/33 MHz microcomputer.

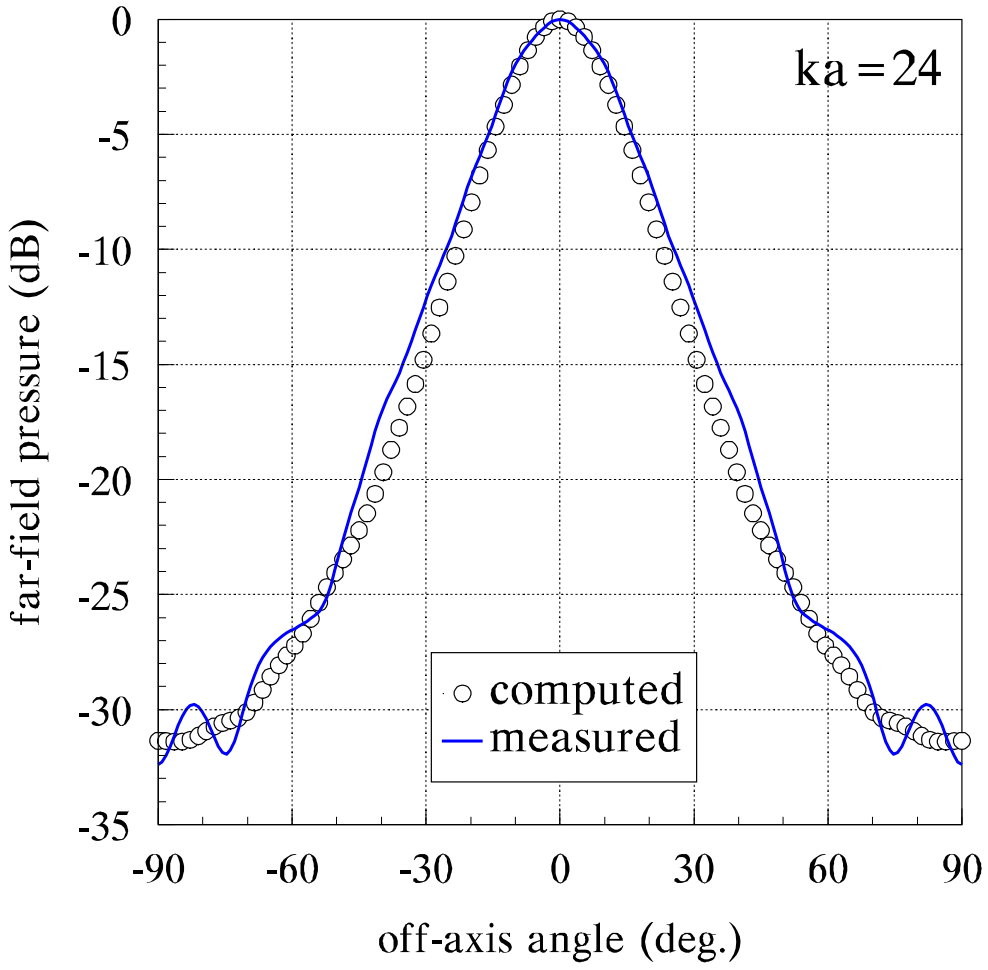

Figure 4.41: Far-field directivity of the tractrix horn at $ka = 24$. The measured far-field directivity was calculated from near-field data. The mouth radius a is used in the normalized frequency ka. The actual frequency of the measurement is 4863 Hz. Analyzer settings: 0–2 kHz bandlimited random noise source, 30 averages, 4096 point data frames resulting in 1601 frequency points. Program parameters: 180 quadratic elements with 12 point Gaussian quadrature rule per element, 35 terms in series expansion of potential on the impedance sphere with 36 point Gaussian quadrature rule. Computation time: 28.1 minutes on a 80486/33 MHz microcomputer.

Chapter 5

Concluding Remarks

Rayleigh's technique as presented here has met with some difficulty and the results that seem quite possible from it have not been achieved. The method has been expanded and clarified as compared to Rayleigh's original exposition, and future developments should be more readily achievable as a result of this work. The idea for a more accurate rate of area expansion has been presented however, and would extend the range of applicability for Webster's horn equation if successful.

A new formulation of the boundary element method has been developed for radiation problems that can be modeled as if they were in an infinite baffle. This formulation avoids the uniqueness difficulties associated with exterior formulations of the boundary element method typically used in radiation problems. This method has been used to solve the problem of a rigid piston in an infinite baffle and is extremely accurate in simultaneously predicting the driving point impedance and the far-field directivity.

Two techniques for measuring acoustic impedance have been developed and compared. The methods show relatively good agreement, but the reaction on the source technique of measuring impedance has been found to be more difficult and less accurate than the new implementation of the two-microphone technique. The implementation of the two-microphone technique that has been described is easy to use, yet extremely accurate and precise.

The concept of a near-field range has been introduced into acoustic testing of horns. The method has been shown to be very accurate and easy to implement. Using the near-field range simplifies the measurement of far-field directivity considerably by eliminating exposure to the natural elements and external sources of noise.

The throat impedance and directivity of the tractrix and exponential horns have been measured and compared. Contrary to long-standing beliefs, the exponential horn was not found to demonstrate optimal low-frequency loading or directivity control. The tractrix horn displayed greater resistive and less reactive loading than the exponential horn. It is also apparent that the rapid flare at the mouth of the tractrix horn results in smaller reflections, which leads to a more monotonic throat impedance. The impedance of the exponential horn contained much larger "ripples," which are a result of the abrupt termination at the mouth. The smooth flare at the mouth of the tractrix horn also resulted in decreased diffraction which yields a smoother on-axis frequency response, and a smoother directivity pattern. The comparison of the horn measurements with predictions by the boundary element method program has revealed the importance of maintaining tolerances in the horn design.

5.1 Suggestions for Further Study

Rayleigh's method for solving the wave equation within a tapered waveguide has merit and warrants further study. Because the method includes the mode conversion resulting from the change in cross-sectional area of the waveguide, the method has the potential to yield an accurate approximation of the rate of area expansion to be used in Webster's horn equation. This expansion rate will be frequency dependent and would extend the useful frequency range of Webster's model.

The boundary element method presented in this work can be extended

in a straightforward manner to rectangular horns. The rectangular horn will require a two-dimensional element such as a nine-noded quadrilateral, and the associated Legendre polynomials would have to be used to represent the potential on the impedance sphere. The symmetry of a rectangular horn is such that only one quadrant of the horn need be modeled.

The robustness of the boundary element method should be explored. It is of practical importance to know the relative affect of the various numerical parameters on the accuracy of the solution. The maximum efficiency of the technique cannot be exploited until this is known. Although it is expected that the parameters would be problem dependent, certain "rules" could probably be established for particular problems such as modeling acoustic horns. Once the optimal efficiency of the numerical algorithms is established, it should be possible to combine the boundary element program with an additional numerical algorithm to optimize the directivity of the horn while maintaining a moderate impedance match between the driver and the horn.

The measurement system used to find the far-field directivity from the near-field pressure should be extended to rectangular horns. The near-field pressure would now have to be measured over a quadrant of the fictitious hemisphere across the mouth of the horn rather than the one dimensional arc that was used in this work. It would also be useful to compare the far-field results from the near-field technique with the directivity actually measured in the far field. This would eliminate any concerns about the accuracy of the method.

Appendix

Appendix A

Electromagnetic—Acoustic Analogies

Analogies are often useful in helping us understand something new in terms of what we already know. Many instructors use these kinds of tools in the classroom when explaining things such as an electrical resistor–inductor–capacitor system in terms of an equivalent mechanical spring–mass–damper system. The mass vibrating on the end of a spring is something that most people are familiar with, perhaps from playing with a paddle-ball or a slinky toy. This familiarity gives some "instant" intuition about the new system being introduced.

Another educational tool is to say that something is similar to something else. Although this may help in understanding a particular phenomenon, it is important to distinguish between "analogy" and "similarity." Solving differential equations for some people may be as easy as catching fish in a barrel. These two activities are similar in that they are both "easy" (for those lucky people), but the activities themselves are hardly analogous. An analogy only results if each and every member of the first system has a direct counterpart in the analogous system that plays an equivalent role. Mathematically worded, both systems must have defining equations that can be made *exactly* the same. If the mathematical models for two systems can be made to be exactly the same, without losing the important physics in the problem, then the analogy will be useful. This type of analogy is what we seek in this section.

A.1 Motivation

Acoustic horns were first analyzed in a thorough manner by A. G. Webster who presented his work in December of 1914 at a meeting of the American Physical Society in Philadelphia. The rapid advancement in the telephone and radio industry at that time caused a flurry of research over the next 20 years, after which most important design issues (based on Webster's one-dimensional theory) had been handled.

The theory of acoustic horns was largely complete before electromagnetic (EM) horns began to appear. Although the electromagnetic horn was seen in demonstrations at the Royal Institution in London as early as 1897 by Professor J. Chunder Bose, the theory and production of EM horns lay dormant until the advent of World War II. High-gain transmitters were needed by the war effort to identify aircraft and assist in their navigation and landing. The first publication which analyzed radiation from a true horn was by Barrow and Chu [58] in 1939.* Since that time, the state-of-the-art in EM horns has progressed rapidly.

In view of the tremendous amount of recent work with EM horns [133], it would be reasonable to wonder if an analogy could be made between the electromagnetic horn and the acoustic horn. Once such an analogy was in place, acoustics would benefit from any progress made in electromagnetics and *vice versa*.

A.2 Fundamental Differences and Similarities

The physics behind electromagnetic waves and acoustic waves is very different. Acoustic radiation occurs when there is a time-varying fluctuation in the density of an elastic medium. The speed of the elastic wave propagation depends

*See J. F. Ramsay [93] for the pre-1900 history of microwaves.

intimately upon the material properties of the medium. Electromagnetic radiation occurs in the presence of time-varying electric or magnetic fields that are caused by the acceleration of electric charge and can travel in a vacuum. Even though the fundamental physics is so different for electromagnetics and acoustics, there are still many reasons that we might suspect an analogy between them to exist. Many phenomena are similar for both types of waves.

Both electromagnetic and acoustic media support wave propagation with and without dispersion. Electrical conduction in electromagnetics causes dispersion, which results from viscosity and heat loss in acoustics. At very high frequencies, both acoustic and electromagnetic theories must account for the atomic or molecular properties of the medium. Electromagnetics must account for atomic resonances if the medium of propagation is not free space. At these resonance frequencies, absorption and dispersion become very pronounced. In acoustics, absorption and dispersion become very pronounced when the period of the acoustic waves is on the order of the relaxation time[†] of the molecules that make up the medium.

A.3 Analytic Similarities

The analytic similarities between electromagnetics and acoustics create many parallels in the methods of analysis, as mentioned by texts covering both fields of study [109, 156, 96, 117], but precise analogies are not easily found. The basic nature of the difficulty arises from the fact that Maxwell's equations are not curl-free and the linear acoustic equations are curl-free. This irrotational nature of the waves in linear acoustics allows the vector problem in acoustics to be posed as a scalar problem by introducing a scalar potential function. This would lead one to think that useful analogies between electromagnetics

[†]The *relaxation time* is the time taken by a molecule, after having absorbed some energy, to re-emit it.

and acoustics will be limited to electromagnetic fields that can be expressed in terms of a scalar potential. An analogy of this type is seen between two-dimensional electrostatics (curl-free fields) and incompressible, steady-state, two-dimensional fluid flow. An analogy of this completeness will be difficult to find for compressible fluids which have a nonzero divergence.

To further explore these analytic parallels, consider the differential form of Maxwell's equations that model the propagation of electromagnetic waves in a source-free medium:

$$\nabla \times \mathbf{E} = -\mu \frac{\partial \mathbf{H}}{\partial t} \tag{A.1}$$

$$\nabla \times \mathbf{H} = \epsilon \frac{\partial \mathbf{E}}{\partial t}. \tag{A.2}$$

The boldface quantities $\mathbf{E}$ and $\mathbf{H}$ represent the vector electric and magnetic intensities, respectively, while μ and ϵ are the magnetic permeability and electric permittivity respectively and represent the material properties of the media. These equations are to be compared to the momentum and continuity equations for linear acoustics:

$$\nabla p = -\rho_0 \frac{\partial \mathbf{u}}{\partial t} \tag{A.3}$$

$$-\nabla \cdot \mathbf{u} = \frac{1}{\rho_0 c_0^2} \frac{\partial p}{\partial t} \tag{A.4}$$

Although suggestive, no direct analogy can be made at this point. In general, it is troubling that the electromagnetic equations are not curl-free and the linearized acoustic equations are curl-free, or irrotational.

To arrive at wave equations for each medium, take the curl of equation (A.1) and substitute for $\nabla \times \mathbf{H}$ from equation (A.2) to yield:

$$\nabla \times \nabla \times \mathbf{E} = -\mu \frac{\partial}{\partial t} \left(\epsilon \frac{\partial \mathbf{E}}{\partial t} \right) \tag{A.5}$$

Now use the vector identity

$$\nabla \times \nabla \times \mathbf{E} = \nabla \left(\nabla \cdot \mathbf{E} \right) - \nabla^2 \mathbf{E} \tag{A.6}$$

and the fact that the divergence of $\mathbf{E}$ must be zero in a source-free field to give the vector wave equation:

$$\nabla^2\mathbf{E} - \mu\epsilon\frac{\partial^2\mathbf{E}}{\partial t^2} = 0. \tag{A.7}$$

In a completely symmetric manner, the vector wave equation for the magnetic field intensity can be found to be

$$\nabla^2\mathbf{H} - \mu\epsilon\frac{\partial^2\mathbf{H}}{\partial t^2} = 0. \tag{A.8}$$

To derive the acoustic wave equation for pressure p, take the divergence of equation (A.3) and subtract it from the time rate of change of equation (A.4) to arrive at

$$\nabla^2 p - \frac{1}{c_0^2}\frac{\partial^2 p}{\partial t^2} = 0. \tag{A.9}$$

For the velocity wave equation, take the gradient of equation (A.4) and subtract it from the time rate of change of equation (A.3) resulting in

$$\nabla\left(\nabla\cdot\mathbf{u}\right) - \frac{1}{c_0^2}\frac{\partial^2\mathbf{u}}{\partial t^2} = 0. \tag{A.10}$$

Combine this result with the vector identity in equation (A.6) and the fact that the acoustic velocity field is curl-free to give the vector wave equation in the acoustic velocity:

$$\nabla^2\mathbf{u} - \frac{1}{c_0^2}\frac{\partial^2\mathbf{u}}{\partial t^2} = 0. \tag{A.11}$$

The wave equations for acoustics and electromagnetics are almost identical except for the detail that the wave equation for pressure is a scalar one, to be contrasted to the vector wave equation for the electric field $\mathbf{E}$. Note that this increased similarity came about after eliminating the more fundamental relationships of Faraday and Ampère from Maxwell's equations, and momentum and continuity from acoustics. It can be seen from comparing the vector and scalar wave equations that the velocity of propagation for the electromagnetic wave is given by $1/\sqrt{\mu\epsilon}$.

Looking at the equations for energy also leads one to suspect some sort of analogy between electromagnetics and acoustics. After doing a unit analysis, it is seen that the product of **E** and **H** has the units of power per unit area. To derive the energy flux equation, dot Faraday's equation with **H** and dot Ampère's equation by **E** and use the vector identity

$$\nabla \cdot (\mathbf{E} \times \mathbf{H}) = \mathbf{H} \cdot (\nabla \times \mathbf{E}) - \mathbf{E} \cdot (\nabla \times \mathbf{H}) \,. \tag{A.12}$$

Now integrate over a volume and use the divergence theorem to obtain:

$$\oint_{\text{surface}} (\mathbf{E} \times \mathbf{H}) \cdot d\mathbf{S} = -\frac{\partial}{\partial t} \int_{\text{volume}} \left(\frac{1}{2} \mu H^2 + \frac{1}{2} \epsilon E^2 \right) dv. \tag{A.13}$$

The scalar quantities E^2 and H^2 are the usual notation for $\mathbf{E} \cdot \mathbf{E}$ and $\mathbf{H} \cdot \mathbf{H}$ respectively. We can obtain a strikingly similar equation by an almost identical method in the acoustic case by dotting the momentum equation by the velocity and multiplying the continuity equation by the pressure, adding the result and integrating over a volume which gives:

$$\oint_{\text{surface}} (p\mathbf{u}) \cdot d\mathbf{S} = -\frac{\partial}{\partial t} \int_{\text{volume}} \left(\frac{1}{2} \rho_0 u^2 + \frac{1}{2} \frac{p^2}{\rho_0 c_0^2} \right) dv. \tag{A.14}$$

If the density ρ_0 is equivalent to the permeability μ, and the quantity representing the acoustic compliance per unit volume, $1/\rho_0 c_0^2$, is equivalent to permittivity ϵ, then the sound speed is analogous to the light speed. This gives a nice equivalence between the right hand sides of the above equations, but the problem of two vectors in electromagnetics versus one vector in acoustics remains. It would seem that a general analogy between electromagnetics and acoustics is not possible. In order to find an analogy, it is necessary to further restrict the system in which the analogy is to exist.

A.4 Guided Waves

In unbounded space far away from any supporting structures, all electromagnetic wave propagation approaches that of a plane wave, or TEM type.[‡] It is possible to establish an analogy between plane waves in electromagnetics and plane waves in acoustics, but this type of wave propagation is not possible in hollow waveguides, so the analogy is not of direct use for acoustic horns. TEM wave propagation is possible on different types of transmission lines and this is why an analogy is possible between electrical transmission lines and acoustic transmission lines.

Only after introducing approximations for a very specific situation, such as a transmission line, have useful analogies been found. Even in these special situations the analogy is not complete, i.e. there is only an analogy between current and velocity, potential and pressure and the analogy does not extend back to the electric and magnetic fields themselves. Even in the simple case of a TEM wave on a transmission line, it would be difficult to make any analogy with boundary conditions that included charges and currents. Also, it is difficult to imagine how TEM waves could exist within an EM horn. A TEM wave in electromagnetics is analogous to the 00-mode or plane-wave mode in an acoustic media. There is no frequency dependence of the phase speed or the impedance of the media. Both of these are possible in acoustics but a plane wave mode in EM cannot exist within the confines of a waveguide (such as a horn). TE or TM waves can exist and the sum of these would be neither TE, TM, or TEM. Both TE and TM modes have perfect analogies, but each of these require conflicting boundary conditions in acoustics so the sum of the two problems would not be physical for the case of an acoustic waveguide. Also, neither TE or TM has a 00-mode for energy propagation. This means that when an analogy is found, it

[‡]A TEM (Transverse Electromagnetic) wave is a wave in which the electric and magnetic field intensities are in a direction transverse to, or normal to, the axis of propagation.

will not include the 00-mode, which is the dominant mode for acoustic horns.

For TEM waves a perfect analogy can be drawn between acoustic waves and electromagnetic waves. TEM waves do not have a cut-off frequency, whereas TM and TE waves do. For transmission lines, a TEM mode is possible so it is possible to draw a complete analogy between acoustic waves and electromagnetic waves, but for single conductor waveguides, a TEM mode cannot be supported, so a practical analogy seems unlikely.

Bibliography

(in chronological order)

[1] Lord Rayleigh, "On the Approximate Solution of certain Problems relating to the Potential," *Proceedings of the London Mathematical Society*, **7**:70, 1876.

[First publication containing Rayleigh's method of successive iteration. In this method, Rayleigh poses a partial differential equation as an infinite-order ordinary differential equation and presents a method for an approximate solution.]

[2] Strutt, John William, Baron Rayleigh, *The Theory of Sound*, pages 113–115, page 181, MacMillan Co., 1877, second edition 1894, reprint 1926, 1929, Dover reprint 1945.

[Expressions given for solution within conical horn and for resonant frequencies. The electrical analogy concerning resonators is mentioned.]

[3] James Clerk Maxwell, *A Treatise on Electricity and Magnetism*, volume 2, third edition, Claredon Press, 1891. Unabridged version republished by Dover, 1954.

[On pages 282–283 is a discussion of the analogy between mechanical stress and electromagnetic fields. Maxwell notes that "We have asserted nothing as yet with respect to the mode in which this state of stress is originated and maintained in the medium." This statement may imply difficulty in finding an analogy that included the boundary conditions.]

[4] E. Picard, *Traité d'analyse*, volume 2, Gauthiers-Villars & Cie, Paris, 1893.

[Convergence proof for method of successive approximation on page 301.]

[5] Oliver Heaviside, *Electro-magnetic Theory*, volume II, The Electrician Publishing Co., 1894. (Reprinted by Dover, 1950)

[6] John Tyndall (1820–1893), *Sound*, D. Appleton and Company, 1896.

[The frontispiece shows an early application of a horn as a signaling station to warn approaching ships. It is referred to as a "steam-siren," and was 16 1/2 ft long, 5 in. in diameter at the throat and 2 ft, 3 in. at the mouth. Two disks, one fixed at the throat and the other rotating behind it, have slits which allow a strong puff of steam under 70 lbs of pressure to escape when the slits

coincide. The pitch of the note is controlled by the frequency of rotation of the rear disk. It is not know whether the horn used in this design was of the exponential type or otherwise. The text refers to it as a conical trumpet, but it is not quite conical in the frontispiece of the text which displays this horn. These investigations began on the 19th of May, 1873 on South Foreland, near Dover in England.]

[7] Larmor, "On the Mathematical Expression of the Principle of Huyghens," *The Proceedings of the London Mathematical Society*, Series II, **1**:1, 1903.

[8] E. H. Barton, "On spherical radiation and vibrations in conical pipes," *Philosophical Magazine and Journal of Science*, **15**(6):69–81, January–June 1908.

[This work only deals with resonances in a cone; radiation from the cone is only mentioned in the title. Repeats what is covered in Lord Rayleigh's text but without using the velocity potential which is claimed to add excessive difficultly for a large interested audience.]

[9] A. E. Kennelly and G. W. Pierce, "The Impedance of Telephone Receivers as Affected by the Motion of their Diaphragms," *Proceedings of the American Academy of Science*, **48**:113+, 1912.

[This paper defines the concept of mechanical impedance and draws the analogy between electrical and mechanical parameters.]

[10] John William Strutt, Baron Rayleigh, "On the propagation of sound in narrow tubes of variable section," *Philosophical Magazine*, **31**:89–96, 1916. (republished as article 402 in *Scientific Papers*, Dover 1964)

[This paper treats the problem of waves in a duct with slowly varying cross section, and the problem of a sudden step in the duct diameter. A new mathematical method which yields a semi-analytical solution *via* a perturbation type approach with Picard's method of iteration is presented. The zeroth-order approximation is identical to Webster's horn equation although Rayleigh did not likely know of Webster's work.]

[11] Arthur Gordon Webster, "Acoustical Impedance, and the Theory of Horns and of the Phonograph," *Proceedings of the National Academy of Science*, **5**:275–282, 1919. Read in December of 1914 at the meeting of the American Physical Society at Philadelphia. Reprinted in *Benchmark Papers in Acoustics* Volume 4:*PHYSICAL ACOUSTICS*, edited by R. Bruce Lindsay, pages 58–65, Dowden, Hutchinson & Ross, Stroudsburg, Pennsylvania, 1973.

[This paper is famous for being the beginning of horn theory in general, and the first publication concerning acoustical impedance. In this sense, even though Webster wasn't the first to utilize the so-called, "Webster" horn equation, it is appropriate that we honor Webster's contribution by connecting his name with the horn equation.

The impedance of a straight tube, power horns and conical horns are found and mention is made of Stewart using the results given during World War I. Webster points out that bells of most horns are of three types; power type (later termed the Bessel horn), exponential, or Gaussian, and also suggests that more complicated horn geometries may be handled by dividing them into sections.

The solution of the horn equation given by Webster is followed by a general technique for determining the two-port parameters (transmission matrix) for arbitrary contours where two independent solutions are known. This is the first publication presenting acoustic two-port theory.

It has been suggested [186] that Webster did not intend the horn equation derivation to be for plane waves, but this would seem to be contradicted by Webster's statement, "Let us consider a tube of infinitesimal cross section σ varying as a function of the distance x from the end of the tube." Webster's experiments [12] used long horns of narrow cross section.]

[12] Arthur Gordon Webster, "Experiments on the Vibration of Air in Conical Horns," *Proceeding of the National Academy of Science*, **6**:316–320, 1920.

[Webster presents the first published measurements of on-axis pressure in a conical horn, which largely validates his earlier theory. Most of the discrepancy he feels is due to his rough estimate of the open end. He says, "It will be seen that the theory is very substantially verified, the defect in it being due to the very rough estimate made about the correction of the open end which, as I stated in my paper on horns, is far from being accurate."]

[13] G. W. Stewart, "The Performance of Conical Horns," *Physical Review*, series II, **16**(4):313–326, 1920.

[Stewart experimentally studies conical horns; resonant characteristics are examined and an end correction is found. This is the first known published paper using spherical wave fronts in the impedance calculations for the conical horn. Only 256 Hz and 512 Hz responses are examined.]

[14] A. E. Kennelly and K. Kurokawa, "Acoustic Impedance and its Measurement," *Proceedings of the American Academy of Arts and Sciences*, **56**(1):1–42, February 1921.

[A lengthy discussion of telephone receivers and impedance, followed by a tutorial on the analogy between electrical and acoustical transmission lines.]

[15] G. W. Stewart, "Acoustic Wave Filters," *Physical Review*, series II, **20**:528–540, 1922. Reprinted in *Benchmark Papers in Acoustics*, Volume 4:*Physical Acoustics*, edited by R. Bruce Lindsay, pages 83–95, Dowden, Hutchinson & Ross, Stroudsburg, Pennsylvania, 1973.

[The idea of acoustic impedance presented in Webster's paper is used here to model lumped parameter acoustic circuits. Defines acoustic inertance and capacitance (instead of compliance; the impedance analogy was the only one

is use at the time; Webster used condenser instead of capacitor in his paper [11]) and uses these to construct both low-pass and high-pass acoustic filters.]

[16] C. R. Hanna and J. Slepian, "The Function and Design of Horns for Loud Speakers," *Transactions of the American Institute of Electrical Engineers*, **43**:393–411, February 1924.

[Design considerations are discussed extensively for exponential horns. Loading of the diaphragm is shown to be important for flatting the overall frequency response. Throat area and diaphragm chamber volume is discussed relative to radiating efficiency, and the shape and mouth of the horn is considered. It is shown that the exponential horn probably provides the "optimum" loading. A very interesting discussion here on the physics of reflections from the open end of a tube and exponential horn that lead to the conclusion that the mouth of an exponential horn is as large as it need be when $k_c r_m = 1$. This same theory leads to the fact that higher frequencies lead to less and less reflection from the mouth which is contrary to the findings by Keele (1973) [118]. The derivation of the horn equation is the first that does not assume infinitesimal cross sections (plane waves), but draws the fronts of constant amplitude and phase as curved. Morse (1936) [51] follows this approach in his text. Hanna and Slepian conclude that the horn equation is less accurate near cut-off, but this is a result of mistaking phase for group velocity.

Discussion at the end of this article: E. W. Kellogg suggests folding up the horn, "Another question of practical interest is whether it has been found possible to coil up the horn without impairing its action." and points out the analogy to the tapered electrical transmission line which has been in use for years (first studied by Heaviside [5]). L. P. Rundle points out that "In nearly all of the better grades of radio loud-speaker horns there is at least one right-angle bend; in others there are two and in still others a circle and a half, i.e., six right-angle bends." revealing folded horns already being used in practice, although nothing was yet published in the literature. Fletcher points out the problem with nonlinear distortion for small throat diameters based on the fact that ordinary conversation often contains SPL's of greater than 50 dynes/cm^2 (108 dB's). A. Nyman points out that constant directivity would be a desirable trait.

Note that both the authors and Kellogg use "velocity of propagation" to describe the phase velocity, i.e. $c_{\text{phase}} = \omega/\gamma$ where ω is the radian frequency and γ is the quantity which gives the phase shift per unit length. Kellogg clearly understands the difference but Hanna and Slepian seem in doubt.]

[17] A. N. Goldsmith and J. P. Minton, "The Performance and Theory of Loud Speaker Horns," *Proceedings of the Institute for Radio Engineers*, **12**:423–478, 1924.

[Sixteen conical horns are constructed and tested. Based on plane-wave assumptions, conical, exponential and parabolic horns are studied theoretically. The authors conclude that conical horns are superior to exponential horns at some frequencies.]

[18] V. A. Hoersch, "Non-radial Harmonic Vibrations within a Conical Horn," *Physical Review*, serial II, **25**:218–224, 1925.

[Inspired by the concept of an optimum angle of amplification described in Stewart's paper(1920), Hoersch shows that other types of vibrations may exist in a conical horn that are not plane, and may give rise to this optimum angle. Two different modal patterns are plotted but the coefficients (which depend on the termination at the mouth) are not given.]

[19] V. A. Hoersch, "Theory of the Optimum Angle in a Receiving Conical Horn," *Physical Review*, serial II, **25**:225–?, 1925.

[20] G. W. Stewart, "Theory of the Optimum Angle of a Receiving Conical Horn," *Physical Review*, serial II, **25**:230–?, 1925.

[21] K. Kobayashi, "The performance and design of the sound radiator consisting of the acoustic transformer and the horn," *Institute of Electrical Engineers of Japan Journal*, (461):1437–1444, 1926.

[In Japanese. This is an early example of a complete design of horn and transducer. The electrical impedance is used as a design parameter and conical and exponential horns are tested. Based on this theory, the appropriate dimensions of an exponential horn of finite length are given. Unfortunately, I cannot read Japanese, so more cannot be said.]

[22] Irving B. Crandall, *Theory of Vibrating Systems and Sound*, pages 152–174, D. Van Nostrand Company, Inc., 1927.

[Contains a discussion complete with references for conical horns, exponential horns, and finite exponential horns. The terminating condition at the mouth of the horn is also discussed and argument made for placing the impedance at the mouth with the equivalent impedance "seen" by a spherical source. Note that the phase velocity is still not differentiated clearly from "velocity of propagation" in this text. For example, the phase velocity is referred to as "modified velocity of sound" on p. 239.]

[23] W.[arren] P.[erry] Mason, "A Study of the Regular Combination of Acoustic Elements, with Applications to Recurrent Acoustic Filter, Tapered Acoustic Filters, and Horns," *Bell System Technical Journal*, **6**:258–275, 1927. Reprinted in *Benchmark Papers in Acoustics*, Volume 4:*Physical Acoustics*, edited by R. Bruce Lindsay, pages 96–113, Dowden, Hutchinson & Ross, Stroudsburg, Pennsylvania, 1973.

[This paper firmly establishes modeling acoustic horns as sections of uniform cylindrical waveguide. Also shown is that the piecewise uniform model converges to the Webster equation. It is the first paper to extend the idea of acoustic impedance to distributed systems, although this concept was definitely suggested by Webster in his paper.]

[24] Stuart Ballantine, "On the Propagation of Sound in the General Bessel Horn of Infinite Length," *Journal of the Franklin Institute*, **203**:85–102, 1927.

[This paper studies a family of horns represented by area $= A_0 x^m$ which transform Webster's equation into an equation of Bessel type. Ballantine terms this family of horns Bessel horns, in analogy to Heaviside's earlier work with Bessel electric lines [5]. The value of m in the area expansion above determines the "Bessel flaring" of the horn and Ballantine reveals that, "The effect of increasing Bessel flaring is to augment the response for low notes in quite the same fashion as in the exponential horn, except that no critical frequency exists." Ballantine also critically reviews the assumptions behind linear horn theory and points out that significant nonlinear distortion will occur in high power public address systems with small throats. Ballantine reveals his disbelief in the existence of a cut-off frequency in the exponential horn by arguing, "it seems unquestionable that the existence of a critical frequency is spurious and due only to the nature of Webster's approximate method and its failure at this frequency; spontaneously diffusive propagation at any frequency violates our physical intuition." Note: The phase velocity is referred to as "the apparent velocity of sound."]

[25] C. R. Hanna, "On the Propagation of Sound in the General Bessel Horn of Infinite Length," *Journal of the Franklin Institute*, **203**:849–853, 1927.

[Argues that the Bessel horns presented by Ballantine [24] converge to the exponential horn, giving further evidence of the superiority of the exponential contour.]

[26] E. C. Wente and A. L. Thuras, "A High Efficiency Receiver for Horn-Type Loudspeaker of Large Power Capacity," *Bell System Technical Journal*, **7**(1):140–?, January 1928.

[27] Marcus O'Day, "40. The function of a horn in acoustics," abstracts, minutes of the Pomona meeting, *Proceedings of the American Physical Society*, page 328, June 15, 1928.

[Derives an equation saying $p = 1/S\, F(t - x/c)$ for all horns but this can't be correct in the presence of reflections and doesn't match the solution for the conical horn. Perhaps O'Day intended to write $p = 1/\sqrt{S}\, F(t - x/c)$.]

[28] Oliver Dimon Kellogg, *Foundations of Potential Theory*, J. Springer, 1929. Republished by Dover, 1954.

[29] P. Wilson and G. W. Webb, *Modern Gramophones and Electrical Reproducers*, ch. V, app. II, Cassell, London, 1929.

[30] H. Bouasse, *Tuyaux et Résonateurs*, Librairie Delagrave, 15, Rue Soufflot, 15, Paris, 1929.

[Chapter 10 is on the theory of cones and contains a derivation of Webster's equation beginning with the Helmholtz equation. Cylindrical, conical, exponential, and Bessel contours are considered. No references.]

[31] Kôzi Satô, "On the Sound Field due to a Conical Horn with a Source at its Vertex," *Japanese Journal of Physics*, **5**(3):103–109, 1929.

[Discusses directional radiation from a conical horn based on a curved surface at the mouth. The conical horn is assumed to be mounted in a rigid sphere. Purely spherical waves are assumed inside the horn for both the sound source and the wave reflected from the horn mouth. An analytical solution of the wave eq. is assumed exterior to the horn the interior/exterior solutions are then matched at the mouth to find the modal coefficients. Directivity pattern are plotted for both near and far field for several opening angles of the conical horn. This solution is more or less equivalent to finding the directivity pattern of a spherically-curved circular piston. I would expect that the solution is fairly valid except that it could not be used for the interior pressure field.]

[32] George Walter Stewart (1876–1956) and Robert Bruce Lindsay (1900–), *ACOUSTICS, A Text on Theory and Applications*, pages 132–158, D. Van Nostrand Co. Inc., 250 Forth Ave., New York, 1930.

[Plane-wave theory is utilized in all work presented here. Impedance theory is discussed and exponential, conical, hyperbolic and parabolic horns are all treated. Discusses end correction for an open tube. Applies reciprocal theorem of Helmholtz to horns. Note: Refers to cut-off of exponential as "spurious result" on p. 146.]

[33] C. R. Hanna, "Theory of the Horn-Type Loud Speaker," *Journal of the Acoustical Society of America*, **2**:150–156, 1930.

[An early tutorial that reviews the relevant theory behind horn loudspeakers. The transformer nature of the horn is covered, as well as throat size, mouth size, flare rate, and easy design methods for exponential horns.]

[34] Irving Wolff and Louis Malter, "Directional Radiation of Sound," *Journal of the Acoustical Society of America*, **2**:201–241, October 1930.

[An early measurement of the directivity of a rectangular mouthed horn driven by an 8 in. cone-type driver.]

[35] Harry F. Olson, "A New High Efficiency Theatre Loudspeaker of the Directional Baffle Type," *Journal of the Acoustical Society of America*, **2**:485–498, April 1931.

[Gives the equations and equivalent circuit model of a low frequency horn driven by a cone-type driver. Efficiency is predicted and compares well to measurements.]

[36] Edward W. Kellogg, "Means for Radiating Large Amounts of Low Frequency Sound," *Journal of the Acoustical Society of America*, **21**:94–110, July 1931.

[Arguments are made to determine how many acoustic watts are needed for sound reproduction and what type of reproduction devices would be able to deliver this power. Baffled arrays and horn loaded assemblies are discussed. Of particular interest are the figures showing exponential horns fitted to room corners. Kellogg also mentions that the horn would have to be folded for most practical applications. This may be what sparked Paul Klipsch's idea for his corner horn [60].]

[37] Whitaker, *Physics in Sound Recording, Institute of Physics*, November 1931.

[This paper presents electromechanical analogies for the gramophone and reports on the general progress of the transducers which are relying less and less on resonance and thus have flatter frequency responses. Reference from Wood's *Acoustics* [61, p. 523]]

[38] Horance Lamb, *Hydrodynamics*, sixth edition, Cambridge University Press, 1932. Republished by Dover, 1945.

[39] P. B. Flanders, "A Method of Measuring Acoustic Impedance," *Journal of the Acoustical Society of America*, **4**:402–410, 1932.

[Describes an apparatus that uses two know loads (anechoic and rigid) to find the impedance of a third unknown load. Data is presented showing the impedance of a cylindrical tube, a conical and exponential horn, and a hole in a thin plate. Mention is made that Kennelly and Kurokawa were probably the first to attempt to measure acoustic impedance.]

[40] William M. Hall, "Comments on the Theory of Horns," *Journal of the Acoustical Society of America*, **3**:552–561, 1932.

[Hall points out the many assumptions made in the current horn theory: *i*) uniform, isotropic fluid, *ii*) neglect viscosity in medium and on wall *iii*) ignore effect of gravity *iv*) irrotational motion and *v*) infinitesimal vibration. Experimental data is shown of the pressure fields within a conical and exponential horn and it may be clearly seen that the planar theory is in error. This paper is somewhat classic in that it contains the first published measurements (to the author's knowledge) of the entire acoustic pressure field interior to a horn and including the mouth region. Notes: The "velocity of propagation" is explicitly defined here as $c \equiv \sqrt{\gamma P_0/\rho_0}$. This work was part of a thesis at Massachusetts Institute of Technology under the direction of Prof. Fay, 1932.]

[41] William M. Hall, *An Investigation of Sound Fields in Regions Restricted by Finite Boundaries*, Master of Science Thesis, Massachusetts Institute of Technology, 1932. (79 pages)

[This thesis describes in detail the background work for the above paper in J.A.S.A. Also described are the condenser microphone construction and throat impedance measurements. Notes: Thesis was signed off on Sept. 26, 1931 by R. Fay.]

[42] Rocard, "Sur la propagation des ondes sonores d'amplitude finie," "The Propagation of Sound Waves of Finite Amplitude," *Comptes rendus hebdomadaires des seances de l'Academie des sciences*, **196**:161–164, 16 January 1933. ISSN: 0001-4036, OCLC: 1124612

[In the first theoretical analysis of finite amplitude effects in the exponential horn, Rocard shows that appreciable amplitude distortion can be introduced in a high efficiency wide frequency range horn by the non-linearities of the air in the horn throat. His result predicts second harmonic power generation that is 6 dB too high (see Goldstein and McLachlan, 1935 [48]).]

[43] N.[orman] W.[illiam] McLachlan, LOUD SPEAKERS*, Theory, Performance, Testing and Design*, pages 177–197, Clarendon Press, Oxford, 1934. (corrected edition published by Dover, 1960)

[McLachlan gives the clearest exposition in his day of conical, exponential, and Bessel horns. Phase velocity is defined as $c' = \omega/k$ although he refers to it as "velocity of propagation" in some instances. The most extensive discussion to date concerning reflections at the mouth is contained here. For finite length, the impedance that an infinite horn would have at the mouth of the finite length horn is assumed correct. It is shown that a piston is a good approximation of the termination impedance for $1.25 < ka < 2.0$ but not outside of this. Hanna and Slepian [16] gave physical arguments for the proper mouth size. McLachlan points out that "To simulate the horn termination identically, not only the impedance but the spatial distribution of radiation would have to be reproduced." The equation modeling finite amplitude propagation in conical and exponential horns is derived but no solution is presented (see McLachlan [72]). Extensive design information is given for practical horn design including measurements of frequency response and directivity.]

[44] N. W. McLachlan, *Bessel Functions for Engineers*, Oxford at the Clarendon Press 1934, second edition 1955.

[A complete analysis of the Bessel horn along with a proof that the Bessel horn of infinite order tends to an exponential horn.]

[45] E. C. Wente and A. L. Thuras, "Loud Speakers and Microphones," *Bell Systems Technical Journal*, **13**:259–277, 1934.

[Discussion of the principles of design for an exponential horn are discussed. Emphasis is on avoidance of distortion due to finite amplitude effects in air, and varying force factor $B\ell$, due to excessive excursion of diaphragm.]

[46] Stanford Goldman, "Supersonic Measurement of the Directional Characteristics of Horns," *Journal of the Acoustical Society of America*, **5**:181–195, January 1934.

[This paper exploits scaling by making a small horn and driving it with a high frequency source. Goldman states, "Since the sound radiated from a horn in any direction is purely a diffraction phenomenon, its low frequency values can be determined by making a smaller, geometrically similar horn and measuring

its directional characteristics at a higher frequency, if the wave-length of the sound is reduced in the same ratio as the linear dimensions of the horn." Directional information is plotted but due to the organization of the material, is difficult to interpret. Added is a discussion of physics at the mouth of the horns.

Note the use of "supersonic" in the title instead of "ultrasonic".]

[47] A. L. Thuras, R. T. Jenkins, and H. T. O'Neil, "Extraneous Frequencies Generated in Air Carrying Intense Sound Waves," *Journal of the Acoustical Society of America*, **6**:173–180, 1935.

[Second harmonic distortion due to finite-amplitude effects is measured in a tube and an exponential horn. Experimental data is presented and the results are impressively close to the theoretical predictions based on: *i*) the second harmonic is generated according to the local pressure along the length of the horn, and *ii*) the second harmonic propagates in the same manner as the fundamental.]

[48] S. Goldstein and N. W. McLachlan, "Sound Waves of Finite Amplitude in an Exponential Horn," *Journal of the Acoustical Society of America*, **6**:275–278, April 1935.

[A theoretical analysis of second harmonic generation in a tube and exponential horn. One example is worked that illustrates how to design a horn to avoid more than −30 dB (standard for high-fi) of second harmonic distortion. The authors point out that Y. Rocard's [42] (1933) result is incorrect (6 dB too high on 2nd harmonic power) due to confusion between Eulerian and Lagrangian coordinates.]

[49] P. Wilson, "Tractrix Horns," *The Gramophone*, **12**:119–120, August 1935.

[Questions assumptions behind tractrix horn and presents a table for making tractrix contours.]

[50] John K. Hilliard, "A Study of Theatre Loud Speakers and the Resultant Development of the Shearer Two-Way Horn System," *Academy research Council Technical Bulletin*, 1936 Volume, pages 1–28, 3 March 1936.

[Note: Douglas Shearer was the head of the Metro-Goldwyn-Mayer sound department and responsible for bringing about and directing this project. Development was engineered by Hilliard.

This is the only reference found that completely discusses the design and construction of a horn loudspeaker followed by results and discussion. The horns used in the two-way design were of the exponential type. The high frequency horn was multi-celled and the low frequency horn was folded. The system boasts a newly designed radial phase plug in the compression horn driver designed by James B. Lansing.

Also published in: Research Council of the Academy of Motion Picture Arts and Sciences, Motion Picture Sound Engineering, pp. 97–115, D. Van Nostrand

Company, Inc., 1938. Note: Douglas Shearer was the technical representative for Metro-Goldwyn-Mayer Studios for the writing of this engineering text.

"Even today this system represents the state of the art in sound systems.," Ivor D. Groves, Jr., Acoustic Transducers, Benchmark papers in acoustics, v. 14, Editor's comment, p. 153, Hutchinson Ross Pub. Co., 1981.

"When the knowledgeable observer considers that the systems these men designed and the concepts they developed are essentially still state-of-the-art in a competitive professional sound marketplace, one is aware of the power of a leader such as John Hilliard." Don Davis, Editor's Note, Journal of the Audio Engineering Society, **26**:843–850 (1978).]

[51] Philip M. Morse, *Vibration and Sound*, second edition, pages 265–293, McGraw-Hill 1948, first edition 1936, reprint by the American Institute of Physics in 1981.

[Over 20 pages concerning propagation of sound in horns. This text seems to be the first work that discusses the physics behind one-parameter waves in a horn and when they are applicable. Presents a general family of horn shapes (second edition only) from Salmon's work (1946) and goes on to explicitly study the conical horn, exponential horn and catenoidal horn. He discusses transmission coefficient, reflection from the open end, and a design problem for the conical horn.

Some confusion about the speed of sound propagation in passed on here by the statement, "This wave travels out of the horn with ever diminishing amplitude, with a velocity (c/τ) larger than the speed of sound in the open." although it is clear that Morse understands that he is talking about the *phase velocity*, which he defines on page 154 as the velocity of propagation for a simple harmonic wave.]

[52] N. W. McLachlan and A. T. McKay, "Transient oscillations in a loud speaker horn," *Proceedings of the Cambridge Philosophical Society. Mathematical and Physical Sciences.* **32**:265–?, 1936.

[53] Harry F. Olson, "Horn Loud Speakers, Part I. Impedance and Directional Characteristics," *RCA Review*, **1**(4):68–83, April 1937.

[Discussion centers on exponential horns although conical horns are shown to be inferior in ratio of resistance to reactance at the throat. The effect of finite length is clearly revealed in a series plotting throat impedance for horns of varying lengths. Much discussion and many figures of experimental data are devoted to directional characteristics of exponential horns. It is found that the horn radiates the same pattern as a piston when the operating wavelength is equal to or greater that the mouth diameter, and is determined by the flare for wavelengths smaller than a mouth diameter. A ring type horn and a multi-celled horn are discussed and measured directivity patterns shown. A practical method for predicting directivity patterns of multi-celled horns is given.]

[54] Harry F. Olson, "Horn Loud Speakers, Part II. Efficiency and Distortion," *RCA Review*, **2**(2):265–277, October 1937.

[Efficiency vs. throat chambers, and temperature is discussed and results shown. Olson, concerned with non-linear distortion, states, "The distortion due to non-linearity of the air is, at the present time, one of the most important as well as troublesome factors in the design of high efficiency loudspeakers for large outputs." Distortion due to non-linear compliance in the throat is also examined, but is found to be small relative to the non-linear compliance of the loudspeaker suspension.]

[55] A. J. Sanial, "Graphs for Exponential Horn Design," *RCA Review*, **2**(2):97–102, 1937.

[This is a paper written for design engineers constructing exponential horns. It contains plots which allow rapid graphical solutions based on equations given in Crandall's text.]

[56] Frank Massa, "Horn-Type Loud speakers—A Quantitative Discussion of Some Fundamental Requirements in Their Design," *Proceedings of the Institute of Radio Engineers*, **26**(6):720–?, June, 1938.

[57] Frank Massa, "Temperature Reduction in High-powered Loudspeakers," *RCA Review*, **3**(2):196–202, October 1938.

[Massa has the clever idea here to increase the power handling of a loudspeaker (which is usually limited by the inability to conduct heat from the voice coil which results in an increase in resistance followed by thermal failure) by placing helium or hydrogen in the voice coil gap instead of air. Both of these gases have heat conduction properties superior to air. Massa demonstrates up to five times greater power handling and much less increase in voice-coil resistance due to cooler operation.]

[58] W. L. Barrow and L. J. Chu, "Theory of the Electromagnetic Horn," *Proceedings of the Institute of Radio Engineers*, **27**:51–64, January 1939. Republished in *Electromagnetic Horn Antennas*, by A. W. Love, IEEE Press, 1976.

[59] J. E. Freehafer, "The Acoustical Impedance of an Infinite Hyperbolic Horn," *Journal of the Acoustical Society of America*, **11**:467–476, April 1940.

[This paper seems to be the first publication showing the three-dimensional solution to the wave equation in a coordinate system other than spherical (for conical horn). The horn studied is in the form of a hyperboloid of one sheet and the wave equation separates in the oblate spheroidal coordinates. Throat impedance is plotted showing low frequency superiority to the conical horn.]

[60] Paul W. Klipsch, "A Low Frequency Horn of Small Dimensions," *Journal of the Acoustical Society of America*, **13**(2):137–144, October 1941. Reprinted with additional comments by the author in *Journal of the Audio Engineering Society*, **27**(3):141–148, March 1979.

[This paper introduces the prototype of the classic KLIPSCHORN, corner-horn loudspeaker, which is still in production. One of the big arguments for horn loading in the low-frequency region is the reduced cone motion that results, leading to less overall distortion because the nonlinearity of the loudspeaker's suspension is the primary cause of distortion.]

[61] Alexander Wood (1879–1950), *Acoustics*, pages 114–122, 530–535, Interscience Publishers, Inc., 1941.

[Discusses the derivation of the horn equation and goes on to consider the conical and exponential contours and actual applications. I found the most interesting material on pages 188–190 which present the horn used in an early application for collecting sound and identifying the direction that it came from. One device referred to as the Claude orthophone was used by the French during WW I to locate gunfire and another used to locate aircraft.]

[62] Paul W. Klipsch, "Improved Low-Frequency Horn," *Journal of the Acoustical Society of America*, **14**(3), January 1943.

[63] Paul W. Klipsch, "A Note on Acoustic Horns," *Proceedings of the I.R.E.*, (Institute of Radio Engineers), **33**:447–449, 1945.

[Using the impedance equation given by Olson in "Horn Loudspeakers," it is pointed out that the resistive component of the throat impedance of a finite exponential horn does not go to zero below the cut-off frequency of the horn as is often thought, but sound radiation will still occur. Practical value of performance below cut-off is discussed (limits excursion, and reduces subsequent harmonic distortion).]

[64] J. B. Lansing and J. K. Hilliard, "An Improved Loudspeaker System for Theaters," *Journal of the Society of Motion Picture Engineers*, **45**(5):339–349, November 1945.

[This work describes the first straight-bass, horn-loaded loudspeaker for motion picture theaters. The low frequency unit utilizes horn loading except at the lowest frequencies where the cabinet functions as a bass reflex enclosure. New features include: Alnico No. 5 permanent magnets and replaceable diaphragms. The efficiency of the high frequency unit at 1000 Hz is noted as 108 dB at 5 ft with 1 W of electrical power. These horns replaced the Shearer horns [50] as the dominant motion picture loudspeaker.]

[65] Paul W. Klipsch, "A High-Quality Loudspeaker of Small Dimensions," *Journal of the Acoustical Society of America*, **17**(2), January 1946.

[66] Vincent Salmon, "Generalized Plane Wave Horn Theory," *Journal of the Acoustical Society of America*, **17**(3):199–211, January 1946.

[Salmon assumes a power series representation of the horn contour and manipulates the Webster horn equation into the one-dimensional Schrödinger equation. The effect of horn contour and frequency are separated. Establishes

a general formula for determining the "cut-off" frequency of any plane-wave horn. Manipulates horn equation into the Ricatti equation. The plane-wave admittance of a horn is shown to be best represented by parallel resistance and mass elements. Horns of similar performance to conical horns are synthesized and theoretical vs. experimental values of pressure along the horn axis is plotted.]

[67] Vincent Salmon, "A New Family of Horns," *Journal of the Acoustical Society of America*, **17**(3):212–218, January 1946.

[Given a desired conductance at the throat of a power type horn, a horn contour is synthesized. The possible contours are shown to be bounded by the conical and hyperbolic cosine shapes. This paper represents a landmark in horn design since it is the first to include a method for synthesizing a general horn contour. The first discussion of hyperbolic horns.]

[68] Harry F. Olson, *Elements of Acoustical Engineering*, second edition, D. Van Nostrand Company, 1947.

[69] Harold Levine and Julian Schwinger, "On the Radiation of Sound from an Unflanged Circular Pipe," *Physical Review*, **73**(4):383–406, 1948.

[This is a theoretical solution of a long-standing problem. Included is the often discussed end correction for the open pipe. The directivity pattern is also plotted showing that the main lobe is nearly identical to that of a baffled piston.]

[70] Osman K. Mawardi, "Generalized Solutions of Webster's Horn Theory," *Journal of the Acoustical Society of America*, **21**(4):323–330, July 1949.

[Comments on the validity of Webster's horn theory at low frequency and says, "The high frequency transmission characteristics are not so important, since the behavior of all horns at high frequencies is very nearly the same." Mawardi is probably referring to the impedance behavior. Transforms Webster horn equation into the Ricatti equation for the impedance and shows its superiority for finding impedance in some cases. Shows that the exponential horn is the only horn whose frequency characteristics remain unchanged along its length. Mawardi makes use of two-port networks and transmission line theory to represent horns of finite length and discusses a technique for finding the input impedance for a horn of arbitrary contour. As a terminating impedance for the horn cap, Mawardi expresses that the spherical impedance function is better than the piston impedance function.]

[71] Winston E. Kock and F. K. Harvey, "Refracting Sound Waves," *Journal of the Acoustical Society of America*, **21**(5):471–481, 1949.

[Sparked by research on dielectric lenses for microwave transmitters, Kock presents this work which would seem to be the first publication regarding using diffraction lenses for altering radiation patterns of horns and conventional cone type loudspeakers. A pyramidal horn is shown with a diffraction grating and data is taken for both with and without the grating. The pyramidal horn

used for the tests is actually a microwave horn. Note the H-band rectangular waveguide used as the throat of the horn.]

[72] N. W. McLachlan, *Ordinary Non-Linear Differential Equations in Engineering and Physical Sciences*, Appendix I, Oxford University Press, 1950.

[Appendix I contains a detailed solution for finite amplitude one-dimensional wave propagation within an exponential horn. The discussion includes transmitted power and influence of flare on second harmonic.]

[73] Lawrence E. Kinsler and Austin R. Frey, *Fundamentals of Acoustics*, pages 298–318, John Wiley and Sons, Inc., 1950.

[Chapter 11 gives a very clear introduction to one-dimensional horn theory. Contains several interesting comments concerning cut-off and exponential vs. conical horns. Contrast the following words with Ballantine (1927) who also expressed disbelief in a cutoff frequency: "In contrast to the simple theory developed above, experimental observations indicate that acoustic waves are propagated through an exponential horn both at and below the cut-off frequency, although the acoustic power transmitted is greatly reduced. The origin of this discrepancy is undoubtedly in the failure of some of the simplifying assumptions made in the derivation of the approximate wave equation." Crandall (1927) is obviously not the only one to disagree with the conclusions in Goldsmith and Minton's paper (1924) [17] since Kinsler and Frey state "...and even below the cut-off frequency, where the exponential horn is theoretically inferior to the conical horn, actual experimental measurements show that this is not true."]

[74] C. T. Molloy, "Response Peaks in Finite Horns," *Journal of the Acoustical Society of America*, **22**(5):551–557, 1950.

[An expression is derived to predict axial response in a hyperbolic horn. Measured response vs. predicted response is shown to confirm theory. Using Levine and Schwinger's results, Molloy plots the radiation impedance of the unbaffled tube. Although not mentioned, the radiation impedance is much closer to that seen by a baffled piston source than seen by a spherical source.]

[75] G. J. Thiessen, "Resonance Characteristics of a Finite Catenoidal Horn," *Journal of the Acoustical Society of America*, **22**(5):558–562, September 1950.

[Expressions are given for impedance of a finite catenoidal horn and comparisons made with conical and exponential horns.]

[76] Fred B. Daniels, "On the Propagation of Sound Waves in a Cylindrical Conduit," *Journal of the Acoustical Society of America*, **22**(5):563–564, September 1950.

[The author uses an equivalent circuit analogy to add the effect of heat conduction and viscosity and shows that this approach matches the limiting cases solved by Rayleigh for very narrow and very wide tubes.]

[77] J. E. White, "A Method for Measuring Source Impedance and Tube Attenuation," *Journal of the Acoustical Society of America*, **22**(5):565–568, September 1950.

[Describes a method similar to that used by standing wave tubes that is useful for measuring attenuation and velocity of sound in gases and also useful for rapid measurement of sound source impedance.]

[78] Paul W. Klipsch, U.S. Patent 2537141, January 9, 1951. (Application date, June 15, 1945)

[In an effort to approach the performance achieved by the more costly multicelled exponential horns, Klipsch presents the earliest example of a sectoral type horn. This horn has inserts in the throat to separate the wave front into the desired radius of curvature. The figures describe an exponential type horn but claim the feature may be applied equally well to other types of horns.]

[79] A. F. Stevenson, "Exact and Approximate Equations for Wave Propagation in Acoustic Horns," *Journal of Applied Physics*, **22**(12):1461–1463, December 1951.

[A general method of solving horn problems is presented. The horn is divided into multiple tubes and the velocity potential in each tube is expanded into its eigenfunctions and matched to the next and the previous sections.]

[80] Bart N. Locanthi, "Application of Electric Circuit Analogies to Loudspeaker Design Problems," *Institute of Radio Engineers Transactions on Audio*, volume PGA-6, March 1952. Reprinted in *Journal of the Audio Engineering Society*, **19**(9):778–785, October 1971.

[A horn loudspeaker is treated partly as a lumped parameter system and partly as a distributed parameter system. The electrical impedance is both measured and predicted *via* the model described with good agreement.]

[81] Philip M. Morse and Herman Feshbach, *Methods of Theoretical Physics*, Part I and Part II, McGraw-Hill, 1953.

[A criterion for applicability of plane waves in a horn is given on page 1353. Also shows that the transient solution in an exponential horn involves a Bessel function of order zero.]

[82] E. G. Richardson, *Technical Aspects of Sound*, Volume I, *Sonic Range and Airborne Sound*, pages 359–361, Elsevier Publishing Co., 1953.

[Just a very brief review of current types of horns. Figures are included showing a compound horn, a multi-cellular horn, and a horn with a diffraction lens on the front for increased beamwidth. Of interest are the two pictures containing spherical wave (tractrix) horns built in Germany by Siemens-Klangfilm. One shows a small two-way system and the other is a large two-way cinema horn that should yield impressive results down to about 27 Hz!]

[83] Daniel J. Plach, "Design Factors in Horn-Type Speakers," *Journal of the Audio Engineering Society*, **1**(4):276–280, October 1953.

[Not much here really; Plach just says the obvious; i.e. if you desire maximum efficiency from a horn down around cutoff (above cutoff it is not very important since the horn looks resistive and no conjugate match is necessary for maximum efficiency, just a resistance match so pick the throat area accordingly) the unloaded resonance of the driver must be higher than the cutoff freq. of the horn. This is obvious since the horn provides a mass load at cutoff which would lower the resonance of the driver so if the final resonance it to be around cutoff, then of course the unloaded resonance must be above cutoff.]

[84] Paul W. Klipsch, "Loudspeaker Developments," *Institute of Radio Engineers Transactions on P.G.A.*, May/June 1953.

[85] Leo L. Beranek, *Acoustics*, pages 259–284, McGraw-Hill, 1954.

[This text is the first to illustrate the design of both the horn and compression driver together with electric circuit analogies. Example calculations are given and nonlinear distortion discussed.]

[86] Frederick Vinton Hunt, *ELECTROACOUSTICS, The Analysis of Transduction, and Its Historical Background*, pages 89–91, Harvard University Press, 1954.

[The first 91 pages of this text are devoted to the history of electroacoustics! It is revealed that A.L. Thuras (1930) of Bell Telephone Laboratories was the first knowledgeable inventor of the bass reflex principle (first applied to dynamic microphones). Loading a diaphragm on each side with different length horns was first suggested by Selden T. Williams in 1928 (R.C.A.). John P. Minton and Abraham S. Ringel (R.C.A.) first proposed a two-way loudspeaker with a passive electrical network in 1925. E.C. Wente patented (1932) the use of the multi-cell exponential horn for coverage purposes. Maximilian Weil pointed out that the corner of a room may be used as an extension of a horn in 1925 which was later explored by Kellogg (1931). Also it appears that Poincaré pioneered using linear two-port equations for describing electromechanical coupling in 1907.]

[87] Sidney E. Levy, Saul J. White, and Abraham B. Cohen, U.S. Patent 2690231, September 28, 1954.

[An unusual looking horn is presented claiming wide angle beam width. The contours converge in the vertical plane while diverging in the horizontal plane. No measured directivity patterns are included.]

[88] Leo L. Beranek, "Loudspeakers and Microphones," *Journal of the Acoustical Society of America*, **26**(5):618–? September 1954.

[89] Robert F. Lambert, "Acoustical Studies of the Tractrix Horn. I," *Journal of the Acoustical Society of America*, **26**(6):1024–1028, November 1954.

[Uses the lossless transmission-line model for tractrix horn. A modified Webster equation is derived but has inconsistent units. Approximate solutions (using WKBJ method) are compared with analog computer simulation and actual measurements. Pressure is measured on axis and throat impedance measurements are compared to simulation using piston termination and hemi-spherical termination at the mouth. The piston termination seems to best match the data.]

[90] A. O. Jensen and R. F. Lambert, "Acoustical Studies of the Tractrix Horn. II," *Journal of the Acoustical Society of America*, **26**(6):1029–1033, November 1954.

[Throat impedance of the tractrix horn is measured using Flander's [39] method. On and off-axis responses are measured for a single and double-celled tractrix horn.]

[91] E. S. Weibel, "On Webster's horn equation," *Journal of the Acoustical Society of America*, **27**(4):726–727, July 1955.

[A stream function approach is used to derive a horn equation similar to Webster's, but the coefficients are defined differently. Assuming the surfaces of constant stream potential coincide with the surfaces of constant phase is correct only in the low-frequency limit ($\nabla^2\phi = 0$), but probably offers a significant improvement over the assumption of plane waves.]

[92] Frederick Vinton Hunt, "Notes on the Exact Equations Governing the Propagation of Sound in Fluids," *Journal of the Acoustical Society of America*, **27**(6):1019–1039, November 1955.

[This paper includes finite amplitude, viscous and thermal effects in the equations of sound propagation. Tensor forms are presented and both material and spatial coordinates are considered.]

[93] J. F. Ramsay, "Microwave antenna and waveguide techniques before 1900," *Proceedings of the Institute of Radio Engineers*, **46**:405–415, February 1958.

[94] Robert H. Randall, *An Introduction to Acoustics*, Addison-Wesley, Reading, Massachusetts, 1959.

[States that there are no "precise" counterparts to the "induction" or "coulomb" fields in acoustics on page 107. Horns are examined from pages 111–125; the analysis closely parallels Morse [51].]

[95] Richard W. Carlisle, "Method of Improving Acoustic Transmission in Folded Horns," *Journal of the Acoustical Society of America*, **31**(8):1135–1137, 1959.

[Carlisle adds a small change in the curved portion of a folded horn used for public address (now termed a re-entrant horn) to improve response.]

[96] Robert Bruce Lindsay, *Mechanical Radiation*, pages 168–171, McGraw-Hill, 1960.

[The analogy between electromagnetic and acoustic fields, is discussed.]

[97] Yûkichi Nomura, Ichirô Yamamura, and Sakari Inawashiro, "On the Acoustic Radiation from a Flanged Circular Pipe," *Journal of the Physical Society of Japan*, **15**(3), 1960.

[The unflanged pipe had been solved since 1948; here the infinite baffled pipe is solved. Radiation impedance, transmission coefficient, power gain function and end correction are all shown as functions of wavelength. This paper is devoid of references to this problem which is approximately treated in Morse's *Vibration and Sound*, (1936, 1948) and solved exactly in Morse and Feshbach's *Methods of Theoretical Physics, part II*, page 1455, 1953.]

[98] James Moir, *High Quality Sound Reproduction*, second edition, pages 507–524, MacMillan Co., 1961.

[Contains design considerations for horns. Exponential (multi-celled), conical and folded horns are all included along with causes of distortion. Directivity of a multi-celled exponential horn is shown as well as diffraction lenses for controlling the beam pattern. Contemporary systems for domestic use are pictured.]

[99] E.[dward] H.[arrington] Lockwood, *A Book of Curves*, Cambridge University Press, 1961.

[Pages 119–124 discuss practical means of producing the tractrix contour, the catenary curve as evolute of the tractrix, and the historical origins of both. C. Huyg(h)ens (Dutch, 1629–1695) solved the tractrix problem (which askes: the path of an object dragged along a horizontal plane by a string of constant length when the other end of the string moves along a straight line in the plane), generalized it, and gave the curve its name. The tractrix problem was first proposed by a French doctor to G. W. Leibniz (German, 1646–1716).]

[100] Paul W. Klipsch, "A New High-Frequency Horn," *I.E.E.E. Transactions on Audio*, November/December 1963.

[101] L. H. Chen and D. G. Schweikert, "Sound Radiation from an Arbitrary Body," *Journal of the Acoustical Society of America*, **35**(10):1626–1632, October 1963.

[This is the basic theory behind a powerful program written to allow for acoustic radiation assuming coupling between the structure and the fluid medium. The example of a piston set in a sphere is used to show the accuracy of the procedure.]

[102] Milton Abramowitz and Irene A. Stegun, *Handbook of Mathematical Functions*, National Bureau of Standards, 1964. Corrected edition republished by Dover, 1972.

[103] Robert E. Collin, *Foundations for Microwave Engineering*, McGraw-Hill, 1966.

[Explicit sections (5.7–5.15) on impedance matching *via* taper or a finite number of straight sections. One-dimensional theory applies directly to one-dimensional acoustic horn approximations.]

[104] R.[aymond] W.[illiam] B.[arrow] Stephens and A. E. Bate, *Acoustics and Vibrational Physics*, second edition, Edward Arnold Pulblishers, London, 1966. First edition published under the title of *Wave Motion and Sound*.

[Analogies between electromagnetic and acoustic fields in waveguides (page 525–536) and also for electrostatics and incompressible, steady-state fluid flow (page 568–569).]

[105] Gordon E. Martin, *On the Propagation of Longitudinal Stress Waves in Finite Solid Elastic Horns*, Dissertation, University of Texas at Austin, 1966.

[106] Edward Eisner, "Complete Solutions of the 'Webster' Horn Equation," *Journal of the Acoustical Society of America*, **41**(4):1126–1146, April 1967.

[Annotated bibliography with 196 references.]

[107] Harry A. Schenck, "Improved Integral Formulation for Acoustic Radiation Problems," *Journal of the Acoustical Society of America*, **44**(1):41–58, 1968.

[The uniqueness difficulties of using the Helmholtz integral equation to solve radiation problems are theoretically proven to exist, but then are removed by a method Schenck calls CHIEF (combined Helmholtz integral equation formulation).]

[108] Y. Ando, "Experimental Study of the Pressure Directivity and the Acoustic Centre of the 'Circular Pipe Horn Loud Speaker'," *Acustica*, **20**:366–369, 1968.

[Experimental study reveals that it is best to use the outside diameter for a pipe of finite wall thickness when predicting the directivity and acoustic center. Nice data is shown using pulsed and continuous tone techniques.]

[109] I.[gnacy] Malecki, *Physical Foundations of Technical Acoustics*, pages 649–651, translated from Polish by Irena Bellert, Pergamon Press, 1969.

[An electroacoustic analogy is attempted in spatial systems but not completed. Difficulties are discussed. It seems as if Malecki states that the electric flux density vector field is curl free, or irrotational. This is not the case for the electrodynamics being discussed, and invalidates the following analogies.]

[110] Y. Ando, "On the Sound Radiation from Semi-Infinite Circular Pipe of Certain Wall Thickness," *Acustica*, **22**:219–225, 1969/70.

[Attention is again turned to the classic problem of radiation from a cylindrical tube with the added complication of finite wall thickness. Expressions are given for the reflection coefficient, end correction, and measurements are also compared with directivity and acoustic center.]

[111] Paul W. Klipsch, "Loudspeaker Performance," *Wireless World*, February 1970.

[112] A. J. Burton and G. F. Miller, "The Application of Integral Equation Methods to the Numerical Solutions of Some Exterior Boundary Value Problems," *The Proceedings of the Royal Society of London*, Serial A, **323**:201–210, 1971.

[113] H. F. Olson, Modern Sound Reproduction, Van Nostrand R., 1972.

[114] M. B. Lesser and J. A. Lewis, "Applications of matched asymptotic expansion methods to acoustics I. The Webster horn equation and the stepped duct," *Journal of the Acoustical Society of America*, **51**(5):1664–1669, 1972.

[115] M. B. Lesser and J. A. Lewis, "Applications of matched asymptotic expansion methods to acoustics II. The open-ended duct," *Journal of the Acoustical Society of America*, **52**(5):1406–1410, 1972.

[The method presented in their first paper is used to solve the open-ended duct problem. The solution compares to order epsilon with the exact solution.]

[116] R. Bruce Lindsay, *Acoustics: Historical and Philosophical Development*, Benchmark Papers in Acoustics, Dowden, Hutchinson & Ross, Inc., Stroudsburg, Pennsylvania, 1973.

[117] Leopold B. Felsen and Nathan Marcuvitz, *Radiation and Scattering of Waves*, Prentice-Hall, Englewood Cliffs, NJ, 1973.

[118] D. B. Keele Jr., "Optimum Horn Mouth Size," presented at the 46th Convention of the Audio Engineering Society, September 10–13, 1973, preprint 933. *Journal of the Audio Engineering Society(Abstracts)*, **21**:748, 1973.

[Using Webster's plane-wave horn theory and terminating the mouth of the horn as a rigid piston, Keele shows that there is an optimum length for an exponential horn, after which the reflections from the mouth begin to increase again. This phenomenon is indeed true if the waves in the mouth of the horn are plane waves (see W. M. Hall's work [40]). This result is difficult to believe, but no experimental work has been presented to confirm or refute it. Note that other accomplished horn designers such as C.A. Henrickson accept the results (see *The New Audio Cyclopedia* [163]).]

[119] Ali Hasan Nayfeh and Demetri P. Telionis, "Acoustic propagation in ducts with varying cross sections," *Journal of the Acoustical Society of America*, **54**(6):1654–1661, 1973.

[Looks at rectangular and circular ducts which vary slowly. The rate of attenuation of higher-order modes is being studied. This work is not particularly applicable to horns which vary too rapidly.]

[120] Peter H. Rogers, "Formal solution of the surface Helmholtz integral equation at a nondegenerate characteristic frequency," *Journal of the Acoustical Society of America*, **54**(6):1662–1666, 1973.

[This is mostly just a mathematical look at a long standing problem but doesn't offer any practical utility for circumventing the difficulty.]

[121] William E. Zorumski, "Generalized Radiation Impedance and Reflection Coefficients of Circular and Annular Ducts," *Journal of the Acoustical Society of America*, **54**(6):1667–1673, 1973.

[Gives the reflection coefficients for a flanged duct with arbitrary duct wall admittance.]

[122] A. H. Benade and E. V. Jansson, "On Plane and Spherical Waves in Horns with Nonuniform Flare, I. Theory of Radiation, Resonance Frequencies, and Mode Conversion," *Acustica*, **31**(3):79–98, 1974.

[123] E. V. Jansson and A. H. Benade, "On Plane and Spherical Waves in Horns with Nonuniform Flare, II. Prediction and Measurements of Resonance Frequencies and Radiation Losses," *Acustica*, **31**(4):185–202, 1974.

[Webster's equation is used to predict the resonance frequencies in trumpets. Both plane-wave and spherical-wave propagation is assumed and the measured resonance frequency is found to lie between the predictions of the two assumptions.]

[124] J. Dinsdale, "Horn Loudspeaker Design," *Wireless World*, **80**(1459):19–24, March; (1461):133–139, May; (1462):186–190, June 1974.

["After a brief historical survey, these articles examine the theory behind the horn-loaded loudspeaker enclosure and explain the basic points to consider when designing horns. The various compromises adopted by different workers are discussed, especially in the area of folding techniques, and the effects of these compromises on audio quality are studied. Finally, outline designs for two domestic horns are given: a 'no-compromise' horn to suit the most fastidious (and enthusiastic) listener, and a 'mini-horn' which provides a more limited performance for those with smaller living rooms (and bank balances), and which, while no more obtrusive than most commercial loudspeaker cabinets, will provide extremely clear and natural reproduction." Tractrix, exponential, and modified exponential (Wilson) horns are discussed. It is stated that the horn only loads the diaphragm while moving in the forward direction, and another horn behind the diaphragm is needed to load during backward motion.]

[125] K. W. Yeow, "Webster Wave Equation in Two Dimensions," *Journal of the Acoustical Society of America*, **56**(1):19–21, July 1974.

[The author presents spinning modes and shows that they also propagate according to Webster's horn equation. It seems to me that for spinning modes it is dangerous to neglect shear forces which would destroy the assumptions here.]

Arthur Gordon Webster (1863–1923) American physicist.

[126] David R. Schaller, "Horn Loudspeaker Output," Letters to the Editor, *Wireless World*, **81**(1471):126, March 1975.

[A response concerning misleading information in Dinsdale's articles. Schaller points out from Olson's *Acoustical Engineering*, page 220, that ". . . a relatively smooth output response frequency characteristic can be obtained from a horn having a mechanical impedance characteristic varying over wide limits."]

[127] Percy Wilson and Geoffrey L. Wilson, "Horn Theory and the Phonograph," *Journal of the Audio Engineering Society*, **23**(3):194–199, April 1975.

[Percy is Geoffrey's father.]

[128] Robert W. Pyle, Jr., "Effective Length of Horns," *Journal of the Acoustical Society of America*, **57**(6):1309–1317, June 1975.

[Based on plane-wave theory, Pyle derives a first-order, nonlinear, ordinary differential equation from which the effective length of horns at any frequency may be found. The results are claimed to be in qualitative agreement with instrument makers.]

[129] D. B. Keele, Jr., "What's So Sacred about Exponential Horns," presented at the 51th Convention of the Audio Engineering Society, preprint 1038, *Journal of the Audio Engineering Society* (Abstracts), **23**:492, July/August 1975.

[This paper describes the research behind the first constant-directivity horn. It gives credit to his boss at Electro-Voice, John Gilliom for coming up with the basic approach. Keele also points out the similarity to Paul Klipsch's horn which was patented *circa* 1945. See Keele's Patent [136].]

[130] W. Eversman, E. L. Cook and R. J. Beckemeyer, "A Method of Weighted Residuals for the Investigation of Sound Transmission in Non-uniform Ducts Without Flow," *Journal of Sound and Vibration*, **38**(1):105–123, 1975.

[Numerical solution of a tube which changes size is given for the first and second modes and compared against other numerical methods.]

[131] Y. Ando, and T. Koizumi, "Sound radiation from a semi-infinite circular pipe having an arbitrary profile of orifice," *Journal of the Acoustical Society of America*, **59**(5):1033–1039, 1976.

[A computer based algorithm is given for computing radiation from ducts with varying profiles that could, of course, include an acoustic horn profile. To demonstrate, insertion loss from a muffler is calculated and the sound pressure level on axis of a loudspeaker is also shown. Neither of these is supported with experimental data and there is no comment on the efficiency of the computer algorithm.]

[132] J. K. Hilliard, "Historical review of horns used for audience-type sound reproduction," *Journal of the Acoustical Society of America*, **59**(1):1–8, January 1976.

[A nice overview of the development of the horn (including many photographs) as used in the commercial industry. The phonograph horn is first mentioned followed by multi-celled horns, folded horns, sectoral horns, and horns with diffusion lenses. The Fletcher horn by Wente and Thuras at Bell Labs, the Shearer horn by Hilliard at MGM studios, and the "Voice of the Theater" horn system by Altec Lansing are all included.]

[133] A. W. Love, editor, *Electromagnetic Horn Antennas*, The Institute of Electrical and Electronics Engineers Press, 345 East 47th Street, New York, NY 10017, 1976.

[A collection of historically important publications in the area of electromagnetic horns.]

[134] William E. Boyce and Richard C. DiPrima, *Elementary Differential Equations and Boundary Value Problems*, third edition, John Wiley & Sons, 1977.

[135] Frederick Vinton Hunt, *ORIGINS IN ACOUSTICS, the Science of Sound from Antiquity to the Age of Newton*, foreword by Robert Edmund Apfel, New Haven and London, Yale University Press, 1978.

[An extensive historical survey. Begins with philosophers on observation, then on to experiments and the beginning of modern acoustic theory (225 references). Early work with horns is discussed with the first reference being 1650 by Athanasius Kircher (nice pictures from Kircher's work, *Phonurgia Nova*, 1673, including horns used by the military to summon troops and horns to be used in residences for paging, music, or eavesdropping are included on pages 139–141), who claims to be the inventor of the loud-speaking trumpet. Sir Samuel Morland (1625–1695) triggered Kircher's claim by a brochure of his entitled *Tuba Stenotoro-Phonica...; Invented and variously Experimented in the Year 1670*. Morland's first instrument was of glass, $32''$ long and $11''$ in diameter at the mouth, but he then progressed to a copper $21'$ horn with a $2'$ mouth. Morland appears to be the first person to investigate experimentally

the directivity of a sound source. Sir John Conyers (1644–1719) first demonstrated the re-entrant folded horn in 1678. The modern exponential horn has its antecedent in the demonstration by Richard Helsham (1680–1738) that "the best form for such tubes ... is generated by the revolution of a logarithmic curve round its axis, as in a tube of this form the elastic bodies will increase in such a manner as most to increase the quantity of motion." In his analysis, Helsham suggested that the air in the horn be subdivided into thin laminae perpendicular to the axis, and he then considered the transmission of motion from one laminae to the next. The conclusion he reached, that the area of any one laminae should be the geometric mean of the areas of its two neighbors, still constitutes a valid basis for arguing the superiority of the exponential form of horn profile. Compare with the analysis of Hanna and Slepian [16].]

[136] D. Broadus Keele, Jr., U.S. Patent 4071112, January 31, 1978.

[This patent is classic in that it is the first constant-directivity (CD) horn patent. In the vertical plane, the design begins with an exponential type throat section which turns into a conical flare and ends with a rapid bell flare. In the horizontal plane, the horn is a wide straight sided type until near the end where it becomes a wide bell type flare. Included are plots of the beam width of both a sectoral exponential horn and the CD horn. The horizontal beam width of the CD horn is constant from 450 Hz to 20 kHz ($\pm 5^\circ$).

Assignee: Electro-Voice, Incorporated, Buchanan, Michigan.]

[137] Clifford A. Henricksen and Mark S. Ureda, "The Manta-Ray Horns," *Journal of the Audio Engineering Society*, **26**(9):629–634, September 1978.

[This article details the design of a new type of constant-directivity horn. The horn wall contour is different in the horizontal and vertical directions to achieve the desired coverage, and the area expansion is quadratic which makes the horn a "Bessel" type (see Ballantine [24]). The appendix includes a discussion on the proper axis of rotation when doing directivity measurements on a horn.]

[138] Martin Greenspan, "Piston Radiator: Some Extensions of the Theory," *Journal of the Acoustical Society of America*, **65**(3):608–621, March 1979.

[On-axis pressures are analytically derived and computed for the rigid piston, simply-supported radiator, clamped radiator, and Gaussian radiator. Impedances "seen" by the sources are also shown as well as total power radiated. (It is interesting to note that the impedance seen by the Gaussian radiator is shown as purely resistive and the total power radiated has both a real and reactive component.) Three-dimensional plots of on-axis transient responses are also added.]

[139] W. Marshall Leach, Jr., "On the Specification of Moving-Coil Drivers for Low-Frequency Horn-Loaded Loudspeakers," *Journal of the Audio Engineering Society*, **27**(12):950–959, December 1979.

[Discusses the synthesis of a horn coupled to a cone driver. Design examples are included; all theory is presented *via* electroacoustic models. Also see *Letters to the Editor* [148].]

[140] S. Iyanaga and Y. Kawada, *Encyclopedic Dictionary of Mathematics*, MIT Press, Cambridge, Mass., 1980, page 998.

[Picard's method of iteration for partial differential equations of the elliptic type is given with convergence criteria.]

[141] Clifford A. Henricksen, and Mark S. Ureda, U.S. Patent 4187926, February 12, 1980.

[This patent assigned to the Altec Corporation (Anaheim, CA) for a constant-directivity horn which is straight sided in the vertical plane except for a small straight flare on the end and is at first parallel and then going to a straight flare at the diffraction slot in the horizontal plane. Two directivity patterns are shown side-by-side against patterns obtained from Don Keele Jr.'s (U.S. Patent 4071112, 1978) showing better low-frequency and mid-frequency performance than the original constant-directivity horn design.]

[142] Y. Kagawa, T. Yamabuchi, T. Yoshikawa, S. Ooie, N. Kyouno, and T. Shindo, "Finite Element Approach to Acoustic Transmission-Radiation Systems and Application to Horn and Silencer Design," *Journal of Sound and Vibration*, **69**(2):207–228, 1980.

[Numerical procedure is outlined for coupling an internal finite element method (FEM) and an external Green's function approach in the solution of a conical and exponential horn. The results of throat impedance don't seem to be a significant improvement over predictions by plane-wave theory. Character based plots are shown of the internal pressure distribution in the horns.]

[143] Shigeru Morita, Noboru Kyono, and Shinichi Sakai, "Acoustic Radiation of a Horn Loudspeaker by the Finite Element Method—A Consideration of the Acoustic Characteristic of Horns," *Journal of the Audio Engineering Society*, **28**(7/8):482–489, July/August 1980.

[144] Samuel Temkin, *Elements of Acoustics*, John Wiley & Sons, 1981.

[145] Bruce C. Edgar, "The Tractrix Horn Contour," *Speaker Builder Magazine*, pages 9–15, February 1981.

[A historical review of the tractrix horn. Various contours for tractrix construction are given on graphical design charts.]

[146] Josef Merhaut, *Theory of Electroacoustics*, pages 182–208, McGraw Hill, 1981.

[147] Tomas Salava, "Measurements of the Input Impedance of Loudspeaker Horns," *Journal of the Audio Engineering Society*, **29**(6):416–420, June 1981.

[148] Edward F. McClain, Jr., "Comments on Reactance Annulling in Horn-Loaded Loudspeaker Systems," *Letters to the Editor, /JAES*, **29**(7/8):523–524, July/August 1981.

[Claims Al Thuras first invented Reactance Annulling. Followed by a discussion from Leach [139] on the technique.]

[149] D. Broadus Keele, Jr., U.S. Patent 4308932, January 5, 1982.

[This patent describes the current state-of-the-art in constant-directivity horns. The entire method for construction of the horn geometry is described in detail. The radius of curvature of the wavefront is established in the vertical plane and then a sharp discontinuity establishes the wavefront curvature in the horizontal direction. The directivity patterns in both horizontal and vertical planes are shown and reveal impressive pattern control, although no comment is made about the loss of uniform loading on the driver. Assignee: James B. Lansing Sound Inc., Northridge, CA.]

[150] Noboru Kyouno, Shinichi Sakai, Shigeru Morita, Tatsuo Yamabuchi, and Yukio Kagawa, "Acoustic Radiation of a Horn Loudspeaker by the Finite Element Method—Acoustic Characteristics of a Horn Loudspeaker with an Elastic Diaphragm," *Journal of the Audio Engineering Society*, **30**(12):896–905, December 1982.

[151] L. M. B. C. Campos, "Some General Properties of the Exact Acoustic Fields in Horns and Baffles," *Journal of Sound and Vibration*, **95**(2):177–201, February 1984.

[This paper deals with one-dimensional horn theory; a historical summary of horn theory is given. The point of the paper is to study further various properties of the Webster horn equation and its possible solutions (110 references).]

[152] John Eargle, "Developments in High Frequency Pattern Control: The Defined Coverage Horn," *dB*, pages 14–15, July 1984.

[A brief essay on the reasons for constant directivity horns followed by an example of the latest in CD horns: The JBL 4660.]

[153] Frank. J. Fahy, "Rapid Method for the Measurement of Sample Acoustic Impedance in a Standing Wave Tube," Letter to the Editor, *Journal of Sound and Vibration*, **97**:168–170, 1984.

[154] A. F. Seybert, B. Soenarko, F. J. Rizzo, and D. J. Shippy, "An Advanced Computational Method for Radiation and Scattering of Acoustic Waves in Three Dimensions," *Journal of the Acoustical Society of America*, **77**(2):362–368, 1985.

[A general formulation based on the Helmholtz integral formula for numerically solving radiation and scattering problems *via* the boundary element

method (BEM) is presented. Quadratic boundary elements are used. The resulting program is tested on the radiation impedance of a sphere and accurately produces the correct solution for values of $ka \leq 5$ after modeling the sphere with 24 triangular elements. Monopole and dipole radiation is also shown to be accurately predicted as well. Scattering from a rigid cylinder and sphere for $ka = 1$ and $ka = 0.1$ are also correctly predicted.]

[155] Norbert N. Bojarski, "The Far Field in Terms of the Spatial Fourier Transform of the Sources and its Implications on the Inverse Problem," *Journal of Applied Physics*, **58**(1):1–4, 1985.

[Bojarski rigorously proves that the far-field acoustic pressure may be represented by the Fourier transform of velocity sources on a plane boundary. It is not original work, but merely serves as a convenient reference. Both acoustic and electromagnetic cases are covered.]

[156] Douglas Samuel Jones, *Acoustic and Electromagnetic Waves*, Oxford University Press, 1986.

[Discusses the parallels in analysis techniques between acoustics and electromagnetics.]

[157] Josef Merhaut, "Impulse Measurement of Horn-Type Loudspeaker Drivers," *Journal of the Audio Engineering Society*, **34**(4):245–254, April 1986.

[158] J. McLean and E. Hixson, "The Modeling of Rigid-Walled Acoustic Horn with Sharp Flare Discontinuities," presented at the 111th meeting of the Acoustical Society of America at Cleveland, OH, May 1986, paper 003.

[159] Earl R. Geddes, "Source Radiation Characteristics," *Journal of the Audio Engineering Society* (Engineering Reports), **34**(6):464–478, June 1986.

[160] A. F. Seybert, B. Soenarko, F. J. Rizzo, and D. J. Shippy, "A special integral equation formulation for acoustic radiation and scattering for axisymmetric bodies and boundary conditions," *Journal of the Acoustical Society of America*, **80**(4):1241–1247, October 1986.

[161] M. A. Milošević and V. M. Gmitrović, "Optimization procedure for computer design of a horn loudspeaker," *Journal of the Audio Engineering Society*, **34**:382, reprint No. 2360, 1986.

[162] Jerome Spanier and Keith B. Oldham, *An Atlas of Functions*, Hemisphere Publishing Corporation, ISBN 0-89116-573-8, 1987.

[163] Glen Ballou, *HANDBOOK FOR SOUND ENGINEERS, The New Audio Cyclopedia*, pages 445–460, Howard W. Sams & Co., a division of Macmillian, Inc., 1987.

[Contains a section written by C. A. Henrickson (designer of the Altec Mantaray horns) on compression horn drivers and horns. Many pictures of drivers are included along with relevant design equations for both drivers and horns. Many horn types are shown in actual commercial examples. Keele's presentation (1973) based on a piston model of mouth impedance is interpreted here as substantiated when Henrickson states, "Recently, Keele has found that the impedance will actually reach an optimum or minimum passband ripple and then begin to ripple more as the horn is lengthened and the mouth size increased."]

[164] Earl Geddes, James Porter, and Yifan Tang, "A Boundary-Element Approach to Finite-Element Radiation Problems," *Journal of the Audio Engineering Society*, **35**(4):211–229, 1987.

[A derivation is given for a "boundary element" used for radiation coupling in finite element modeling. Results are compared with other numerical techniques but no analytical baselines are used and no experimental work is done.]

[165] E. R. Geddes, D. Clark, "A Computer Simulation of Horn-Loaded Compression Drivers," *Journal of the Audio Engineering Society* (Engineering Reports), **35**(7/8):556–566, July/August 1987.

[166] A. F. Seybert and T. K. Rengarajan, "The use of CHIEF to obtain unique solutions for acoustic radiation using boundary integral equations," *Journal of the Acoustical Society of America*, **81**(5):1299–1306, May 1987.

[Compares the CHIEF method of circumventing nonuniqueness in the Helmholtz integral formulation to the gradient method and concludes the CHIEF method is more accurate.]

[167] Leo L.[eroy] Beranek, *Acoustical Measurements*, revised edition, Published by the *American Institute of Physics* for the *Acoustical Society of America*, 1988. (first edition published by John Wiley, 1949)

[Chapter 15 contains standard methods for testing loudspeakers.]

[168] Mario Rossi, *Acoustics and Electroacoustics*, Artech House, 685 Canton St., Norwood, MA 02062, 1988.

[A Patrick R. W. Roe translation of *Electroacoustique*, originally published in French as volume XXI of the *Traité d'Electricité* by the Presses Polytechniques Romandes, Lausanne, Switzerland, 1986.]

[169] E. R. Geddes, "Sound Radiation from Acoustic Apertures," presented at the 85th Convention of the Audio Engineering Society, preprint 2742. *Journal of the Audio Engineering Society* (Abstracts), **36**:1026, 1988.

[170] Arie J. M. Kaizer, A. D. Leeuwestein, "Calculation of the Sound Radiation of a Nonrigid Loudspeaker Diaphragm Using the Finite-Element Method," *Journal of the Audio Engineering Society*, **36**(7/8):539–551, 1988.

[Places a hemisphere over the loudspeaker in an infinite baffle and derives an impedance matrix to use as a boundary condition in the finite element formulation.]

[171] Junichi Hayakawa, Shiro Iwakura, Kaoru Yamazaki, and Susumu Matsuoka, "Improvement in Dome Loudspeaker Characteristics by Using a Spherical-Wave-Front Horn Baffle," *Journal of the Audio Engineering Society*, **36**(7/8):575–584, July/August 1988.

[Here is an example of a tractrix horn being used in a modern loudspeaker application. The measured results show a marked improvement in smoothness of frequency response and directivity, resulting from decreased diffraction at the edges of the loudspeaker.]

[172] J. Kergomard, "General Equivalent Electric Circuits for Acoustic Horns," *Journal of the Audio Engineering Society*, **36**(12):948–955, December 1988.

[Presents a method based on continued fraction expansions to derive an electric circuit model for predicting resonances. Fewer elements are needed for accurate calculation but the model is less physical than the common transmission line model. Discusses validity of Webster's equation by comparing it to spherical waves in a conical horn. This leads to $\frac{1}{2}k\int_{x_1}^{x_2}(dr/dx)^2 \ll 1$ where r is the radius of the horn, k is the wave number, and x represents axial distance.]

[173] U. R. Kristiansen, T. F. Johansen, "The Horn Loudspeaker as a Screen-Diffraction Problem," *Journal of Sound and Vibration*, **133**(3):449–456, 1989.

[The surface of the horn is replace with dipoles is this work. Results show the calculations compare well with measurements for a conical horn.

In contrast to much of the older work which seemed to believe that all horns behaved much the same at high frequencies, Kristiansen is aware of the importance the horn geometry has in determining the directivity pattern when he states: "For higher frequencies, the actual horn shape will play an important part, and interference phenomena between the direct and secondary source distribution on the horn surface will cause the covering angle to vary."]

[174] Josef Merhaut, "Impulse Measurement of Acoustic Impedance," *Journal of the Audio Engineering Society*, **37**(5):343–352, May 1989.

[175] Earl R. Geddes, "Acoustic Waveguide Theory," *Journal of the Audio Engineering Society*, **37**(7/8):554–569, 1989.

[An review of the history of horn theory. Points out that the purpose of the horn has changed from one of optimal driver loading to one of optimal directivity pattern. To predict these radiation patterns, a new waveguide approach is said to be necessary in which a coordinate system is found that allows one parameter wave propagation. It is not necessary that the coordinate system be separable in the usual sense, i.e. $\phi(x,y,z,t) = X(x)Y(y)Z(z)T(t)$ but only

such that $\phi(u,t) = A(u)\exp(i(ku - \omega t))$ where u is the only coordinate variable that enters into the equation. An example is worked to show this idea in one of the 11 fully separable coordinate systems, the oblate spheroidal system. The paper contains several errors and the coordinate system presented does not allow for one-parameter wave propagation. See *Letters to the Editor* [186] for a discussion of this article.]

[176] Allan D. Pierce, *ACOUSTICS, An Introduction to Its Physical Principles and Applications*, pages 357–365, Published by the American Institute of Physics for the Acoustical Society of America, 1989.

[The Webster equation is derived from an integral approach and limits of applicability are given as $\frac{1}{2}rr'(\partial p/\partial x)_0/p_0 \ll 1$ where r is the local radius, prime indicates differentiation w.r.t. the axial coordinate, and the $(\cdot)_0$ subscripts indicate the on-axis pressure and velocity.]

[177] Gary E. Evans, *Antenna Measurement Techniques*, Artech House, 1990.

[Chapter 6 discusses near-field testing ranges for electromagnetic antennas. Includes a bibliography.]

[178] A. F. Seybert, C. Y. R. Cheng, T. W. Wu, "The Solution of Coupled Interior/Exterior Acoustic Problems Using the Boundary Element Method," *Journal of the Acoustical Society of America*, **88**(3):1612–1618, 1990.

[Presents a formulation for separating the domain of a problem into two or more domains and solving them individually, then together. The method is shown to yield the same solution as a single domain method. Seybert claims that this approach overcomes the problem of a single domain approach where the boundary meshes lie very close to one another, creating numerical errors.]

[179] T. Shindo, T. Yoshioka, K. Fukuyama, "Calculation of Sound Radiation from an Unbaffled, Rectangular-Cross-Section Horn Loudspeaker Using Combined Analytical and Boundary-Element Methods," *Journal of the Audio Engineering Society*, **38**(5):340–349, 1990.

[Sections of multi-moded rectangular waveguide are used [79] to model wave propagation in the horn with the Rayleigh integral used at the mouth for a boundary condition. After the field at the mouth of the horn is known, the exterior surface of the horn is used as the radiation source in a boundary element method formulation. Directivity patterns are given in vertical and horizontal planes for several frequencies and show good agreement with measurement.]

[180] Martin Colloms, *High Performance Loudspeakers*, fourth edition, John Wiley & Sons 1991.

[Colloms defines horn cutoff as: "The frequency at which the acoustic impedance becomes reactive rather than resistive, i.e. the resistive component has fallen by 6 dB."]

[181] R. D. Ciskowski and C. A. Brebbia, editors, *Boundary Element Methods in Acoustics*, Computational Mechanics Publications, ISBN 0-945824-87-4, copublished with Elsevier Science Publishing Co., ISBN 1-85166-679-6, 1991.

[182] M. Milošević and M. Gmitrović, "The Computer Design of Horn Loudspeaker Systems," *Acustica*, **74**:209–216, 1991.

[Low frequency optimization of the equivalent horn loudspeaker circuit. Transmission line *ABCD* model of horn contour.]

[183] Robert W. Pyle, Jr., "Notes on Plane-wave Horn Theory," Unpublished, 43 pages, Draft copy dated February 4, 1991.

[A nice collection of one-dimensional horn theory for use in design of musical instruments. Dual contours, transmission matrices, equivalent circuits, effective length and numerical solutions are all covered. Received through private communication.]

[184] Roy Delgado, Kerry Geist, and Jim Hunter, "Tractrix Horns," *Audio Magazine*, pages 36–49, March 1991.

[Plots of phase response of a tractrix horn versus an exponential horn reveal that the tractrix horn has a more nearly constant group delay.]

[185] K. R. Holland, F. J. Fahy, and C. L. Morfey, "Prediction and Measurement of the One-Parameter Behavior of Horns," *Journal of the Audio Engineering Society*, **39**(5):315–337, May 1991.

[186] Gavin R. Putland, "Comments on 'Acoustic Waveguide Theory'," *Journal of the Audio Engineering Society*, **39**(6):469–472, June 1991.

[187] Mapes-Riordan, D., "Horn Modeling with Conical and Cylindrical Transmission Line Elements," *Presented at the 91st Convention of the Audio Engineering Society in New York*, preprint 3194, 4–8 October 1991.

[Points out the advantages of transmission-line element modeling over lumped element modeling. Claims that conical elements are superior to cylindrical elements for horn modeling due to a more rapid convergence and shows results from a computer program to validate claim. Note: It has been noticed during other numerical studies [183] that using conical sections resulted in no improvement over using cylindrical sections in transmission-line modeling, because both element types converged at the same rate for the off-diagonal, two-port matrix elements.]

[188] Jyh-Yeong Hwang, San-Cheng Chang, "A Retracted Boundary Integral Equation for Exterior Acoustic Problem with Unique Solution for All Wave Numbers," *Journal of the Acoustical Society of America*, **90**(2):1167–1180, 1991.

[189] G. Beer & J. O. Watson, *Introduction to Finite and Boundary Element Methods for Engineers*, John Wiley & Sons, 1992.

[190] William H. Press, Saul A. Teukolsky, William T. Vetterling, Brian P. Flannery, *Numerical Recipes in FORTRAN, the art of scientific computing*, Cambridge University Press, 1992.

[191] James S. McLean, John T. Post, and Elmer L. Hixson, "A theoretical and experimental investigation of the throat impedance characteristics of constant directivity horns," *Journal of the Acoustical Society of America*, **92**(5):2509–2526, November 1992.

[Using plane wave horn theory and adding losses, the two-port parameters for a compression horn driver are found and used to find the acoustic impedance at the throat of a modern constant directivity horn. The experimental results compare well with theory.]

[192] Noam Amir, Giora Rosenhouse and Uri Shimony, "Input Impedance of Musical Horns and the 'Horn Function'," *Applied Acoustics*, **38**:15–35, 1993.

[Using the potential function form (Schrödinger wave equation) of Webster's equation, resonance frequencies are computed for musical instrument horns. Piecewise cylindrical and exponential models are used for numerical computations. Optimization is attempted with little success.]

[193] Juha Backman, "A Computational Model of Horn Loudspeakers," Presented at the 94th Convention of the *Audio Engineering Society*, Preprint 3512(E1-5), March 16–19, 1993.

[Claims a new technique for predicting horn performance. The new method is an approximate implementation of the boundary element method but no study is made to understand the implication of the approximation.]

[194] Earl R. Geddes, "Sound Radiation from Acoustic Apertures," *Journal of the Audio Engineering Society*, **41**(4):214–230, April 1993.

[A qualitative discussion of the directivity of bulging wavefronts in the mouth of an aperture. The results are likely pushed beyond applicability for an acoustic horn, since at large values of ka, the assumed velocity distribution is a poor approximation of measured data (see Hall [40]).]

[195] Gavin R. Putland, "Every One-Parameter Acoustic Field Obeys Webster's Horn Equation," *Journal of the Audio Engineering Society*, **41**(6):435–451, June 1993.

[196] Earl R. Geddes, "Acoustic Waveguide Theory Revisited," *Journal of the Audio Engineering Society*, **41**(6):452–461, June 1993.

[197] Paul D. Bauman, A. B. Adamson, and Earl R. Geddes, "Acoustic Waveguides — In Practice," *Journal of the Audio Engineering Society*, **41**(6):462–470, June 1993.

[198] Dan Mapes-Riordan, "Horn Modeling with Conical and Cylindrical Transmission-Line Elements," *Journal of the Audio Engineering Society*, **41**(6):471–484, June 1993.

[199] D. J. Henwood, "The Boundary-Element Method and Horn Design," *Journal of the Audio Engineering Society*, **41**(6):485–496, June 1993.